

Pure Scaling Operators at the Integer Quantum Hall Plateau Transition

Inaugural-Dissertation
zur
Erlangung des Doktorgrades
der Mathematisch-Naturwissenschaftlichen Fakultät
der Universität zu Köln

vorgelegt von
Daniel Johann Wieczorek
aus Dormagen

Köln, 2015

Berichtersteller:

Prof. Dr. Martin R. Zirnbauer
PD Dr. Rochus Klesse

Tag der letzten mündlichen Prüfung:

08.05.2015

Kurzzusammenfassung

Legt man an einen Metalloxid-Halbleiter-Feldeffekttransistor, der bei niedrigen Temperaturen von einem starken magnetischen Fluss durchsetzt ist, eine longitudinale Spannung an, so findet man, dass der transversale Leitwert eine strikte Quantisierung $\frac{ne^2}{h}$ mit einer natürlichen Zahl n zeigt. Gleichzeitig verschwindet in dieser sogenannten Plateau-Region die longitudinale Leitfähigkeit; dies ist der ganzzahlige Quanten-Hall-Effekt. Bei einer ausreichend starken Änderung des Magnetfelds findet ein Quanten-Phasenübergang zwischen den Plateau-Regionen statt, der, in Übereinstimmung mit einem zentralen Paradigma der statistischen Physik, durch eine konforme Feldtheorie beschrieben werden sollte. Ausgehend vom kritischen Chalker-Coddington-Netzwerkmodell, das ein diskretes quantenmechanisches Modell für den Phasenübergang darstellt, schlägt diese Arbeit eine Familie von Observablen als Diskretisierungen konformer Primärfelder vor. Im einfachsten Fall reduzieren sich diese auf das Unordnungsmittel von Momenten des Betragsquadrats stationärer Streuzustände auf einer Kante l des Netzwerks in Anwesenheit eines Punktkontakts c . Für ein ebenes Netzwerk erwartet man dann einen algebraischen Abfall dieser Observable mit dem Abstand zwischen Kontakt und Beobachtungspunkt. Im supersymmetrischen Vertexmodell, das über eine Dualitätstransformation mit dem Netzwerkmodell verbunden ist, entsprechen diese Observablen Zuständen höchsten Gewichts für die Symmetriealgebra $\mathfrak{gl}_{2n|2n}$. In zylindrischer und rechteckiger Geometrie zeigen wir anschließend, dass die Vermutung, dass es sich hierbei tatsächlich um Diskretisierungen von Primärfeldern handelt, numerisch bestätigt werden kann. Abschließend untersuchen wir noch die für die genaue Natur der Kontinuumstheorie äußerst bedeutsame Frage nach der Form des Multifraktalitätsspektrums der konformen Dimensionen dieser Felder. Die Klasse der Observablen ist dabei, im Vergleich zu früheren Arbeiten, derart umfassend, dass eine numerische Klärung der Frage nach der Parabolizität des Spektrums nun greifbarer erscheint.

Abstract

If a longitudinal voltage is applied to a MOSFET subject to low temperature and a strong perpendicular magnetic field, one finds that the transversal conductivity is strictly quantized according to $\frac{ne^2}{h}$ with positive integer n . This is called the plateau region. At the same time, the longitudinal conductivity vanishes; this is the integer quantum Hall effect. Changing the magnetic field eventually results in a quantum phase transition between the plateaus. By a central paradigm of statistical physics this transition should be described by a conformal field theory. Starting from the critical Chalker-Coddington network model, which is a discrete model for this transition, we suggest a family of observables as discretizations of conformal primary fields. In the simplest case these reduce to the disorder average of moments of the absolute value square of stationary scattering states of the network evaluated at a specific link l in the presence of a point contact c . In a plane network algebraic decay with the distance between l and c is expected. The network model is connected to the supersymmetric vertex model by a duality transformation and the suggested observables correspond to highest weight operators of the symmetry algebra $\mathfrak{gl}_{2n|2n}$. Numerical simulations in cylindrical and rectangular geometries provide strong evidence for the conjecture that these observables have indeed the desired properties. Finally, we address the question of the precise form of the multifractal spectrum of conformal dimensions, which is an important one to ask in view of the correct continuum field theory. The family of observables is, compared to work done in the past two decades, quite extensive and will hopefully contribute to a conclusive answer on the parabolicity of the spectrum.

Contents

1	Introduction	1
1.1	The integer quantum Hall effect	2
1.1.1	Landau level quantization	3
1.1.2	Enter disorder, boundaries	4
1.1.3	Laughlin's argument and topological insulators	5
1.2	The network model	6
1.2.1	(Semi-)Classical percolation and its insufficiency	6
1.2.2	The Chalker-Coddington model	7
1.2.3	Localization-delocalization transition	8
1.3	Critical properties and finite size scaling	10
1.4	Recent results on the localization length exponent	13
1.5	Multifractality of critical wavefunctions	14
1.6	Conformal invariance	17
1.7	Point-contact conductances	20
2	Pure Scaling Observables	23
2.1	Preparations	25
2.1.1	Fermionic Fock space	25
2.1.2	Bosonic Fock space	25
2.1.3	Representations and character formulas	26
2.1.3.1	Fermionic Fock space	26
2.1.3.2	Bosonic Fock space	28
2.1.4	Two-point functions and matrix elements	29
2.1.5	Supersymmetric Fock space	30
2.1.6	Application to the network model	30
2.1.7	Lie superalgebras	33
2.2	Single-point observables for $\mathfrak{gl}_{2 2}$	35
2.3	Point contacts and point contact conductances	38
2.4	Multi-point observables for $\mathfrak{gl}_{2 2}$, several contacts	42
2.5	$n + 1$ -point functions of φ_q	44
2.6	Multi-point observables for $\mathfrak{gl}_{2n 2n}$	45
2.7	Casimir eigenvalues	52
2.8	The conceptual background of φ_q	54

3	Numerical Tests	59
3.1	Description of the program code	60
3.2	Results on long cylinders	63
3.2.1	Two-point contact conductances	63
3.2.2	First results on the observables A_1, A_2, A_3	66
3.2.3	2+1-point functions	69
3.2.4	An attempt at finite size scaling for A_1	70
3.3	Results on the rectangle	71
3.3.1	Establishing the scaling behavior of $Z(\tau)$	72
3.3.2	Finite size scaling on the rectangle	73
4	Summary and outlook	77
A	Two-point function on the rectangle	79
B	Program code	83
	Bibliography	96

Chapter 1

Introduction

*Was würde passieren, wenn Sie von einem 56000 km/h
schnellen Rostbraten getroffen würden?*
Prüfungsfrage von Robert B. Laughlin

This chapter serves as an introduction of some aspects of the subject to a general audience—but, to be honest, in view of the very limited and *localized* impact of inaugural dissertations mainly to make the topic easily accessible for subsequent PhD students—and as a motivation for the main part of this thesis. We briefly recall the basic phenomenology and theoretical folklore of the integer quantum Hall effect, motivating the introduction of the Chalker-Coddington network model. It is generally believed to describe the universality class of the quantum phase transition between Hall plateaus and, since its introduction in 1985, has been used widely for numerical simulations—this thesis being no exception. We introduce the localization length, inverse participation ratios and point-contact conductances as important examples of critical observables and discuss the concepts of finite size scaling and multifractality as well as recent numerical work on the critical exponent of the localization length. Especially the investigation of so-called typical point-contact conductances strongly suggests that the paradigm of conformal invariance at a two-dimensional quantum critical point also applies to the integer quantum Hall transition. The search for this conformal field theory has been the subject of numerous publications over the last decades, the most notable suggestions being nonlinear sigma models with target space $\mathrm{PSL}_{2|2}$ over the base manifold $S^3 \times H^3$ including a Wess-Zumino term. The level varies between $k = 1$ [Z99], $k = 8$ [T07] and $k = 1/t$ [BKS⁺00]. Since no conclusive answer has been found so far and the discussion of these suggestions, apart from mentioning that all of these three imply a strictly parabolic multifractal spectrum, would lead us too far astray we omit it here and refer to the literature. 35 years have passed since the discovery of the quantum Hall effect and the basics already found their way into textbooks. This being said it is clear that we can claim neither much originality nor anything near comprehensiveness in this chapter, but still we try to point out some oversimplifications and errors which are repeated quite often. The literature from which the author learned about the subject obviously influenced the selection and presentation of the material in this chapter. Firstly, the textbook by Altland and Simons [AS10] gives a general introduction as well as a

discussion of Pruisken’s field theory of the plateau regime. For the early theoretical and numerical approaches, up to the investigation of wavefunction multifractality, the textbook by Janßen, Viehweger, Fastenrath and Hajdu [JVF⁺94] as well as the review by Huckestein [H95] still serve as a valuable source of information, especially concerning localization and scaling aspects of the topic. The recent and extensive review by Kramer, Ohtsuki and Kettmann [KOK05] focuses on the random network model aspect and also covers much of the material in our first three subsections. The review by Evers and Mirlin [EM08] discusses the much broader context of Anderson transitions, the integer quantum Hall transition falling into the unitary symmetry class A in the Altland-Zirnbauer classification scheme [AZ97]. Our treatment of multifractality was mainly inspired by this article. Furthermore, the introduction into scaling and renormalization by Cardy [C96] as well as the “big yellow book” on conformal field theory [FMS97] have been used. Thus, as far as folklore is concerned which can either be found in the literature just mentioned or even in lecture courses on statistical mechanics, condensed matter or quantum field theory we refrain from cluttering the text with too many citations (since the author aims at a PhD in theoretical physics rather than humanities).

1.1 The integer quantum Hall effect

The classical Hall effect is well-known from high-school physics: A thin rectangular piece of metal in the $x - y$ -plane is subjected to a magnetic field $Bdx \wedge dy$. If one applies a voltage V_x in x -direction (and thus a current I_x flows through the sample), a voltage V_y proportional to I_x and B is induced across the sample.

In 1980, von Klitzing, Dorda and Pepper [KDP80] discovered that an analogous experiment on a two-dimensional electron gas—realized in the inversion layer of a MOSFET—in a strong magnetic field $B \sim 15T$ at low temperatures $T \sim 1K$ yields well-defined plateaus of the Hall resistance

$$\rho_{xy} = \frac{1}{n} \frac{h}{e^2} \quad n \in \mathbb{N} \quad (1.1)$$

as a function of the magnetic field. These are accompanied by a vanishing longitudinal resistance $\rho_{xx} = 0$. The experimental results are shown in figure 1.1.

The fact that the Hall conductance $\sigma_{xy} = \rho_{xy}^{-1}$ is integer when measured in units of $\frac{e^2}{h}$ coined the name integer quantum Hall effect. Apart from 1985’s nobel prize, the astonishing accuracy of (1.1) established the von Klitzing constant

$$R_K = \frac{h}{e^2} = 25812.807557(19)\Omega \quad (1.2)$$

as a practical standard for electrical resistance in 1990. This effect can be understood only via a combination of localization due to disorder and the Landau level quantization of electrons in a magnetic field. Surprisingly, broken translational invariance of the system is crucial for the very existence of a quantized Hall conductivity: Let us consider a homogeneous electron gas in a translationally invariant system which is placed in a perpendicular magnetic field $Bdx \wedge dy$. If no external electric field is applied, no current is flowing. On the other hand, in an inertial system moving with

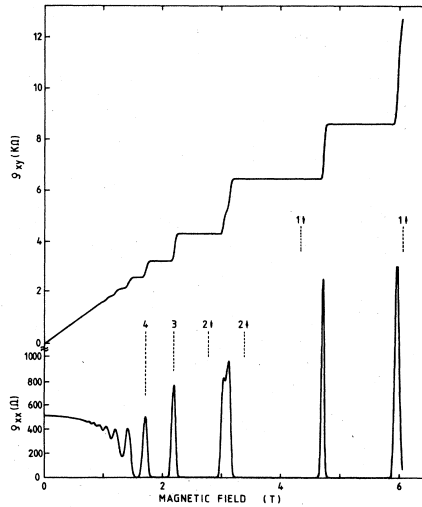


Figure 1.1: Longitudinal resistance ρ_{xx} and Hall resistance ρ_{xy} vs. strength of magnetic field, taken from [K85].

velocity ve_x a current density $j = -v\rho dy \wedge dz$ is observed. Furthermore, the magnetic field in the system at rest is transformed into an electrical field $E = -vBdy$ in the co-moving frame, so that we find $\sigma_{xy} = \frac{\rho}{B}$ for the Hall conductivity. Since the argument is independent of the speed v , we can conclude that translational invariance implies $\sigma_{xy} \sim B$.

1.1.1 Landau level quantization

The quantum mechanics of a two-dimensional non-interacting electron gas can be described by the Hamiltonian

$$H = \frac{1}{2m^*} \left[\left(-i\hbar\partial_x + \frac{1}{2}eBy \right)^2 + \left(-i\hbar\partial_y - \frac{1}{2}eBx \right)^2 \right] \quad (1.3)$$

where m^* is the effective mass and the symmetric gauge $A = \frac{1}{2}B(xdy - ydx)$ has been chosen. Introducing complex coordinates $z = x + iy$, $\bar{z} = x - iy$ and operators $b = \sqrt{2} \left(l\partial_{\bar{z}} + \frac{z}{4l} \right)$, $a = \sqrt{2} \left(l\partial_z + \frac{\bar{z}}{4l} \right)$, where $l = \sqrt{\frac{\hbar}{eB}}$ is the magnetic length, and noting $\partial_{\bar{z}}^\dagger = -\partial_z$, H assumes the form of a harmonic oscillator

$$H = \frac{\hbar eB}{m^*} \left(b^\dagger b + \frac{1}{2} \right). \quad (1.4)$$

Since a, a^\dagger do not appear at all, each energy eigenvalue $E_n = \frac{\hbar eB}{m^*} \left(n + \frac{1}{2} \right)$ is hugely degenerate; there are $n_B = \frac{B}{\Phi_0}$ states per unit area in each Landau level, where $\Phi_0 = h/(2e)$ is the magnetic flux quantum. We notice that proportionality to B is also expected in the classical picture. Fixing the kinetic energy of an electron and thus its speed v , the radius of its cyclotronic motion is $r = \frac{mv}{eB}$, i.e. the larger B ,

the more cyclotronic orbits fit into a unit area without interfering. Denoting the number of electrons per unit area by n_e , the filling factor $n = \frac{n_e}{n_B}$ gives the number of filled Landau levels, but only for $n \in \mathbb{N}$ the plateau values of the conductance are assumed, which leads to the conclusion that essential ingredients are missing for an explanation of the effect.

1.1.2 Enter disorder, boundaries

Adding static disorder via a random potential to the Hamiltonian,

$$H = H_0 + V(r) , \quad (1.5)$$

has the effect that the infinitely sharp Landau levels are broadened into bands. The density of states then qualitatively looks as shown in figure 1.2.

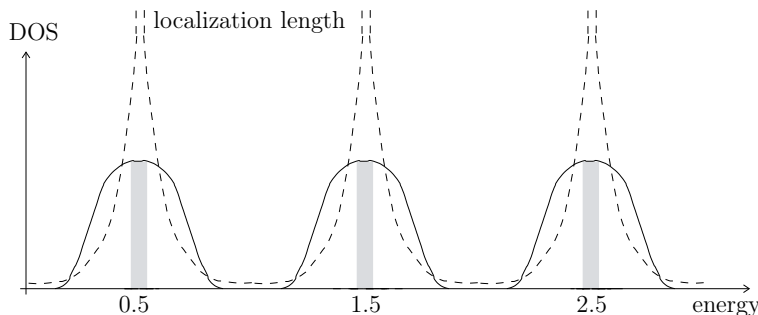


Figure 1.2: Qualitative picture of the dependence of the density of states (solid lines) and the localization length (dashed lines). Adapted from [KOK05].

States in the band tails turn out to be exponentially localized, i.e. their wavefunctions decay as $|\Psi(r)|^2 \sim \exp(-r/\xi)$, where ξ is the so-called localization length¹, whereas extended states exist only in the band centers. Now, if the Fermi energy lies in the so-called incompressible spectral region, where the density of states vanishes, or in the band tails, there are no extended states available for zero-temperature dc transport, implying $\rho_{xx} = 0$. Furthermore, a strong change in the Fermi level is needed to change the filling factor over the incompressible region, which leads to a constant Hall conductivity there. However, contrary to the treatment in many introductory texts, the existence of a broad plateau also requires an explanation of why the continuous change of the filling factor in the band tails does not affect the Hall conductance. As it turns out, this is due to the fact that only delocalized states contribute to the Hall conductance. From the viewpoint of non-commutative geometry this was already explained in the classic article by Belissard, van Elst and Schulz-Baldes [BES94]. On the other hand, in the shaded central regions of the compressible spectral region extended states are available for electric transport and since a large number of states falls into a small energy interval, the filling factor and thus the Hall conductivity changes drastically near the band center when the Fermi energy is varied.

¹Notice that this definition can be grasped intuitively, but it suffers from the drawback that it cannot be employed to calculate ξ , since the wavefunction is not known exactly.

The boundaries of a real sample have the effect of bending the Landau levels in the vicinity of the sample edges as shown in figure 1.3 for a clean conductor.

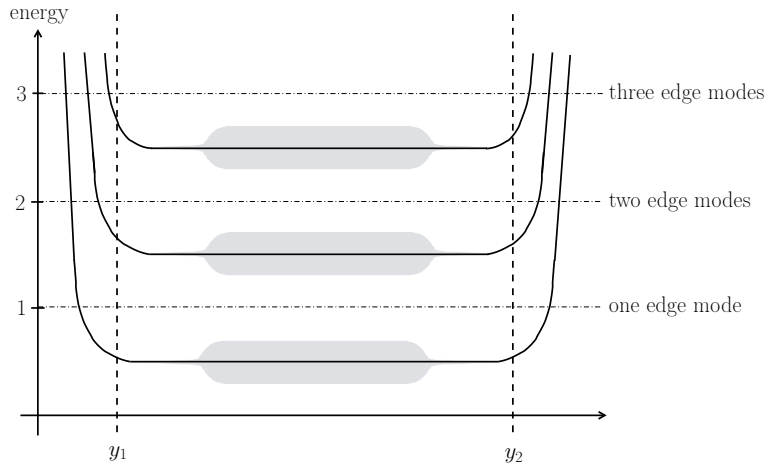


Figure 1.3: Landau levels in the presence of disorder and a boundary, adapted from [B88] and [AS10].

If the Fermi energy lies between the bulk Landau levels, the crossing points with the deformed levels correspond to edge states which acquire a velocity along the edges of the sample

$$v_{jk} = \frac{1}{\hbar} \frac{dE_{jk}}{dy_0} \frac{dy_0}{dk}, \quad (1.6)$$

where y_0 denotes the center coordinate of the cyclotronic motion. The form of the spectrum then implies that the edge states are chiral. Finally, taking disorder into account again, in the plateau regime there are localized bulk states which do not contribute to electrical transport as well as chiral edge modes which escape localization by the very presence of the boundary. This is the hallmark of systems that are nowadays called topological insulators [KM05]. Büttiker [B88] demonstrated that in a theoretical treatment of the precise experimental setup -a four-terminal measurement with disorder in the sample and in the contacts taken into account- the prefactor n in (1.1) corresponds to the number of chiral edge states.

1.1.3 Laughlin's argument and topological insulators

The term *topological* insulator indicates that there is also another perspective on the robustness of the Hall conductance quantization: In his famous gedankenexperiment, Laughlin [L81] considered a cylinder connected to charge reservoirs and pierced by a magnetic field perpendicular to its surface together with a magnetic flux tube along its symmetry axis, see figure 1.4. A time-dependent flux results in an electromotive force in azimuthal direction which in turn causes a charge transfer between the reservoirs. By gauge invariance, pumping integer multiples of a flux quantum Φ_0 through the system leaves the Hamiltonian invariant and it can be shown that the number of transported charges in one pump cycle equals the Hall conductance in units of $\frac{e^2}{h}$. However, as pointed out by Avron and Seiler [AS03], although the

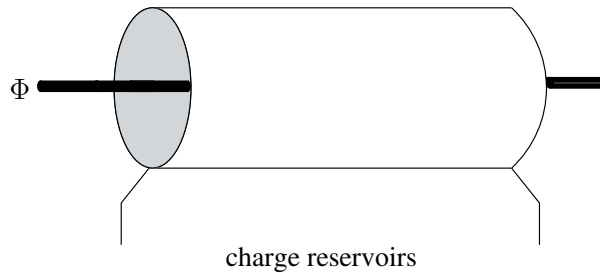


Figure 1.4: Setup of the Lauglin gedankenexperiment, adapted from [AS03].

charge transported in any individual cycle is integer, quantum mechanics does not forbid the number of charges to change between cycles per se. Thus, an explanation for the quantization of the average transferred charge is also needed: It is possible to write down a single-particle effective Hall Hamiltonian $H(\phi, \theta)$ that depends on two angular variables ϕ, θ with period ϕ_0 . θ is chosen such that the Hall current can be written as $I = c\partial_\theta H(\phi, \theta)$. Furthermore, if the ground state is gapped and its energy is independent of ϕ , then the ground state expectation value of the Hall current is given by

$$\langle \Psi_0 | I | \Psi_0 \rangle = \hbar c^2 K U , \quad (1.7)$$

where U is the driving electromotive force and $Kd\phi \wedge d\theta$ is the Berry curvature (or rather its pullback) of the ground state line bundle over the parameter space torus T . In this way, the Hall conductance receives a geometric interpretation. The averaging procedure over pump cycles then corresponds to averaging over the torus, i.e. to the integral $\frac{1}{2\pi} \int_T K$. This is an integer, since we can consider a closed loop on the torus, which divides the torus into two disconnected components. By Stokes' theorem, we can calculate the Berry phase around this loop by integrating over any of these components, and the resulting phases have to be equal up to integer multiples of 2π . Shrinking the loop this argument continues to hold, so the integral above is indeed an integer. This is the celebrated Chern number, which is a prime example of a topological invariant, since it measures the homotopy class into which the Hamiltonian falls. Changing the homotopy class can only be achieved through a continuous deformation of the Hamiltonian if the energy gap closes at some point, giving an explanation for the robustness of the quantum Hall plateaus.

1.2 The network model

Further physical insight into the nature of the plateau transition can be gained by considering two simplified models, namely the percolation model and the random network model, where the latter is also tailor-made for numerical simulations.

1.2.1 (Semi-)Classical percolation and its insufficiency

In the experimental setup, the two-dimensional electron gas is confined to the inversion layer of a MOSFET. Randomly distributed impurities in the semiconducting material generate a long-range correlated, random electric potential. In the high magnetic field (or semiclassical) limit, this can be assumed to vary significantly only

on length scales much larger than the magnetic length l . In this semiclassical picture the wavefunction of the electron is essentially confined to a strip of width $\sim l$ around the equipotential lines carrying a current density along these. This is also expected classically, since the motion is directed due to the presence of a magnetic field. In this picture it is easy to see that for very low energy E the electron encircles potential valleys, whereas for very high energies the motion takes place around hill-tops. In both cases the wavefunctions correspond to exponentially localized states [KS83]. As E is increased, an equipotential line visits more and more valleys, and at a critical energy E_c it percolates through the whole system. This corresponds to the classical percolation threshold and the localization length ξ_P , in this context defined as the correlation length of a percolating equipotential line, diverges as

$$\xi \sim |E - E_c|^{-\nu_P} . \quad (1.8)$$

$\nu_P = \frac{4}{3}$ has been calculated exactly [SD87], but this value differs from the experimentally observed value ~ 2.38 [LVX⁺09]. This large discrepancy can be resolved by noting that two salient features of quantum mechanics has been ignored so far: quantum tunneling at saddle points and quantum interference. We briefly mention that the semiclassical argument [MS88] by Mil'nikov and Sokolov which ignores interference received far too much acclaim by heavy recitation in the past since it is essentially wrong. A combination of percolation and quantum tunneling alone reproduces the percolation exponent $\frac{4}{3}$, as was shown in [HK97].

1.2.2 The Chalker-Coddington model

The Chalker-Coddington network model [CC88] unites all the important ingredients. Let us consider a network of current loops which encircle potential maxima and minima. At any saddle point of the potential, two incoming currents (ψ_0, ψ_2) and two outgoing (ψ_1, ψ_3) currents meet², see figure 1.5.

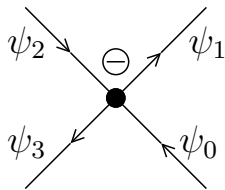


Figure 1.5: A node in the network model.

Conservation of probability flux enforces the relation $|\psi_1|^2 + |\psi_3|^2 = |\psi_0|^2 + |\psi_2|^2$ which can be expressed conveniently by a unitary scattering matrix S ,

$$\begin{pmatrix} \psi_1 \\ \psi_3 \end{pmatrix} = S \begin{pmatrix} \psi_0 \\ \psi_2 \end{pmatrix} , \quad S \in \text{U}_2 . \quad (1.9)$$

Instead of considering a random potential landscape, the effect of disorder can equivalently be captured by a regular network of current loops with scattering matrices

²The counting of links is chosen such that it is compatible with chapter 3.

randomly drawn from U_2 according to Haar measure. Furthermore, every $S \in U_2$ can be written by the polar decomposition as

$$S = \begin{pmatrix} e^{i\phi_1} & 0 \\ 0 & e^{i\phi_3} \end{pmatrix} \begin{pmatrix} r & -t \\ t & r \end{pmatrix} \begin{pmatrix} e^{i\phi_0} & 0 \\ 0 & e^{i\phi_2} \end{pmatrix}. \quad (1.10)$$

The transmission and reflection probabilities t^2 and r^2 are subject to the constraints $t^2 + r^2 = 1$ and $r, t \in [0, 1]$. This implies that we can instead consider non-random scattering at saddle points and absorb the effect of randomness into the link currents ψ_i .

The Chalker-Coddington network model is then defined as follows: Consider a square lattice where each elementary square, called plaquette, has a definite sense of circulation that alternates between neighboring plaquettes. The links of the network are directed accordingly, so that two incoming and two outgoing links meet at each vertex of the lattice. The Hilbert space of the model is

$$\mathcal{H} = \bigoplus_{l \in \text{links}} \mathbb{C}_l, \quad (1.11)$$

i.e. a complex number is assigned to each link. The wave function evolves in discrete time as

$$|\psi(t+1)\rangle = U |\psi(t)\rangle, \quad U = U_s U_r. \quad (1.12)$$

U_s describes unitary scattering at the vertices, i.e. the transfer from incoming to outgoing links. U_r is diagonal in the link basis and describes the propagation along links by assigning to each link a random, independent and uniformly distributed U_1 phase. Apart from a rotation by 90° in figure 1.5, the deterministic part U_s is assumed to be the same at all nodes, i.e. the probability for an incoming current to be scattered to the left resp. to the right is the same all over the network. This is called the isotropic point. The probability of being scattered into one direction is, in fact, the only parameter in the Chalker-Coddington model, since all information like Fermi energy, strength of the magnetic field and properties of randomness are encoded in the scattering at saddle points.

1.2.3 Localization-delocalization transition

The localization-delocalization transition can easily be visualized by considering a network in the strip geometry as shown in figure 1.6. Let us imagine that this is a sketch of a real system which is connected to external leads at the left and the right edge.

There are two extremal cases: For $t = 0, r = 1$ left turns are forbidden and there is no path which connects left and right edge, since there are only closed current loops in the bulk of the strip. This is the trivial insulating phase. On the other hand, if only left turns are allowed, there exist two delocalized edge states with opposite chirality. This is the quantum Hall phase. In between lies the isotropic point $r = t = \frac{1}{2}\sqrt{2}$ where both directions become equally probable.

We mention that the definition of the model employing a unitary time evolution is a more recent viewpoint introduced in [KM97]. The original model was formulated for the strip geometry using transfer matrices which relate the wave function amplitudes

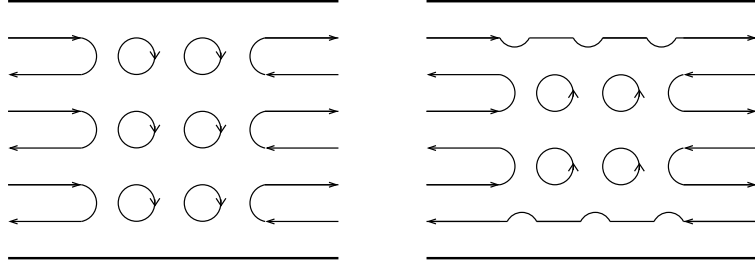


Figure 1.6: Trivial insulator (left), quantum Hall insulator with two edge channels (right).

on the left-hand side to the ones on the right-hand side of each vertex,

$$\begin{pmatrix} \psi_1 \\ \psi_0 \end{pmatrix} = T \begin{pmatrix} \psi_2 \\ \psi_3 \end{pmatrix}, \quad S \in \text{U}_2. \quad (1.13)$$

The transfer matrix T is related to S in (1.10) by

$$T = \begin{pmatrix} e^{-i\phi_1} & 0 \\ 0 & e^{i\phi_0} \end{pmatrix} \begin{pmatrix} \frac{1}{r} & \frac{r}{t} \\ \frac{r}{t} & \frac{1}{t} \end{pmatrix} \begin{pmatrix} e^{i\phi_2} & 0 \\ 0 & e^{-i\phi_3} \end{pmatrix}. \quad (1.14)$$

The shortest strip possible consists of two horizontal layers as shown in figure 1.7.

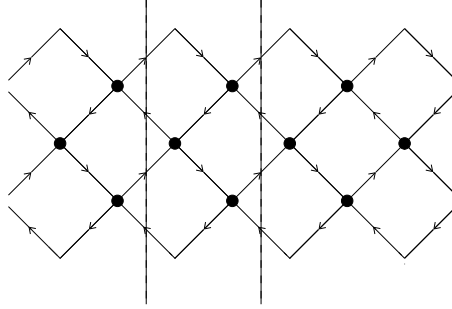


Figure 1.7: A section of a strip of width 2. The section between dashed lines is the building block of this strip.

For a width of W plaquettes, W incoming and W outgoing links on the left are connected to as many links of each type on the right by a transfer matrix T_W . The transfer matrix of a strip of length L is then given by the L th power T_W^L . This approach has been used to study the localization length: By Oseledec's theorem [O68] the matrix

$$T_W^\infty := \lim_{L \rightarrow \infty} (T_W^L T_W^{L\dagger})^{\frac{1}{2L}} \quad (1.15)$$

has only positive eigenvalues, and since T is symplectic, there is a basis in which the underlying operator has the matrix representation

$$\mathcal{T}^\infty = \text{diag}(e^{\gamma_{W/2}}, \dots, e^{\gamma_1}, e^{-\gamma_1}, \dots, e^{-\gamma_{W/2}}), \quad (1.16)$$

where $\gamma_1 \leq \dots \leq \gamma_{W/2}$ are called Lyapunov exponents. Each of these gives a scale

on which the corresponding eigenstate decays, which motivates

$$\xi = \frac{1}{\gamma_1} . \quad (1.17)$$

We remark that in a numerical simulation one must not multiply a large number of transfer matrices, since the magnitude of the elements will decrease rapidly, rendering the result useless. Instead, after m multiplications a QR-decomposition must be performed [KOK05]:

$$T_{W,k} T_{W,k+1} \cdots T_{W,k+m-1} V_k = V_{k+1} \omega_i , \quad (1.18)$$

where V_0 is the unit matrix, V_k are orthonormal $2W \times 2W$ matrices and ω_k are $2W \times 2W$ upper triangular matrices. For a strip of length $L = mn$ this yields

$$T_M^L = V_{n+1} \omega_n \omega_{n-1} \cdots \omega_1 . \quad (1.19)$$

1.3 Critical properties and finite size scaling

After recalling the general philosophy of finite size scaling, we discuss the critical properties of the model in terms of the divergence of the localization length as the critical point is approached as well as the critical wave function and transport properties.

Quantum phase transitions occur, strictly speaking, only in the thermodynamic limit of infinite system size. They are characterized by a power law divergence of certain observables F_∞ with respect to a reduced control parameter, most commonly the reduced Fermi energy ϵ ,

$$F_\infty(\epsilon) \sim \epsilon^{-\mu} . \quad (1.20)$$

It is a hallmark of a critical phenomenon in general that no physical length scale exists at the critical point, because otherwise exponential decay of thermodynamic quantities is expected, the length scale governing the distance at which the quantity has dropped by a factor of e^{-1} . There are two extremal cases where length scales are absent, the first of which being entirely uninteresting: The relevant scale could vanish or diverge. Near the critical point it is assumed in finite size scaling that the only relevant scale is set by the correlation length ξ_{corr} of order parameter fluctuations, which diverges as

$$\xi_{\text{corr}}(\epsilon) \sim \epsilon^{-\nu} . \quad (1.21)$$

This is the finite size scaling hypothesis. For a system of finite width W , the observables will depend on the ratio $\frac{W}{\xi_{\text{corr}}(\epsilon)}$. In principle the critical energy ϵ_c in the infinite system does not coincide with its counterpart in the finite system. However, we are interested in the localization-delocalization transition in the Chalker-Coddington model, which occurs when left- and right-scattering are equally probable, regardless of system size.

The finite size (one parameter) scaling hypothesis postulates the existence of a scaling function which becomes constant at small x and has a universal power law decay at large x ,

$$\tilde{f}(x) \sim x^{-\frac{\mu}{\nu}} , \quad (1.22)$$

such that near the critical point we have

$$F_W(\epsilon) = W^{\frac{\mu}{\nu}} \tilde{f} \left(\frac{W}{\xi_{\text{corr}}(\epsilon)} \right). \quad (1.23)$$

We notice that as $W \rightarrow \infty$ the scaling (1.20) is recovered. Furthermore, if the correlation length of the finite system itself is considered, $\mu = \nu$ and thus

$$\xi_{\text{corr},W}(\epsilon) = W \tilde{f} \left(\frac{W}{\xi_{\text{corr}}(\epsilon)} \right). \quad (1.24)$$

This phenomenological approach can be justified by a renormalization group argument: In the thermodynamic limit, the system is defined by a Hamiltonian with a set of coupling constants $\{k_i\}$ living on a lattice with finite lattice constant a . In a renormalizable theory one demands that if the lattice constant is rescaled as $a \rightarrow ba$, the free energy can be kept fixed if only the coupling constants in the Hamiltonian are changed to a new set $\{k'_i\}$. In this way, a “dynamical” system

$$\{k'_i\} = R(\{k_i\}) \quad (1.25)$$

is defined. The absence of a physical length scale at the critical point implies that rescaling has no effect. Thus we have to look at fixed points of the transformation R . It is then reasonable to consider the linear approximation of the dynamical system in the vicinity of such a fixed point. The corresponding mapping is usually assumed to possess a set of eigenvalues $\lambda_i := b^{y_i}$ such that (1.25) takes the form

$$\phi'_i = b^{y_i} \phi_i, \quad (1.26)$$

where the eigenvectors $\{\phi_i\}$ are $\{k_i\}$ -dependent scaling fields—although they are not fields in the sense of any field theory—which parametrize the distance from the critical point. Obviously, there are three distinct possibilities for the values y_i can take:

- Scaling fields with $y_i > 0$ are called relevant, because the RG flow will drive the system away from the fixed point.
- $y_i < 0$ corresponds to irrelevant fields, since the flow is directed towards the fixed point.
- The fields with $y_i = 0$ are called marginal.

Thermodynamic quantities F can then be expressed as functions of the scaling fields and the length scale W which has been reached after several iterations of the RG transformation. Furthermore, by construction they also get at most rescaled under the transformation, which implies the existence of an (analytic) scaling function f with

$$F(W, \phi_1, \phi_2, \dots) = W^\omega f(\phi_1 W^{y_1}, \phi_2 W^{y_2}, \dots). \quad (1.27)$$

This expression coincides with the finite size scaling hypothesis (1.22) in the thermodynamic limit if there is only one relevant field, $\phi_1 \sim t + O(t^2)$, and $y_1 = \frac{1}{\nu}$,

which can be seen by writing

$$\phi_1 W^{y_1} = \left(W \phi_1^{\frac{1}{y_1}} \right)^{y_1}, \quad (1.28)$$

i.e. $\phi_1 \sim \xi^\nu$.

In the network model, the probability of a right turn at the vertices is the single parameter which drives the system through the localization-delocalization transition. This is conveniently parametrized by the energy x measured from the center of the Landau band scaled by the Landau band width, which is related to the coefficients r, t in the transfer matrix as

$$t = \frac{1}{\sqrt{e^{2x} + 1}}, \quad r = \frac{1}{\sqrt{e^{-2x} + 1}}. \quad (1.29)$$

A useful quantity to study is the so-called MacKinnon-Kramer-variable or reduced localization length

$$\Lambda_W(x) = \frac{\xi_W(x)}{W}. \quad (1.30)$$

The rationale behind this definition is as follows: If the choice of x is such that the system flows towards the localized phase, $\xi_W(x)$ only grows with W until it reaches the order of the localization length of the truly infinite system, so $\Lambda_W(x)$ goes to zero. In the delocalized phase, on the other hand, Λ diverges with W . At criticality, the system is expected to be invariant under scale transformations, so once W is sufficiently large so that irrelevant contributions are suppressed we have $\xi \sim W$ and thus $\Lambda_W(x)$ has a finite limit Λ_c . Let us now suppose that it is sufficient to consider one relevant and one irrelevant scaling field in (1.27),

$$\Lambda_W(x) = f(\phi_1 W^{\frac{1}{\nu}}, \phi_2 W^y). \quad (1.31)$$

As discussed before, in the vicinity of the critical energy $x = 0$ the relevant scaling field decays at least linearly in x while the expansion of the irrelevant fields in x has to start with a constant term. Usually, the expansion of the scaling fields is truncated after the first nonvanishing order, so that we have

$$\Lambda(W; x) = f(c_1 x W^{\frac{1}{\nu}}, c_2 W^y), \quad (1.32)$$

which can then be expanded for small $xW^{\frac{1}{\nu}}$ to give

$$\Lambda_W(x) = \Lambda_c \left(1 + \sum_{k=1} a_k W^{ky} \right) + \sum_{k=1} \left(x W^{\frac{1}{\nu}} \right)^k \sum_{l=0} b_l W^{ly}. \quad (1.33)$$

This result is unpleasant in that many fitting parameters are involved. A slight improvement can be achieved by imposing periodic instead of reflecting boundary conditions on the strip, i.e. by considering a long cylinder of circumference W . In this way the network model acquires a kind of particle-hole-symmetry, since in this geometry it is invariant under transposition of r and t , which in turn implies that

$\Lambda_W(x)$ is an even function of x :

$$\Lambda_W(x) = \lambda(W) + x^2 \tilde{\lambda}(W) + \mathcal{O}(x^4 W^{\frac{4}{\nu}}) \quad (1.34)$$

$$\lambda(W) = \Lambda_c(1 + a_1 W^y + a_2 W^{2y} + \dots) \quad (1.35)$$

$$\tilde{\lambda}(W) = \tilde{\Lambda} W^{\frac{2}{\nu}}(1 + a'_1 W^y + a'_2 W^{2y} + \dots). \quad (1.36)$$

1.4 Recent results on the localization length exponent

Recent work tries to keep as much as seven coefficients in the scaling ansatz. The largest simulations were carried out by Obuse et al. [OGE12] on cylinders³ in the range⁴ $8 \leq W \leq 192$. Fitting such a large set of parameters poses a difficult problem, since the goodness of fit measure χ^2 might have several local minima in which a fitting algorithm could get stuck depending on its initial values. To overcome this difficulty the authors invented what they call “stability map analysis”: for different subsets of the data, i.e. taking only a restricted range of the available circumferences into account, fittings with a random ensemble of 1000 different initial values are employed, which the authors claim to yield global minima of χ^2 . The resulting values for the most interesting quantities ν, y, Λ_c are quite sensitive to the inclusion of a_1 and a'_1 into the fitting procedure. In this way each data set yields specific parameter values and error bars, and the reported values are obtained by taking the mean of the individual values for each parameter combined with the union of all error bars, which are then called “practical error bars“. An example is shown in figure 1.8 and we mention that the depicted situation is generic for the presented analysis, i.e. different data sets give incompatible ranges for the parameters.

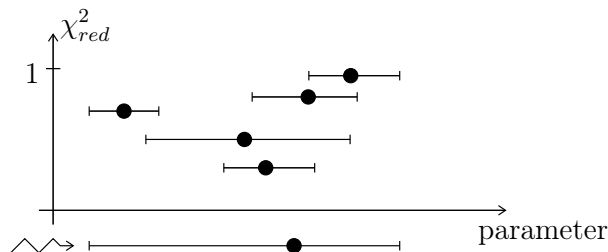


Figure 1.8: Practical error bar as union of all individual error bars.

According to the companion paper [OBL⁺13] the authors believe that this issue is due to truncation in (1.34) and could be, at least in principle, resolved by an improved data set. The results of this analysis are $\nu = 2.62 \pm 0.06$, $\frac{\Lambda_c}{\pi} = 0.257 \pm 0.02$ and $0.4 \leq |y| \leq 0.6$.

The most recent work along these lines has been carried out by Nuding, Klümper and Sedrakyan [NKS14]. They use a seemingly less sophisticated method to extract the parameters, namely fitting 200 times with a random ensemble of initial parameters and afterwards taking the mean and standard deviation for the obtained parameters, to arrive at a compatible value of $\nu = 2.593 \pm 0.0297$. The irrelevant exponent turns out incompatible, $y = -0.145 \pm 0.0677$.

³The system length is not stated in the paper.

⁴Notice that here we count in plaquette units, while the paper counts links.

Although the localization length is an obvious quantity to study, the fact that it is self-averaging implies that only limited information on the precise nature of the transition can be gained from this approach. In combination with the longstanding problems in multi-parameter fits for the data as the system is driven towards the critical point, we find it favorable to have observables at hand which could be studied right at the critical point.

1.5 Multifractality of critical wavefunctions

As a step towards this goal, let us now consider the properties of critical wavefunctions of the closed network. Being unitary, the time evolution operator U of the Chalker-Coddington network model has a set of $\dim \mathcal{H}$ eigenvalues of unit modulus,

$$U |\psi_k\rangle = \exp(i\omega_k) |\psi_k\rangle , \quad (1.37)$$

where ω_k are called quasi-energies. For fixed k , the time evolution can be redefined as $U \rightarrow \exp(-i\omega_k)U$ without altering the nature of the randomness, so that $|\psi_k\rangle$ is a so-called stationary wavefunction for the redefined dynamics. We remark that although any state satisfying (1.37) is a stationary state in the ordinary sense, the nomenclature of the field reserves the term stationary wavefunction resp. stationary state for eigenvectors of U with quasi-energy 0. At the critical point, $r = t = \frac{1}{\sqrt{2}}$, the normalized wavefunction ψ defines a multifractal measure which in turn gives rise to multifractal observables [J94], an example of which being the moments of the inverse participation ratios

$$P_q = \sum_{\text{links } \mathbf{r}} |\psi(\mathbf{r})|^{2q} . \quad (1.38)$$

We denote the ensemble average, i.e. the average of P_q with respect to link disorder, by $\mathbb{E}\{P_q\}$. This quantity shows scaling with the system size L ,

$$\mathbb{E}\{P_q\} = L^d \mathbb{E}\{|\psi(\mathbf{r})|^{2q}\} \sim L^{-\tau(q)} . \quad (1.39)$$

Here, the values $\tau(0) = -d$ and $\tau(1) = 0$ follow directly from the definition (1.38), d being the space dimension. Furthermore, the function τ is convex and non-decreasing. In the simplest case one could imagine, τ is a linear function $\tau(q) = d(q-1)$, but this is not the case for the critical wavefunctions of the network model and, due to strong spatial fluctuations, for any critical wavefunction at an Anderson transition. One then defines the anomalous scaling dimension Δ_q by

$$\tau(q) = d(q-1) + \Delta_q , \quad (1.40)$$

which governs the decay of spatial correlations of moments of the wavefunction,

$$L^{d(q_1+q_2)} \mathbb{E}\{|\psi^{2q_1}(\mathbf{r})\psi^{2q_2}(\mathbf{r}')|\} \sim L^{-\Delta_{q_1}-\Delta_{q_2}} \left(\frac{|\mathbf{r}-\mathbf{r}'|}{L}\right)^{\Delta_{q_1+q_2}-\Delta_{q_1}-\Delta_{q_2}} . \quad (1.41)$$

The heuristic reasoning behind this equation is that the correlator falls off as a power of $\frac{|r-r'|}{L}$ in the absence of length scales,

$$\mathbb{E}\{|\psi^{2q_1}(\mathbf{r})\psi^{2q_2}(\mathbf{r}')|\} = c(L) \left(\frac{|l-l'|}{L}\right)^X. \quad (1.42)$$

If the distance between the observation links is of the order of the system size, the wavefunctions are statistically independent, so that

$$c(L) \sim L^{-d(q_1+q_2)+\Delta_{q_1}+\Delta_{q_2}}, \quad (1.43)$$

while for separations smaller than the microscopic scale set by the lattice constant one effectively has $l=l'$, so that

$$\mathbb{E}\{\psi^{2(q_1+q_2)}\} \sim L^{-d(q_1+q_2)+\Delta_{q_1+q_2}}. \quad (1.44)$$

Only recently has it been proven in the framework of supersymmetric non-linear sigma models that the anomalous dimensions should obey exact symmetry relations [MFM⁺06],[GMZ13]. At the quantum Hall transition reflection symmetry around $q = \frac{1}{2}$ is theoretically expected, i.e.

$$\Delta_q = \Delta_{1-q}. \quad (1.45)$$

We give an elementary proof of this relation in section 2.7. The behavior of the multifractal spectrum as well as the scaling behavior of the whole distribution function $P(|\psi|^2)$ is summarized by the so-called singularity spectrum $f(\alpha)$. Defining the variable $\alpha = -\frac{\ln|\psi|^2}{\ln L}$, the distribution functions $P(|\psi|^2)$ and $P(\alpha)$ are related as

$$P_q = \int |\psi|^{2q} P(|\psi|^2) d|\psi|^2 = \int L^{-\alpha q} P(\alpha) d\alpha. \quad (1.46)$$

In order to reproduce (1.39), the distribution must have the form

$$P(\alpha) \sim L^{f(\alpha)-d}, \quad (1.47)$$

where $f(\alpha)$ is the Legendre transform of $\tau(q)$,

$$\alpha = \tau'(q), \quad f(\alpha) = \alpha q - \tau(q), \quad (1.48)$$

and it is understood implicitly that q is a function of α which comes from inverting the relation $\alpha = \tau'(q)$. By the properties of $\tau(q)$ and the general properties of the Legendre transform, f is a convex function on \mathbb{R}_0^+ with a unique maximum at α_0 which corresponds to $q = 0$. By

$$\mathbb{E}\{\ln |\psi|^2\} = \frac{d}{dq} \Big|_{q=0} \mathbb{E}\{|\psi|^{2q}\} \sim L^{-\alpha_0} \quad (1.49)$$

we see that this exponent governs the scaling of the typical value of the probability

$$P_q^{typ} := e^{\mathbb{E}\{\ln |\psi|^2\}}. \quad (1.50)$$

The simplest non-trivial singularity spectrum is parabolic,

$$f(\alpha) = d - \frac{(\alpha - \alpha_0)^2}{4(\alpha_0 - d)}, \quad (1.51)$$

the corresponding scaling dimension also being parabolic:

$$\tau(q) = d(q - 1) - \gamma q(q - 1), \quad \gamma = \alpha_0 - d. \quad (1.52)$$

In general, this should also be a reasonable approximation to the spectrum in the region where the anomalous dimension is small compared to $d(q - 1)$, i.e. in the case $\gamma q \ll d$. This form entails that the distribution of the wavefunction amplitudes is log-normal,

$$P(|\psi|^2) = \frac{1}{\sqrt{2\pi}\sigma|\psi|^2} \exp\left(-\frac{(\ln|\psi|^2 - \mu)^2}{2\sigma^2}\right), \quad (1.53)$$

where $\mu = \alpha_0 \ln L$ and $\sigma^2 = (\alpha_0 - d) \ln L$. This is the paradigm of a distribution which is broad on all length scales, implying that for quantities like (1.39) tail contributions are essential. For numerical simulations we thus see that large ensemble sizes are crucial to capture the multifractal exponents adequately. Whether or not such an approximation is exact is a central question to ask, since Δ_q is related directly to the spectrum of an underlying conformal field theory and thus provides the possibility to rule out certain suggestions. There were several attempts to answer this question by investigation of the scaling behavior of inverse participation ratios in the Chalker-Coddington model. Using square networks containing up to $2 \cdot 10^6$ links⁵ Evers et al. found no significant deviations from parabolicity [EMM01]. However, seven years later the same authors reinvestigated toric networks of the same sizes with moderately improved ensemble sizes⁶ and refined fitting methods to report small deviations [EMM08],

$$\Delta_q = 2q(1 - q) \left[b_0 + b_1 \left(q - \frac{1}{2} \right)^2 + \dots \right], \quad (1.54)$$

with $b_0 = 0.1291(2)$ and $b_1 = 0.0029(3)$. Almost in parallel, Obuse et al. [OSF⁺08] found $2b_0 = 0.2599$ and $2b_1 = 0.0065$ on quadratic cylinders of $1.3 \cdot 10^5$ links with comparable statistics, but without giving error bars. Furthermore, the union of these authors extended the notion of multifractality to the scaling of moments of the local density of states near the surface of a system [SGL⁺06]. More pronounced fluctuations are expected in this region, giving rise to a new set of surface multifractal dimensions. Together with an analytical argument as well as numerics in symmetry class C [OSF⁺07a], this lead to the expectation that if deviations from parabolicity are present, they should be more pronounced at the surface. Indeed, in this case $2b_0 = 0.370$ and $2b_1 = 0.042$ was reported in [OSF⁺08]. We will come back to this issue in section 3.3.

We close this section with some remarks on the possible singularities in the spectrum

⁵The boundary conditions are not specified in the paper.

⁶A factor of 8 has been gained by keeping eight critical wavefunctions for each realization of disorder.

$\tau(q)$. In the case of bounded observables like participation ratios or conductances, exact parabolicity cannot hold for arbitrary real q because f is defined in the range $\alpha \in \mathbb{R}_0^+$ and $\alpha = 0$ corresponds to q_c with $\tau'(q_c) = 0$, meaning that for parabolic f we have $\tau(q) = -f(0)$ for $q \geq q_c$. In the case $f(0) < 0$ this behavior is called termination, while for $f(0) = 0$ one speaks of freezing, where in the latter regime the inverse participation ratios (1.38) are constant with respect to system size when $q \geq q_c$. The third possibility is $\lim_{\alpha \rightarrow 0} f(\alpha) = -\infty$, where $\tau(q)$ just increases monotonously. All three cases are summarized in figure 1.9.

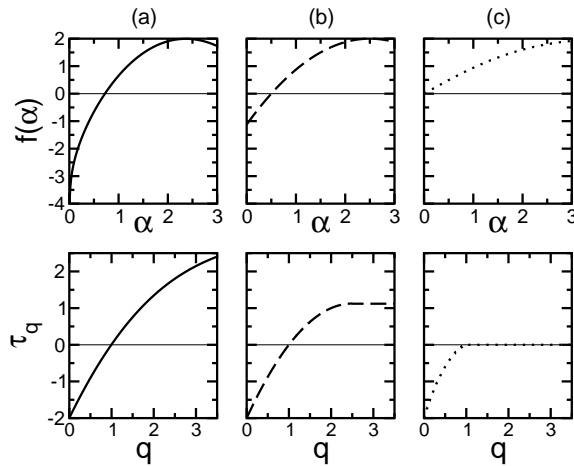


Figure 1.9: Possible behavior of the singularity spectrum (upper row) and the scaling dimension (lower row) for multifractal wavefunctions; no singularity (left), termination (center) and freezing (right). Figure taken from [EM08].

1.6 Conformal invariance

Apart from critical wavefunctions, scale invariance also holds for energy level statistics and the distribution of the two-terminal conductance at criticality, which have not been discussed here. For details, see [KOK05]. The self-similar fixed point theory which describes the phase transition should be invariant under more general transformations than just linear rescaling. At least one expects global translations and rotations to be symmetries, but if the interactions involved are short-ranged, the global symmetries are generally believed to be promoted to local ones. The most general transformation is then conformal, i.e. it leaves the metric invariant up to rescaling by a function or, put differently, preserves angles between tangent vectors of curves. Conformal transformations are quite constrained in arbitrary dimension. By Liouville's theorem the only transformations that are conformal in $d > 2$ are concatenations of translations, similarities, orthogonal transformations and inversions. The situation changes drastically in $d = 2$, where the conformal group becomes infinite-dimensional and contains all holomorphic maps, so it is customary to work in complex coordinates (z, z^*) . A central role is played by scaling operators $\phi(z, z^*)$ which are called primary fields and transform under a conformal

map $z \mapsto w(z), z^* \mapsto w^*(z^*)$ as

$$\phi'(w, w^*) = \left(\frac{dw}{dz}\right)^{-h} \left(\frac{dw^*}{dz^*}\right)^{-h^*} \phi(z, z^*), \quad (1.55)$$

where h and h^* are called the holomorphic resp. antiholomorphic dimension.

Primary fields can be regarded as algebraic objects: The holomorphic generators of conformal transformations are $l_n = -z^{n+1}\partial_z$, $n \in \mathbb{Z}$, which obey

$$[l_n, l_m] = (n - m)l_{n+m}. \quad (1.56)$$

Analogous relations hold in the antiholomorphic case; this is called the Witt algebra. In a conformal quantum field theory, a leading role is played by the Virasoro algebra, which is a central extension of the Witt algebra. The commutation relations are modified according to

$$[L_n, L_m] = (n - m)L_{n+m} + \frac{c}{12}n(n^2 - 1)\delta_{n+m,0}. \quad (1.57)$$

Here, L_n are the modes of the stress-energy tensor, which is related to the change of correlations functions under diffeomorphisms of the Riemann surface on which the theory is defined. c is the so-called central charge. Primaries are highest weights with respect to the Virasoro algebra, which means $L_n\phi = 0$ for $n > 0$ and $L_0\phi = h\phi$. Two- and three-point functions of such fields are severely constrained by the transformation property (1.55). A combined rotation and scaling, $z \mapsto \lambda w = \lambda e^{i\theta}z$, gives

$$\langle \phi(w_1, w_1^*)\phi(w_2, w_2^*) \rangle = \lambda^{-2\Delta} e^{-2si\theta} \langle \phi(z_1, z_1^*)\phi(z_2, z_2^*) \rangle, \quad (1.58)$$

where $\Delta = h + h^*$ is the usual scaling dimension and $s = h - h^*$ is called the spin—to be distinguished from quantum mechanical spin. Here, we will only be concerned with the case of spinless fields, so from now on we only consider $h = h^*$. By rotational and translational invariance, the two-point function can only depend on the distance $z_{12} := |z_1 - z_2|$ and, by the behavior under rescaling, has to be proportional to $z_{12}^{-2\Delta}$. Furthermore, if we consider two primary fields, the correlator has to be invariant under a transposition of the coordinates z_1 and z_2 . On the other hand, the prefactors in the transformation (1.55) will be affected by this change, so the correlator can only be nonvanishing for two primary fields of the same conformal dimension. We thus have

$$\langle \phi_1(z_1, z_1^*)\phi_2(z_2, z_2^*) \rangle = \frac{C_{12}}{z_{12}^{2\Delta}}. \quad (1.59)$$

When we write such an equation we have a continuum field theory in mind. Superimposing a lattice with lattice constant a over the domain on which the fields live, correlators of this type can be interpreted as limits

$$\lim_{a \rightarrow 0} a^{-2\Delta} \langle \phi_1^{\text{lat}}(\mathbf{r}_1)\phi_2^{\text{lat}}(\mathbf{r}_2) \rangle \quad (1.60)$$

of correlators of local lattice fields ϕ_i^{lat} . The dimension Δ is exactly such that this continuum limit makes sense [C08].

In a similar fashion as before, three-point functions can be fixed up to normalization as

$$\langle \phi_1(z_1, z_1^*) \phi_2(z_2, z_2^*) \phi_3(z_3, z_3^*) \rangle = \frac{C_{123}}{z_{12}^{\Delta_1 + \Delta_2 - \Delta_3} z_{13}^{\Delta_1 + \Delta_3 - \Delta_2} z_{23}^{\Delta_2 + \Delta_3 - \Delta_1}}. \quad (1.61)$$

Both of these results continue to hold in dimensions $d > 2$, since only global conformal transformations are needed to derive them. For our purposes a particularly useful feature of $d = 2$ is given by the fact that subsets of the full complex plane may be mapped to geometries which are convenient from the viewpoint of numerical simulations, the most well-known example being the cylinder. Let us consider the mapping

$$w : \mathbb{C} - \{0\} \rightarrow \left\{ z \in \mathbb{C} \mid -\frac{W}{2} \leq \Im(z) \leq \frac{W}{2} \right\}, \quad z \mapsto w(z) = \frac{W}{2\pi} \ln z \quad (1.62)$$

from the punctured complex plane to a strip of vertical width W with periodic boundary conditions, which is thus effectively an infinitely long cylinder of circumference W , see figure 1.10. The two-point functions of two primary fields with the

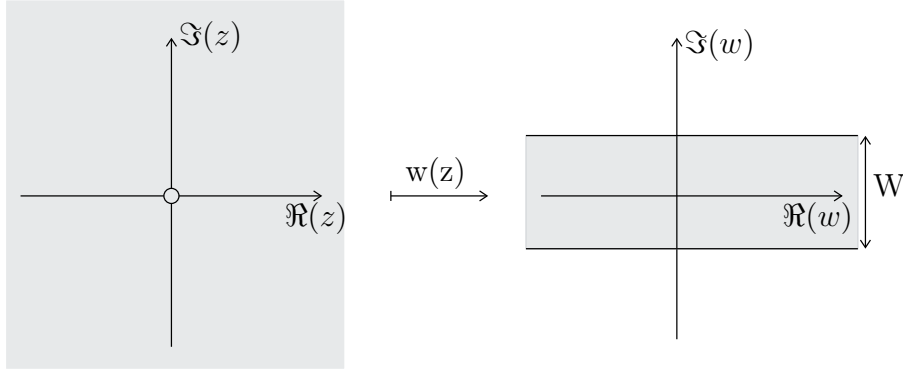


Figure 1.10: Mapping from the infinite punctured plane to the strip with periodic boundary conditions in the vertical direction.

same conformal dimension h transform as

$$\langle \phi(w_1, w_1^*) \phi(w_2, w_2^*) \rangle = \left| \frac{W}{\pi} \sinh \left(\frac{\pi}{W} w_{12} \right) \right|^{-2\Delta}, \quad (1.63)$$

where $w_{12} = w_1 - w_2$. In appendix A we utilize this machinery to give an expression for the two-point functions on the rectangle which uses the notion of boundary conformal field theories [C04]. As we will see, the resulting two-point functions become much more peculiar than in the case of a long cylinder, which reduces to exponential decay with length scale $\xi_W = \frac{W}{2\pi\Delta}$ at distances $w_{12} \gg W$. The objective is thus to find observables which correspond to two-point functions, study these in different geometries and check whether the decay matches the prediction from conformal field theory—if it does, this provides strong evidence in support of conformal symmetry at the critical point because of the non-trivial transformation properties.

1.7 Point-contact conductances

From a theoretical point of view, point-contact conductances are natural observables to consider: ohmic contacts are attached at distant points of a sample and the conductance between two of them is measured. In the Chalker-Coddington model, this setup translates to the following construction: A set of links $\{\mathbf{c}_1, \dots, \mathbf{c}_n\}$ is severed, which effectively makes for n incoming and n outgoing links. One unit of probability flux is injected into the incoming links, the application of U evolves the discrete time by one unit and the procedure is iterated. The outgoing links serve as drains for probability flux, i.e. wavefunction amplitude that is scattered into one of the selected links is removed from the network. The wavefunction at time $t + 1$ can thus be calculated from the wavefunction at time t by the following procedure:

$$|\psi(t + 1)\rangle = U \left(Q |\psi(t)\rangle + \sum_{l=1}^n a_l |\mathbf{c}_l\rangle \right) . \quad (1.64)$$

$|\mathbf{c}_l\rangle$ denotes the unit vector corresponding the link at position \mathbf{c}_l and $\sum_{l=1}^n |a_l|^2 = 1$ and $Q = 1 - \sum_{l=1}^n |\mathbf{c}_l\rangle \langle \mathbf{c}_l|$ is a projection operator that implements the draining action of the outgoing links. We then consider stationary states (in the sense defined above) of this open-network dynamics, $|\psi(t + 1)\rangle = |\psi(t)\rangle$, and refer to them as scattering states. In the presence of n point contacts a basis of the space of scattering states is then furnished by

$$|\psi_k\rangle = U(1 - QU)^{-1} |\mathbf{c}_k\rangle . \quad (1.65)$$

This is derived from (1.64) by letting $a_l = \delta_{lk}$ and solving the stationarity condition. The physical interpretation of $|\psi_k\rangle$ is simply that probability flux is injected only into the link at \mathbf{c}_k . Notice that the presence of the contacts, embodied in Q , introduces a unitary deficit in the time evolution, so that the inverse $(1 - QU)^{-1}$ exists. With respect to the closed-network time evolution operator U , the scattering states are almost stationary. Strictly speaking, the state defined by (1.65) is an element of the closed-network Hilbert space \mathcal{H} , so $\langle \mathbf{c}_k | \psi_k \rangle$ is the probability flux which is supposed to leave the open system after each time step. Applying U to $|\psi_k\rangle$, this amplitude is then scattered into the two links which usually receive a contribution from the contact, but the amplitudes on all the other links stay constant by the stationarity condition. If only one contact is present, we have $\langle \mathbf{c}_1 | \psi_1 \rangle = e^{i\phi}$ by unitarity, so $|\psi_1\rangle$ is (literally) a stationary state for the closed network where the random phase $e^{i\phi_1}$ on the link corresponding to the contact is redefined as $e^{i(\phi_1 - \phi)}$. The set of scattering states is tailor-made to define a scattering matrix $S = (S_{jk})$ with matrix elements $S_{jk} = \langle \mathbf{c}_j | \psi_k \rangle$ which formally relates incoming to outgoing states. In the case $n = 2$, the Landauer-Büttiker formula states that the two-point contact conductance $T_{\mathbf{c}_1 \mathbf{c}_2}$ between the links $\mathbf{c}_1, \mathbf{c}_2$, measured in units of $\frac{e^2}{h}$, is given by

$$T_{\mathbf{c}_1 \mathbf{c}_2} = |S_{12}|^2 . \quad (1.66)$$

Using S , a further correspondence between open and closed networks can be established. Being a unitary matrix, S has n eigenvalues of unit modulus in the naïve sense. By this we mean column vectors v_j such that $Sv_j = e^{i\phi_j} v_j$, ignoring mo-

mentarily that the vector v_j on the left, viewed as an invariant object, lives in a different space than the one on the right. By the same reasoning as above, the states $\sum_{l=1}^n (v_j)_l |\psi_l\rangle$ are stationary states for the network in which the phases on all links which correspond to the contacts are multiplied by $e^{-i\phi_j}$. The relation between open and closed networks was uncovered by Klesse and Zirnbauer in [KZ01], where it was also shown that

$$2\pi\nu \mathbb{E} \left\{ |\psi(\mathbf{c}_1)|^2 f \left(\frac{|\psi(\mathbf{c}_2)|^2}{|\psi(\mathbf{c}_1)|^2} \right) \right\} = \mathbb{E}\{F(T_{\mathbf{c}_1\mathbf{c}_2})\}. \quad (1.67)$$

The function F is defined as

$$F(x) = \int_0^{2\pi} \frac{d\phi}{2\pi} f(x^{-1}|1 - e^{i\phi}\sqrt{1-x|^2}) \quad (1.68)$$

and ψ is a stationary wavefunction of the closed network. Although this formula is remarkable in its own right, it also had implications for numerical tests involving the two-point contact conductance: Given a stationary state, every pair of links for which the relative position agrees with the relative position of the point contacts can give a statistically independent contribution to the average on the left-hand side, thus greatly enhancing the statistics. Furthermore, since the two-point contact conductance is invariant under a change of l and m , we have

$$\left\langle |\psi(\mathbf{c}_2)|^2 f \left(\frac{|\psi(\mathbf{c}_2)|^2}{|\psi(\mathbf{c}_1)|^2} \right) \right\rangle = \left\langle |\psi(\mathbf{c}_1)|^2 f \left(\frac{|\psi(\mathbf{c}_1)|^2}{|\psi(\mathbf{c}_2)|^2} \right) \right\rangle. \quad (1.69)$$

For the special choice $f(x) = x^q$, the left-hand side can also be transformed into the right hand side by the transformation $q \rightarrow 1 - q$. By our observation that the scattering states are effectively stationary closed-network states as we move away from the contact, we can fix $\psi(\mathbf{c}_1) = 1$ and conclude that the symmetry (1.45) continues to hold at the level of disorder averages of wavefunction amplitudes, i.e.

$$\langle |\psi(\mathbf{c}_2)|^{2q} \rangle = \langle |\psi(\mathbf{c}_2)|^{2(1-q)} \rangle. \quad (1.70)$$

To the best of our knowledge this result has not been known so far.

The Chalker-Coddington network model is known to be related to a supersymmetric vertex model by a duality transformation. This construction will be reviewed thoroughly in the next chapter. The model possesses the Lie supergroup $\mathrm{GL}_{2|2}$ as a global symmetry group and it was shown in [JMZ99] that point contacts translate to vertex model operators which are broad in the sense that they are coherent superpositions of operators which transform irreducibly with respect to a single continuous series of $\mathrm{GL}_{2|2}$. Assuming that these operators are in one-to-one-correspondence with primary fields of a yet unknown conformal field theory which describes the plateau transition of the integer quantum Hall effect, it was derived that the disorder average of the typical two-point contact conductance decays as a pure power,

$$\exp \mathbb{E}\{\ln T_{\mathbf{c}_1\mathbf{c}_2}\} \sim |\mathbf{c}_1 - \mathbf{c}_2|^{-X_{\mathrm{typ}}}. \quad (1.71)$$

In [KZ01], equation (1.67) has been used on long cylinders to show that the decay coincides with the conformal field theory prediction

$$T^{\text{typ}} = \left| \frac{W}{\pi a} \sinh \frac{\pi x}{W} \right|^{-X_{\text{typ}}}, \quad (1.72)$$

where a is a nonuniversal lattice spacing, which strongly supports conformal invariance at the critical point. We reproduced these results as a test for our code, see section 3.2.1. A drawback of this observable comes from the functional equation of the logarithm, which implies that studying typical moments of $T_{c_1 c_2}$ does not yield any information on the fractal dimensions Δ_q apart from its value at $q = 1/2$. On the other hand, a vertex model calculation by [JMZ99] presented in section 2.3 clearly indicates that the two-point contact conductance does not show pure algebraic decay, which gives a major motivation for this thesis.

In the following, we will first construct a family of vertex model operators which are supposed to be lattice approximations to primary fields. We will then give, on the other side of the duality, network model observables some of which turn out to be so simple that it is quite surprising they have not been found earlier just by accident. These will then, as we already announced, be studied in different geometries to provide further evidence for conformal invariance and to shed some more light on the question of parabolicity.

Chapter 2

Pure Scaling Observables

*Ist das so,
oder ist es vielleicht viel leichter?
Wir sind Helden*

In this chapter we explain the mathematical background of the observables we suggested in our letter [BWZ14]. We start with the passage from the network model to the supersymmetric vertex model. This is done by introducing a supersymmetric Fock space, also called spinor-oscillator module, at every link. With knowledge from Gaussian integration one can immediately understand why both bosons and fermions are needed: we will be interested in calculating the components of scattering states (1.65), which are matrix elements of $U(1 - QU)^{-1}$. Evaluating “two-point functions” in the complex n -dimensional case,

$$\int d(v^\dagger, v) \bar{v}_i v_j e^{-v^\dagger A v} = \pi^n \det(A)^{-1} (A^{-1})_{ji} , \quad (2.1)$$

matrix elements of A^{-1} are generated together with an inverse determinant which would cause trouble when averaging over disorder. This factor can be removed by an additional fermionic Gaussian integral. This is a cornerstone of the supersymmetry approach to disorder.

Anticipating that we do not only have to calculate the matrix elements in (1.65) on their own, but rather moments of their absolute values like in (1.66), we will have to introduce a second, dualized copy of the constructions advertised so far, which goes under the names “negatively charged” or “advanced” particles. The factorization property (1.12) of the time evolution operator in the network model carries over to the supersymmetric setting. However, in the latter picture the disorder average can be computed easily by projection onto the zero-charge subspace of the large Fock space, which turns out to be an irreducible representation of the Lie superalgebra $\mathfrak{gl}_{2|2}$. From a mathematical perspective this is an instance of Howe duality [H89]. We then turn to the general case, where the link space \mathbb{C} is replaced by $\mathbb{C}^n \otimes \mathbb{C}$, which could be interpreted as introducing n replicas resp. flavors for each link. The construction outlined above also works in this case, with the modification that the relevant Lie superalgebra is now $\mathfrak{gl}_{2n|2n}$. This enhancement makes room for more

complex observables.

The objects which we suggest on symmetry grounds as lattice versions of conformal primary fields are highest weight vectors for the action of $\mathfrak{gl}_{2n|2n}$. In the case $n = 1$ these correspond to moments of the local wavefunction amplitudes of the scattering state (1.65). In our letter [BWZ14], we predicted algebraic decay with the distance between contact \mathbf{c} and observation link \mathbf{r} in the infinite plane network:

$$\mathbb{E}\{|\psi(\mathbf{r})|^{2q}\} \sim |\mathbf{r} - \mathbf{c}|^{-2\Delta_q} . \quad (2.2)$$

The general result was as follows. Consider a set of nearby links $R = \{\mathbf{r}_1, \dots, \mathbf{r}_n\}$ in the network model for the purpose of (non-invasive) observation, and define for $i, j, m = 1, \dots, n$:

$$A_m = \text{Det } K^{(m)} , \quad K_{ij} = \sum_{k=1}^n \psi_k(\mathbf{r}_i) \overline{\psi_k(\mathbf{r}_j)} , \quad (2.3)$$

where $K^{(m)}$ denotes the upper-left $m \times m$ sub-matrix of K . The contacts used to define the basis scattering states lie also nearby in a region C which is distant from R . Suppose now that coarse graining of the lattice takes the contact and observation regions (C and R) to single points, i.e. $\mathbf{r}_i \rightarrow \mathbf{r}$ and $\mathbf{c}_i \rightarrow \mathbf{c}$ for all i , while \mathbf{r} and \mathbf{c} remain distinct. Denoting disorder averages by $\mathbb{E}\{\dots\}$ and CFT correlators as $\langle \dots \rangle$, we then claim that

$$\mathbb{E} \left\{ \left(A_1^{q_1 - q_2} A_2^{q_2 - q_3} \dots A_n^{q_n} \right) (R, C) \right\} = a^{2\Delta_{q_1 \dots q_n}} \langle \tilde{\varphi}_{q_1 \dots q_n}(\mathbf{r}) \Pi_0(C) \rangle , \quad (2.4)$$

where q_1, \dots, q_n are complex numbers, $\tilde{\varphi}_{q_1 \dots q_n}$ is a CFT primary field with scaling dimension $\Delta_{q_1 \dots q_n}$, the operator $\Pi_0(C)$ represents the contacts, and a is the non-universal scale parameter of the network. The operators $\varphi_{q_1 \dots q_n}$ we construct in this chapter are conjectured to be lattice discretizations of the primary fields $\tilde{\varphi}_{q_1 \dots q_n}$. Even though $\Pi_0(C)$ is not a pure scaling field, it here contributes a definite scaling dimension $\Delta_{q_1 \dots q_n}$ due to the orthogonality principle for two-point functions. For an infinite planar network we predict that the observable in (2.4) depends on the distance between the contact and observation regions as a pure power $|\mathbf{r} - \mathbf{c}|^{-\Delta_{q_1 \dots q_n}}$. The observables on the left-hand side of (2.4) are the open-network analogues of the ones constructed in [GMZ13] in the context of nonlinear sigma models for the Anderson transition.

Furthermore, we calculate the eigenvalues of Casimir invariants on the irreducible representations into which the highest weight operators $\varphi_{q_1 \dots q_n}$ fall, since the scaling dimensions $\Delta_{q_1 \dots q_n}$ are linear combinations of these eigenvalues on symmetry grounds. We then close this chapter by offering a larger perspective on the conceptual origin of the observables presented here.

The full basis-invariant backbone of the algebraic constructions presented in the preparatory section can be found in [CFZ05], which we adapt to our situation. Here, each link contributes a summand \mathbb{C} to the Hilbert space of the network model. For each of these link Hilbert spaces we choose the obvious basis $1 \in \mathbb{C}$ and work with fermionic and bosonic creation and annihilation operators on the corresponding Fock space.

2.1 Preparations

2.1.1 Fermionic Fock space

We begin with some preparations and discuss group representations on exterior and symmetric powers of complex vector spaces. The necessity comes from the fact that, given a Hilbert space \mathcal{H} of dimension d , fermionic Fock space $\wedge(\mathcal{H})$ is given by the direct sum of all exterior powers of \mathcal{H} ,

$$\wedge\mathcal{H} = \bigoplus_{k=0}^{\infty} \wedge^k \mathcal{H}, \quad (2.5)$$

which is graded by k . Notice that for a d -dimensional Hilbert space the direct sum on the right-hand side contains only $d + 1$ terms, since $\wedge^k \mathcal{H} = 0$ for all $k > d$. The element $|0\rangle := 1 \in \wedge^0 \mathcal{H} = \mathbb{C}$ is commonly called the vacuum state. Once an orthonormal basis $\{e_j\}$ of \mathcal{H} has been chosen, it is possible to define corresponding particle creation and annihilation operators f_i^\dagger and f_j . The f_j annihilate the vacuum, $f_j |0\rangle = 0$ for all j . Furthermore, they obey the Clifford algebra or canonical anticommutation relations (CAR)

$$\{f_i, f_j^\dagger\} = \delta_{ij}, \quad \{f_i, f_j\} = \{f_i^\dagger, f_j^\dagger\} = 0. \quad (2.6)$$

The Hilbert space scalar product $\langle \cdot, \cdot \rangle$ naturally induces a scalar product on Fock space such that the states

$$(f_1^\dagger)^{n_1} (f_2^\dagger)^{n_2} \dots (f_d^\dagger)^{n_d} |0\rangle \quad (2.7)$$

for $n_l \in \{0, 1\}$ form an orthonormal basis of $\wedge\mathcal{H}$. This justifies the notation f_i^\dagger , i.e. this operator is the adjoint operator of f_i with respect to the Fock space scalar product. The fully occupied state $f_1^\dagger \dots f_d^\dagger |0\rangle$ is then dual to the state $\langle \Omega| := \langle 0| f_d \dots f_1$, and the mapping τ defined as extension of

$$|0\rangle \mapsto \langle \Omega|, \quad f_j^\dagger |0\rangle \mapsto \langle \Omega| f_j \quad (2.8)$$

is called particle-hole transformation. This mapping is well-known in physics from the stable second quantization of the Dirac field.

2.1.2 Bosonic Fock space

An analogous construction can be made on the bosonic side, where bosonic Fock space is defined as the symmetric algebra of \mathcal{H} ,

$$S\mathcal{H} = \bigoplus_{k=0}^{\infty} S^k \mathcal{H}, \quad (2.9)$$

differing from fermionic Fock space by the fact that this direct sum is always infinite. Again, $|0\rangle := 1 \in S^0 \mathcal{H} = \mathbb{C}$ is the vacuum state and there are creation and annihilation operator b_i^\dagger and b_j which obey the Weyl algebra or canonical commutation

relations (CCR)

$$[b_i, b_j^\dagger] = \delta_{ij}, \quad [b_i, b_j] = [b_i^\dagger, b_j^\dagger] = 0. \quad (2.10)$$

They are also adjoint with respect to the induced Fock space scalar product and an orthonormal basis of $S\mathcal{H}$ is given by $(n_l \in \mathbb{N}_0)$

$$(b_1^\dagger)^{n_1} (b_2^\dagger)^{n_2} \dots (b_l^\dagger)^{n_l} \dots |0\rangle. \quad (2.11)$$

2.1.3 Representations and character formulas

2.1.3.1 Fermionic Fock space

Now, let $\text{GL}(\mathcal{H})$ be the group of complex linear invertible transformations of \mathcal{H} , which acts on \mathcal{H} by its fundamental representation $\rho_+^{1,F} : g \mapsto gv$ for $g \in \text{GL}(\mathcal{H})$ and $v \in \mathcal{H}$. The first superscript refers to the degree and F to fermions, while the subscript $+$ indicates that this construction is related to what has been called "retarded" or "positively charged particles" in the literature, to be distinguished from the dualized case later on. For this part it is most convenient to formulate the action of group elements on the Fock spaces in an invariant manner. $\rho_+^{1,F}$ induces a representation $\rho_+^{k,F} : \text{GL}(\mathcal{H}) \rightarrow \text{GL}(\wedge^k \mathcal{H})$ by letting g act on each constituent of an exterior product of degree k ,

$$\rho_+^{k,F}(g)(v_1 \wedge \dots \wedge v_k) = gv_1 \wedge \dots \wedge gv_k, \quad (2.12)$$

and thus the direct sum of these is a representation on Fock space $\wedge \mathcal{H}$ which we denote by ρ_+^F . It has the property that the alternating sum of its characters is a determinant,

$$\sum_{k=0}^d (-1)^k \text{Tr} \rho_+^{k,F}(g) = \text{Det}(\text{Id} - g). \quad (2.13)$$

This can be seen by first considering a diagonalizable g with eigenvalues $\{\lambda_1, \dots, \lambda_d\}$: The action of $\rho_+^F(g)$ on a product of eigenvectors of g is

$$\rho_+^F(g)(v_{i_1} \wedge \dots \wedge v_{i_k}) = \lambda_{i_1} \dots \lambda_{i_k} v_{i_1} \wedge \dots \wedge v_{i_k}. \quad (2.14)$$

The right-hand side can be rewritten as

$$\prod_{i=1}^d (1 - \lambda_i) = \sum_{k=0}^d (-1)^k \sum_{1 \leq i_1 < \dots < i_k \leq d} \lambda_{i_1} \dots \lambda_{i_k} \quad (2.15)$$

which proves the assertion. A general $g \in \text{GL}(\mathcal{H})$ can be Jordan decomposed into a diagonalizable and a nilpotent part the latter of which does not contribute.

Since $\wedge \mathcal{H} = \wedge^{\text{odd}} \mathcal{H} \oplus \wedge^{\text{even}} \mathcal{H}$ is a \mathbb{Z}_2 -graded vector space, the left-hand side of (2.13) coincides with the supertrace $\text{STr}_{\wedge \mathcal{H}} := \text{Tr}_{\wedge^{\text{even}} \mathcal{H}} - \text{Tr}_{\wedge^{\text{odd}} \mathcal{H}}$ so that we have

$$\text{STr}_{\wedge \mathcal{H}} \rho_+^F(g) = \text{Det}(\text{Id} - g). \quad (2.16)$$

On the other hand, a transformation $g \in \text{GL}(\mathcal{H})$ acts on the dual space \mathcal{H}^* as $g\phi := \phi \circ g^{-1}$ by demanding that the pairing between vectors and linear forms

is invariant. We want the representations $\rho_-^{k,F}$ of $\text{GL}(\mathcal{H})$ on $\wedge^k \mathcal{H}^*$ to contain an additional determinant factor,

$$\rho_-^{k,F}(g)(\phi_1 \wedge \cdots \wedge \phi_k) = \text{Det}(g)(\phi_1 \circ g^{-1}) \wedge \cdots \wedge (\phi_k \circ g^{-1}). \quad (2.17)$$

The reason for this choice is that in top dimension $\rho_-^{d,F}$ reduces to the trivial representation, since the space $\wedge^d \mathcal{H}^*$ is one dimensional. Any invertible mapping g acting on a non-trivial element in this space gives, by extension of the usual dual action, just a rescaling by $\text{Det}(g^{-1})$. As we will see shortly, ρ_+^F and ρ_-^F are isomorphic by the particle-hole transformation τ . For odd d even and odd subspaces are interchanged by τ and (2.16) becomes

$$\text{STr}_{\wedge \mathcal{H}^*} \rho_-^F(g) = \text{Det}(g - \text{Id}). \quad (2.18)$$

We now discuss how the constructed representations look when expressed in the usual second-quantized language, which is most conveniently done on the infinitesimal level. For this we fix an orthonormal basis $\{e_1, \dots, e_n\}$ in \mathcal{H} . The Lie algebra $\mathfrak{gl}(\mathcal{H})$ of $\text{GL}(\mathcal{H})$ is just $\text{End}(\mathcal{H})$, so that with respect to the chosen basis each element $X \in \mathfrak{gl}(\mathcal{H})$ has a matrix representation (X_{ij}) . This can be used to define the second-quantized operators

$$X \mapsto \sum_{i,j} f_{+i}^\dagger X_{ij} f_{+j}, \quad X \mapsto \sum_{i,j} f_{-i} X_{ij} f_{-j}^\dagger \quad (2.19)$$

which define Lie algebra representations on $\wedge \mathcal{H}$ and $\wedge \mathcal{H}^*$ respectively. We will now show that both of them come from linearizing ρ_\pm^F at the identity, i.e.

$$(\rho_+^F)_*(X) := \frac{d}{dt} \rho_+^F(e^{tX})|_{t=0} = \sum_{i,j} f_{+i}^\dagger X_{ij} f_{+j} \quad (2.20)$$

and

$$(\rho_-^F)_*(X) := \frac{d}{dt} \rho_-^F(e^{tX})|_{t=0} = \sum_{i,j} f_{-i} X_{ij} f_{-j}^\dagger. \quad (2.21)$$

To this end we notice that both of them are derivations of exterior algebras by the definition of the creation and annihilation operators. It is thus sufficient to show that they agree in degree $k = 1$ with the linearization of $\rho_\pm^{1,F}$. On $\mathcal{H} = \wedge^1 \mathcal{H}$ the infinitesimal action of $\rho_+^{1,F}(e^{tX})$ is by applying X to $v \in \mathcal{H}$. On a single particle state $v = \sum_l a_l f_{+l}^\dagger |0\rangle$ we have

$$\begin{aligned} \left(\sum_{i,j} f_{+i}^\dagger X_{ij} f_{+j} \right) v &= \sum_{i,j,l} a_l f_{+i}^\dagger X_{ij} f_{+j} f_{+l}^\dagger |0\rangle \\ &= \sum_{i,j,l} a_l f_{+i}^\dagger X_{ij} (\delta_{jl} - f_{+l}^\dagger f_{+j}) |0\rangle \\ &= \sum_i \left(\sum_j X_{ij} a_j \right) f_i^\dagger |0\rangle \end{aligned} \quad (2.22)$$

by CAR. In the dual case, by using $\text{Det}(e^{tX}) = e^{t\text{Tr}(X)}$ and the product rule, the linearization of $\rho_-^{1,F}(e^{tX})$ reads

$$\frac{d}{dt}\rho_-^{1,F}(e^{tX})|_{t=0} = \text{Tr}(X) - X^T. \quad (2.23)$$

On single hole states $\phi = \sum_l a_l \langle 0| f_l$, this coincides with the action of X by noting

$$\sum_{i,j} f_{-i} X_{ij} f_{-j}^\dagger = \sum_i X_{ii} - \sum_{i,j} f_{-j}^\dagger (X^T)_{ji} f_{-i}. \quad (2.24)$$

In summary, we have obtained the relations

$$\rho_+^F(e^X) = e^{f_{+i}^\dagger X_{ij} f_{+j}}, \quad \rho_-^F(e^X) = e^{f_{-i} X_{ij} f_{-j}^\dagger}. \quad (2.25)$$

2.1.3.2 Bosonic Fock space

We proceed with an analogous development on the bosonic side. Denoting the symmetric product by \vee , the representation ρ_+^B literally works as on the fermionic side,

$$\rho_+^{k,B}(g)(v_1 \vee \cdots \vee v_k) = gv_1 \vee \cdots \vee gv_k. \quad (2.26)$$

A minor complication arises from the fact that the direct sum $S\mathcal{H} = \bigoplus_{k=0}^{\infty} S^k \mathcal{H}$ is infinite. The sum of characters does not exist for all $g \in \text{GL}(\mathcal{H})$, so the domain has to be restricted to the semigroup of contractions,

$$\text{GL}^<(\mathcal{H}) = \{T \in \text{GL}(\mathcal{H}) \mid \langle Tv|Tv \rangle < \langle v|v \rangle\}. \quad (2.27)$$

We remark that this restriction is not in conflict with our goal of expressing components of stationary scattering states (1.65), since the operator QU used in their definition is a contraction. For any diagonalizable $T \in \text{GL}^<(\mathcal{H})$ any eigenvalue obviously has absolute value less than 1. By the same reasoning as around equation (2.13), we have

$$\text{Tr} \rho_+^{k,B}(g) = \sum_{i_1=0}^{\infty} \cdots \sum_{i_d=0}^{\infty} \lambda_1^{i_1} \cdots \lambda_d^{i_d} = \prod_{i=1}^d (1 - \lambda_i)^{-1}, \quad (2.28)$$

where the second equality comes from the summation formula of the geometric series together with $|\lambda_i| < 1$. This leads, again by Jordan decomposition, to the general formula for $g \in \text{GL}^<(\mathcal{H})$,

$$\text{Tr}_{S\mathcal{H}} \rho_+^B(g) = \text{Det}^{-1}(\text{Id} - g). \quad (2.29)$$

On $S\mathcal{H}^*$ we use the representation ρ_-^B defined in degree k as

$$\rho_-^{k,B}(g)(\phi_1 \vee \cdots \vee \phi_k) = \text{Det}^{-1}(g)(\phi_1 \circ g^{-1}) \vee \cdots \vee (\phi_k \circ g^{-1}). \quad (2.30)$$

As opposed to the fermionic side, the representations ρ_{\pm}^B are not isomorphic—this can be understood heuristically from the fact that there is no such thing as a fully occupied bosonic state, so the trivial representation is not contained in ρ_-^B . Furthermore,

the character is now only defined on anti-contractions

$$\mathrm{GL}^>(\mathcal{H}) = \{T \in \mathrm{GL}(\mathcal{H}) \mid \langle Tv|Tv \rangle > \langle v|v \rangle\} \quad (2.31)$$

and we have

$$\mathrm{Tr}_{S\mathcal{H}^*} \rho_-^B(g) = \mathrm{Det}^{-1}(g - \mathrm{Id}) . \quad (2.32)$$

Finally, at the Lie algebra level, $X \in \mathfrak{gl}(\mathcal{H})$ second-quantizes as

$$X \mapsto \sum_{i,j} b_{+i}^\dagger X_{ij} b_{+j} , \quad X \mapsto - \sum_{i,j} b_{-i} X_{ij} b_{-j}^\dagger , \quad (2.33)$$

which can be summarized by

$$\rho_+^B(e^X) = e^{b_{+i}^\dagger X_{ij} b_{+j}} , \quad \rho_-^B(e^X) = e^{-b_{-i} X_{ij} b_{-j}^\dagger} . \quad (2.34)$$

However, it is important to remark that the first formula holds for $\Re(X) < 0$, while the second one is true for $\Re(X) > 0$, relating to contractions and anti-contractions respectively. The minus sign in the second formula comes from the CCR.

2.1.4 Two-point functions and matrix elements

The analogues to bosonic two-point functions with respect to a quadratic action are in our case for arbitrary i, j

$$\begin{aligned} \langle b_{+i}^\dagger b_{+j} \rangle_{S\mathcal{H}} &:= \mathrm{Tr}_{S\mathcal{H}} \left(b_{+i}^\dagger b_{+j} \rho_+^B(T) \right) \\ &= \mathrm{Det}^{-1}(1 - T) \langle j | T (1 - T)^{-1} | i \rangle \\ \langle b_{-i} b_{-j}^\dagger \rangle_{S\mathcal{H}^*} &:= \mathrm{Tr}_{S\mathcal{H}^*} \left(b_{-i} b_{-j}^\dagger \rho_-^B(T) \right) \\ &= \mathrm{Det}^{-1}(T - 1) \langle j | (1 - T^{-1})^{-1} | i \rangle . \end{aligned} \quad (2.35)$$

We will give a proof of the positive charge relation, the negative one follows in the same fashion. We use the formal notation $b_+^\dagger X b_+ := \sum_{i,j} b_{+i}^\dagger X_{ij} b_{+j}$, write 1 for the unity matrix and let $E_{ij} = |i\rangle \langle j|$ be the ij th elementary matrix. Notice that E_{ij} squares to zero if $i \neq j$ while $E_{ii}^2 = E_{ii}$, so

$$e^{tE_{ij}} = \begin{cases} 1 + tE_{ij} & \text{if } i \neq j; \\ 1 + (e^t - 1)E_{ii} & \text{if } i = j. \end{cases} \quad (2.36)$$

In the following calculation we assume $i \neq j$:

$$\begin{aligned} \mathrm{Tr}_{S\mathcal{H}} \left(\rho_+^B(T) b_{+i}^\dagger b_{+j} \right) &= \mathrm{Tr}_{S\mathcal{H}} \left(\rho_+^B(T) b_{+i}^\dagger E_{ij} b_{+j} \right) \\ &= \frac{d}{dt} \Big|_{t=0} \mathrm{Tr}_{S\mathcal{H}} \left(\rho_+^B(T) e^{tb_{+i}^\dagger E_{ij} b_{+j}} \right) \\ &= \frac{d}{dt} \Big|_{t=0} \mathrm{Det}^{-1}(1 - T e^{tE_{ij}}) \\ &= \frac{d}{dt} \Big|_{t=0} \mathrm{Det}^{-1}((1 - T)(1 - t(1 - T)^{-1} T E_{ij})) \end{aligned}$$

$$\begin{aligned}
&= \text{Det}^{-1}(1-T) \frac{d}{dt} \Big|_{t=0} \exp \text{Tr} \left(\sum_{k=1}^{\infty} \frac{1}{k} t^k \left((1-T)^{-1} T E_{ij} \right)^k \right) \\
&= \text{Det}^{-1}(1-T) \text{Tr} \left((1-T)^{-1} T E_{ij} \right) \\
&= \text{Det}^{-1}(1-T) \langle j | (1-T)^{-1} T | i \rangle .
\end{aligned} \tag{2.37}$$

If we instead consider the case $i = j$ the fourth line has to be replaced by

$$\frac{d}{dt} \Big|_{t=0} \text{Det}^{-1} \left((1-T)(1 - (e^t - 1)(1-T)^{-1} T E_{ii}) \right) \tag{2.38}$$

and again only the first order term $(1-T)^{-1} T E_{ii}$ contributes to the logarithm series.

2.1.5 Supersymmetric Fock space

The four Fock space representations $\rho_{\pm}^{B/F}$ can now be combined to a single one. To this end, we introduce the supersymmetric Fock space

$$\mathcal{F} := \wedge \mathcal{H} \otimes \wedge \mathcal{H}^* \otimes S\mathcal{H} \otimes S\mathcal{H}^* \tag{2.39}$$

together with the representation

$$\rho := \rho_+^F \otimes \rho_-^F \otimes \rho_+^B \otimes \rho_-^B . \tag{2.40}$$

From now on, unless stated otherwise, we use Fock space as synonymous to supersymmetric Fock space. In our situation we will insert a contraction T_+ in the positive charge and an anti-contraction T_- in the negative charge sector, although in principle we are free to insert four different group elements. We denote the average of an operator $A \in \text{End}(\mathcal{F})$ by

$$\langle A \rangle_{\mathcal{F}} = \text{STr}(\rho(T_+, T_-)A) , \tag{2.41}$$

where STr is the supertrace over \mathcal{F} , i.e. the ordinary trace in the bosonic and the supertrace in the fermionic parts. The average of bosonic bilinears is then given by

$$\langle b_{+i}^\dagger b_{+j} \rangle_{\mathcal{F}} = (T(1-T)^{-1})_{ji} \tag{2.42}$$

$$\langle b_{-i}^\dagger b_{-j} \rangle_{\mathcal{F}} = ((1-T^{-1})^{-1})_{ji} , \tag{2.43}$$

where the determinants in (2.35) have been canceled due to the presence of fermions.

2.1.6 Application to the network model

In the network model the draining of probability flux at the contacts is implemented by the operator $Q = 1 - \sum_{l=1}^n |c_l\rangle \langle c_l| =: 1 - P$. Notice that P and Q are orthogonal projectors on complementary subspaces and P is of low rank. We then define the positive charge and negative charge single-particle operators

$$T_{+, \epsilon} = (\epsilon P + Q) U \rho_+^B(T) \quad T_{-, \epsilon}^{-1} = U^{-1} \left(\frac{1}{\epsilon} P + Q \right) . \tag{2.44}$$

In the second quantized language this pair of operators relates to projection onto the Fock space vacuum at the contact links,

$$\pi_0(C) := \sum_{l=1}^n |0_{c_l}\rangle \langle 0_{c_l}| , \quad (2.45)$$

by the following calculation:

$$\begin{aligned} \lim_{\epsilon \rightarrow 0^+} \rho(T_{+, \epsilon}, T_{-, \epsilon}^{-1}) &= \rho(U, U^{-1}) \lim_{\epsilon \rightarrow 0^+} e^{\ln \epsilon \sum_{l=1}^n b_{+, c_l}^\dagger b_{+, c_l} + b_{-, c_l} b_{-, c_l}^\dagger + f_{+, c_l}^\dagger f_{+, c_l} - f_{-, c_l} f_{-, c_l}^\dagger} \\ &= \rho(U, U^{-1}) \pi_0(C) . \end{aligned} \quad (2.46)$$

Let us now consider the case of a single contact, $n = 1$, and introduce the following key objects for an observation link at \mathbf{r} , where we now make use of the spatial structure of the actual network and write the position of the link under investigation as an argument of the operators:

$$\begin{aligned} \mathcal{Z}_q(\mathbf{r}, \mathbf{c}) &= \langle (B_-^\dagger B_-)^q(\mathbf{r}) \pi_0(\mathbf{c}) \rangle_{\mathcal{F}} \\ B_-^\dagger &= b_+^\dagger - e^{i\alpha} b_-, \quad B_- = b_+ - e^{-i\alpha} b_-^\dagger . \end{aligned} \quad (2.47)$$

Here, $e^{i\alpha}$ is any fixed unitary number. B_- and B_-^\dagger commute and B_- does not annihilate any state in Fock space. To see this we consider its action on a general state $|c\rangle = \sum_{m,n} c_{mn} (b_+^\dagger)^m (b_-^\dagger)^n |0\rangle$:

$$\begin{aligned} B_- |c\rangle &= \sum_{m,n} c_{mn} (b_+ - e^{i\alpha} b_-^\dagger) (b_+^\dagger)^m (b_-^\dagger)^n |0\rangle \\ &= \sum_{m,n} c_{mn} \left(m (b_+^\dagger)^{m-1} (b_-^\dagger)^n - e^{i\alpha} (b_+^\dagger)^m (b_-^\dagger)^{n+1} \right) |0\rangle \\ &= \sum_{m,n \geq 1} (m c_{mn} - e^{i\alpha} c_{m+1, n-1}) (b_+^\dagger)^{m-1} (b_-^\dagger)^n |0\rangle \\ &\quad + \sum_{n \geq 0} c_{0n} (b_-^\dagger)^n |0\rangle , \end{aligned} \quad (2.48)$$

from which we see that only for $c_{mn} = 0$ for all m, n the result vanishes. It follows from $\langle v | B_-^\dagger B_- |v\rangle = \|B_- |v\rangle\|^2$ that $B_-^\dagger B_-$ is a strictly positive operator and thus it is meaningful to consider its q th power for any $q \in \mathbb{C}$. Since we consider non-interacting particles, or equivalently, the "action" $\rho(T_+, T_-)$ with respect to which we average is quadratic, we can apply Wick's theorem. Thus for $q \in \mathbb{N}$ we have

$$\mathcal{Z}_q(\mathbf{r}, \mathbf{c}) = q! \mathcal{Z}_1(\mathbf{r}, \mathbf{c})^q , \quad (2.49)$$

which can be continued analytically to $q \in \mathbb{C}$. We now show how $\mathcal{Z}_1(\mathbf{r}, \mathbf{c})$ is related to the scattering state $|\psi\rangle$. To this end, we introduce the operator

$$g := QU(1 - QU)^{-1} + (1 - U^{-1}Q)^{-1} , \quad (2.50)$$

which will appear due to the basic relations (2.42). g is self-adjoint,

$$\begin{aligned}
g &= QU(1 - QU)^{-1} + (1 - U^{-1}Q)^{-1} \\
&= 1 + \sum_{k=1}^{\infty} ((QU)^k + (U^{-1}Q)^k) \\
&= (1 - QU)^{-1} + U^{-1}Q(1 - U^{-1}Q)^{-1} = g^\dagger.
\end{aligned} \tag{2.51}$$

We thus have

$$\begin{aligned}
\mathcal{Z}_1(\mathbf{r}, \mathbf{c}) &= \langle (b_+^\dagger b_+ + b_- b_-^\dagger)(\mathbf{r}) \pi_0(\mathbf{c}) \rangle_{\mathcal{F}} \\
&\stackrel{(2.42)}{=} \langle \mathbf{r} | g | \mathbf{r} \rangle \stackrel{(2.51)}{=} \frac{1}{2} \langle \mathbf{r} | g + g^\dagger | \mathbf{r} \rangle \\
&= \frac{1}{2} \langle \mathbf{r} | (1 + QU)(1 - QU)^{-1} + (1 + QU^\dagger)(1 - QU^\dagger)^{-1} | \mathbf{r} \rangle \\
&= \langle \mathbf{r} | (1 - U^{-1}Q)^{-1} U^{-1} (1 - Q) U (1 - U)^{-1} | \mathbf{r} \rangle \\
&= \langle \mathbf{r} | (1 - U^{-1}Q)^{-1} U^{-1} | \mathbf{c} \rangle \langle \mathbf{c} | U (1 - U)^{-1} | \mathbf{r} \rangle \\
&= |\psi(\mathbf{r})|^2,
\end{aligned} \tag{2.52}$$

where the last step uses the unitary relation between scattering states with incoming-wave and outgoing-wave boundary conditions. The terms with mixed charge indices in $B_+^\dagger B_-$ do not contribute, since $\rho(U)$ does not mix charges. Taking the disorder average is now straightforward, since the time evolution operator of the network decomposes as $U = U_s U_r$ with a diagonal random disorder part

$$U_r = \exp(\text{diag}(i\theta_1, \dots, i\theta_d)). \tag{2.53}$$

We thus have $\rho(U) = \rho(U_s)\rho(U_r)$, where U_r second quantizes as

$$\rho(U_r) = \prod_{\text{links } l} \exp\left(i\theta_l \left(b_+^\dagger b_+(\mathbf{r}_l) + f_+^\dagger f_+(\mathbf{r}_l) - b_-^\dagger b_-(\mathbf{r}_l) - f_-^\dagger f_-(\mathbf{r}_l)\right)\right). \tag{2.54}$$

Therefore, integrating out the random phases projects to the zero charge sector, where the number of positive charge particles equals the number of negative charge particles, on the Fock space attributed to each link *individually*. For any charge-conserving operator $A \in \text{End}(\mathcal{F})$ we thus obtain

$$\mathbb{E}\{\langle A \rangle_{\mathcal{F}}\} = \mathbb{E}\{\text{STr}' A \rho(U_s)\rho(U_r)\} = \text{STr}' A \rho(U_s), \tag{2.55}$$

where STr' is STr restricted to the charge-neutral sector. In this way we arrive at what is called a vertex model \mathcal{V} and denote vertex model averages by

$$\langle A \rangle_{\mathcal{V}} = \text{STr}' A \rho(U_s). \tag{2.56}$$

From a mathematical perspective taking the disorder average should be regarded as a linkwise projection onto the \mathfrak{u}_1 -invariant subspaces V_l , called vertex model module, of the single link supersymmetric Fock spaces

$$\mathcal{F}_l = \wedge \mathbb{C} \otimes \wedge \mathbb{C}^* \otimes S\mathbb{C} \otimes S\mathbb{C}^*. \tag{2.57}$$

There is, at the same time, an action of the Lie superalgebra $\mathfrak{gl}_{2|2}$ on this subspace which commutes with the \mathfrak{u}_1 action.

2.1.7 Lie superalgebras

We briefly digress and recall some basic notions of linear superalgebra. A \mathbb{Z}_2 -graded vector space V over the field $\mathbb{K} = \mathbb{R}$ or \mathbb{C} is a vector space with a direct sum decomposition $V = V_1 \oplus V_0$. In the case $V_1 = \mathbb{K}^p$, $V_0 = \mathbb{K}^q$ one writes $V = \mathbb{K}^{p|q}$. The nonzero elements of V_0 are called even, the ones of V_1 odd, and all elements which are either even or odd are called homogeneous. The grading comes with a parity function $|\cdot|$ which takes the value τ on V_τ . Every $X \in \text{End}(V)$ has a block representation

$$X = \begin{pmatrix} A & B \\ C & D \end{pmatrix}, \quad (2.58)$$

where $A \in \text{End}(V_1)$, $B \in \text{Hom}(V_0, V_1)$, $C \in \text{Hom}(V_1, V_0)$ and $D \in \text{End}(V_0)$. $\text{End}(V)$ is a \mathbb{Z}_2 -graded vector space in the natural way, $\text{End}(V)_0 = \text{End}(V_1) \oplus \text{End}(V_0)$, $\text{End}(V)_1 = \text{Hom}(V_0, V_1) \oplus \text{Hom}(V_1, V_0)$. Thus $\text{End}(V)$ carries a natural bracket operation which is defined for homogeneous elements $X, Y \in \text{End}(V)$ by

$$[X, Y] = XY - (-1)^{|X||Y|} YX. \quad (2.59)$$

The bracket is then linearly extended to non-homogeneous elements in $\text{End}(V)$ and we notice that for $X, Y \in \text{End}(V)_1$ we have $[X, Y] = \{X, Y\}$, while in all other homogeneous cases the bracket coincides with the ordinary commutator. The structure $\mathfrak{gl}(V) := (\text{End}(V), [\cdot, \cdot])$ is then called general linear superalgebra of V . We are primarily interested in the case $V = \mathbb{C}^{p|q}$ and write $\mathfrak{gl}_{p|q}$.

A Cartan subalgebra $\mathfrak{h} \subset \mathfrak{g}$ of a Lie superalgebra is defined as the Cartan subalgebra of the even part of \mathfrak{g} , which consists of arbitrary complex diagonal $n \times n$ -matrices for the case at hand. Concentrating on $\mathfrak{gl}_{2n|2n}$ from now on, we introduce $2n + 2n$ linear functionals

$$\Psi_1, \dots, \Psi_{2n}, \Phi_1, \dots, \Phi_{2n} \in \mathfrak{h}^* \quad (2.60)$$

such that every $H \in \mathfrak{h}$ can be written as

$$H = \text{diag}(\Psi_1(H), \dots, \Psi_{2n}(H), \Phi_1(H), \dots, \Phi_{2n}(H)), \quad (2.61)$$

as a choice of basis for \mathfrak{h}^* . The adjoint action of the Cartan subalgebra on $\mathfrak{gl}_{2n|2n}$,

$$\mathfrak{h} \rightarrow \text{End}(\mathfrak{gl}_{2n|2n}), \quad H \mapsto [H, \cdot] \quad (2.62)$$

can be diagonalized as $[H, X] = \alpha(H)X$, where the (nonzero) functionals α are called roots. The corresponding eigenvectors X are said to span root spaces $\mathfrak{gl}_{2n|2n}^\alpha$. Depending on the parity of the eigenvector, roots are called even or odd. By an elementary calculation we have

$$[E_{ij}, E_{kl}] = \delta_{jk} E_{il} - \delta_{il} E_{kj}, \quad \{E_{ij}, E_{kl}\} = \delta_{jk} E_{il} + \delta_{il} E_{kj}. \quad (2.63)$$

Here, E_{ij} is the elementary matrix which has a 1 on position (i, j) and is zero elsewhere. From this we conclude that the even roots of $\mathfrak{gl}_{2n|2n}$ are $\Psi_k - \Psi_{k'}$ and $\Phi_k -$

$\Phi_{k'}$ for $k \neq k'$. The odd roots are $\Psi_k - \Phi_{k'}$ and $\phi_k - \psi_{k'}$, without restrictions on k, k' . In the standard basis of $\mathbb{C}^{2n|2n}$ corresponding to the block matrix decomposition (2.58) the off-diagonal elementary matrices span the corresponding root spaces. As in the case of classical Lie algebras, the roots come in pairs and we need to fix a set of positive roots Δ^+ in order to define what a highest resp. lowest weight is. To this end, we introduce the following ordering in \mathfrak{h}^* :

$$\Phi_1, \dots, \Phi_n, \Psi_1, \dots, \Psi_{2n}, \Phi_{n+1}, \dots, \Phi_{2n}. \quad (2.64)$$

Any difference $x - y$ of functionals in this sequence is then a positive root if y occurs later than x , e.g. $\Psi_1 - \Phi_{n+1}$. Any choice of positive roots amounts to a Cartan decomposition

$$\mathfrak{gl}_{2n|2n} = \mathfrak{n}^- \oplus \mathfrak{h} \oplus \mathfrak{n}^+, \quad \mathfrak{n}^\pm = \sum_{\alpha \in \Delta^+} \mathfrak{gl}^{\pm\alpha} \quad (2.65)$$

of the Lie superalgebra into its Cartan subalgebra and positive resp. negative root spaces, which enables us to define the notion of highest weights in analogy to the classical case.

With respect to (2.64), the positive root spaces are spanned by strictly upper triangular elementary matrices E_{ij} , $i < j$. One must, however, pay attention to the grading: the *abstract* block decomposition in (2.58) does not carry over naively to this choice of basis. For further convenience in calculations we thus introduce a formal grading vector

$$s = \left(\underbrace{1, \dots, 1}_n, \underbrace{-1, \dots, -1}_{2n}, \underbrace{1, \dots, 1}_n \right), \quad (2.66)$$

so that the root vector E_{ij} has the grade $s_i s_j$. In $\mathfrak{gl}_{2|2}$, elementary matrices thus have the parity to which they correspond in the following scheme, where e stands for even and o stands for odd:

$$\begin{pmatrix} e & o & o & e \\ o & e & e & o \\ o & e & e & o \\ e & o & o & e \end{pmatrix}. \quad (2.67)$$

In contrast, (2.60) corresponds to the choice

$$S = \left(\underbrace{1, \dots, 1}_{2n}, \underbrace{-1, \dots, -1}_{2n} \right). \quad (2.68)$$

Having the charged particle picture in mind, $\mathfrak{gl}_{2n|2n}$ admits a direct sum decomposition

$$\mathfrak{gl}_{2n|2n} = \mathfrak{gl}_{2n|2n}^{(-2)} \oplus \mathfrak{gl}_{2n|2n}^{(0)} \oplus \mathfrak{gl}_{2n|2n}^{(2)}, \quad (2.69)$$

where the central term $\mathfrak{gl}_{2n|2n}^{(0)}$ is a Lie sub-superalgebra,

$$\mathfrak{gl}_{2n|2n}^{(0)} = \mathfrak{gl}_{n|n} \oplus \mathfrak{gl}_{n|n}, \quad (2.70)$$

which, for the choice (2.64), consists of block-diagonal matrices

$$\mathfrak{gl}_{2n|2n}^{(0)} \ni g = \begin{pmatrix} A & 0 \\ 0 & D \end{pmatrix}, \quad A, D \in \mathfrak{gl}_{n|n} \quad (2.71)$$

and we have the inclusion $\mathfrak{gl}_{2n|2n}^{(\pm 2)} \subset \mathfrak{n}^\pm$.

2.2 Single-point observables for $\mathfrak{gl}_{2|2}$

We are now in the position to return to the single link case, where the significance of the decomposition (2.69) will become apparent. Let us define the formal vectors of creation and annihilation operators

$$\bar{c} = \begin{pmatrix} b_+^\dagger & f_+^\dagger & f_- & -b_- \end{pmatrix}, \quad c = \begin{pmatrix} b_+ & f_+ & f_-^\dagger & b_-^\dagger \end{pmatrix}. \quad (2.72)$$

The linear extension of the map

$$\sigma : \mathfrak{gl}_{2|2} \rightarrow \text{End}(V), \quad E_{ab} \mapsto J_{ab} = \bar{c}_a c_b \quad (2.73)$$

is then a Lie superalgebra homomorphism, i.e. σ respects the bracket,

$$\sigma([X, Y]) = [\sigma(X), \sigma(Y)], \quad (2.74)$$

and is compatible with the grading of V . All second quantized operators in the image of σ are charge-conserving bilinears. The upper-left block A in (2.71) acts only on the positive charge sector, whereas D acts on the negative charge sector of V . The other blocks, $\mathfrak{gl}_{2|2}^{(\pm 2)}$, act by two creation resp. two annihilation operators and thus raise resp. lower the particle number by 2 while leaving the total charge invariant. The module V thus has the structure shown in figure 2.1. It is a lowest weight

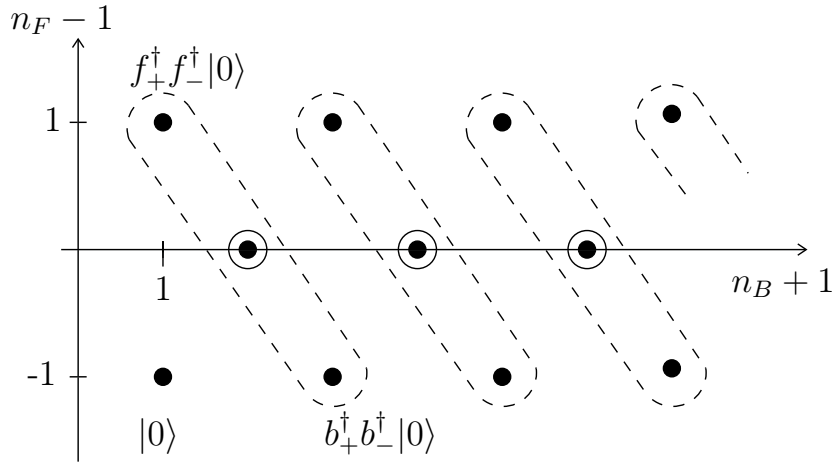


Figure 2.1: Weight diagram of V . n_F/n_B are the numbers of fermions/bosons.

module generated by the action of $\sigma(\mathfrak{gl}_{2|2}^{(2)})$, i.e. by applying the operators $b_+^\dagger f_-^\dagger$, $b_+^\dagger b_-^\dagger$, $f_+^\dagger f_-^\dagger$, $f_+^\dagger b_-^\dagger$ to the Fock space vacuum state $|0\rangle$. The latter lies in V because

it is invariant under the action of \mathfrak{u}_1 specified in (2.54). Furthermore, it is a lowest weight state with respect to our choice of positive roots, i.e. it is annihilated by all Fock space operators which correspond to strictly lower triangular matrices. We remark that there is no fundamental difference between lowest and highest weight representations, but from a physical perspective it seems more natural to regard the "empty" vacuum as the lowest state of the module. From the way how $\mathfrak{gl}_{2|2}$ acts on V it is immediately clear that V contains no $\mathfrak{gl}_{2|2}$ -invariant subspaces and thus it is an irreducible representation.

This module contains some additional structure: For every $n \in \mathbb{N}^+$, a four-dimensional irreducible representation of $\mathfrak{gl}_{2|2}^{(0)}$ with lowest weight $(b_+^\dagger b_-^\dagger)^n |0\rangle$ is contained in V . This is indicated by the diagonal boxes in figure 2.1.

The Lie algebra \mathfrak{su}_2 can be realized in the fermion-fermion sector (which is the central, even block in (2.67)). The vertical pairs of dots at even boson numbers are fundamental representations, while the dots and the circle at odd boson numbers are two trivial representations of SU_2 .

Furthermore, $\mathfrak{su}_{1,1}$ can be realized in the boson-boson sector and every horizontal series of dots resp. circles is an infinite dimensional unitary representation of $SU_{1,1}$ which belongs to the so-called discrete series. We will come back to this point in the next section.

Up to now, the focus was on a single link Fock space \mathcal{F}_l resp. vertex model module V_l . The whole Fock space \mathcal{F} resp. vertex model space \mathcal{V} associated to the Hilbert space of the network model is a tensor product over links,

$$\mathcal{V} = \bigotimes_{\text{links } l} V_l, \quad \mathcal{F} = \bigotimes_{\text{links } l} \mathcal{F}_l. \quad (2.75)$$

Recall that given a group representation $\rho : G \rightarrow GL(V)$ we can form a representation on $V \otimes V$ by letting ρ act on every factor,

$$\begin{aligned} \tilde{\rho} : G &\rightarrow (GL(V) \otimes GL(V) \hookrightarrow GL(V \otimes V)) \\ g &\mapsto \rho(g) \otimes \rho(g). \end{aligned} \quad (2.76)$$

The corresponding Lie algebra representation $\rho_* : \mathfrak{g} \rightarrow \text{End}(V)$ follows from linearizing the former one and using the product rule,

$$\begin{aligned} \tilde{\rho}_* : \mathfrak{g} &\rightarrow (\text{End}(V) \otimes \text{End}(V) \hookrightarrow \text{End}(V \otimes V)) \\ g &\mapsto \rho_*(g) \otimes \text{Id} + \text{Id} \otimes \rho_*(g). \end{aligned} \quad (2.77)$$

The operator $(B_-^\dagger B_-)^q$ which we related to the local wavefunction amplitude has the special significance of being a highest weight of an irreducible $\mathfrak{gl}_{2|2}$ -representation itself. This can be seen as follows. Let us change the basis of generators E_{ab} we used in the representation (2.72) according to

$$\overline{E}_{ab} = U E_{ab} U^{-1}, \quad (2.78)$$

where the transformation on U and its inverse are given by

$$\begin{aligned} U &= \frac{1}{\sqrt{2}} \left(E_{++} \otimes \text{Id}_2 + E_{+-} \otimes \sigma_1 + e^{i\alpha} E_{-+} \otimes \sigma_1 - e^{i\alpha} E_{--} \otimes \text{Id}_2 \right), \\ U^{-1} &= \frac{1}{\sqrt{2}} \left(E_{++} \otimes \text{Id}_2 + e^{-i\alpha} E_{+-} \otimes \sigma_1 + E_{-+} \otimes \sigma_1 - e^{-i\alpha} E_{--} \otimes \text{Id}_2 \right). \end{aligned} \quad (2.79)$$

Notice that U does not correspond to a unitary transformation Fock space, so operators which are adjoint in one representation will not be adjoint in the transformed representation. $E_{\tau\tau'}$ denotes a 2×2 elementary matrix. We thus get the representation

$$\bar{\sigma} : \bar{E}_{ab} \mapsto \bar{J}_{ab} = \bar{C} E_{ab} C, \quad (2.80)$$

where

$$\begin{aligned} \bar{C} &= \bar{c} \cdot U = \frac{1}{\sqrt{2}} \begin{pmatrix} B_-^\dagger & F_+^\dagger & F_-^\dagger & B_+^\dagger \end{pmatrix}, \\ C &= U^{-1} \cdot c = \frac{1}{\sqrt{2}} \begin{pmatrix} B_+ & F_+ & F_- & B_- \end{pmatrix}^T, \end{aligned} \quad (2.81)$$

and

$$\begin{aligned} B_\pm &= b_+ \pm e^{-i\alpha} b_-^\dagger, & B_\pm^\dagger &= b_+^\dagger \pm e^{i\alpha} b_-, \\ F_\pm &= f_+ \pm e^{-i\alpha} f_-^\dagger, & F_\pm^\dagger &= f_+^\dagger \pm e^{i\alpha} f_-. \end{aligned} \quad (2.82)$$

These operators obey the following (anti-)commutation relations:

$$\begin{aligned} \{F^\dagger, F^\dagger\} &= \{F, F\} = \{F^\dagger, F\} = 0, \\ [B^\dagger, B^\dagger] &= [B, B] = [B^\dagger, B] = 0, \\ [B_\pm, B_\mp^\dagger] &= \{F_\pm, F_\mp^\dagger\} = 2. \end{aligned} \quad (2.83)$$

In the first two lines the index is dropped because the charge is irrelevant. Using the upper case operators, the Cartan subalgebra \mathfrak{h} is represented by

$$\begin{aligned} \bar{J}_{11} &= \bar{\sigma}(\bar{E}_{11}) = \frac{1}{2} B_+^\dagger B_-, & \bar{J}_{22} &= \bar{\sigma}(\bar{E}_{22}) = \frac{1}{2} F_-^\dagger F_-, \\ \bar{J}_{33} &= \bar{\sigma}(\bar{E}_{33}) = \frac{1}{2} F_+^\dagger F_+, & \bar{J}_{44} &= \bar{\sigma}(\bar{E}_{44}) = \frac{1}{2} B_-^\dagger B_+. \end{aligned} \quad (2.84)$$

The operator

$$\varphi_q := (B_-^\dagger B_-)^q \in \text{End}(V) \quad (2.85)$$

is a highest weight vector with respect to the adjoint action of $\mathfrak{gl}(2|2)$ on $\text{End}(V)$. It has weight $(q, 0, 0, -q)$, i.e.

$$[\bar{J}, \varphi_q] = \alpha(\bar{J})\varphi_q \text{ for all } \bar{J} \in \bar{\sigma}(\mathfrak{h}) \quad (2.86)$$

with $\alpha = q(\overline{\Phi}_1 - \overline{\Phi}_4)$, $\overline{\Phi}_i \in \mathfrak{h}$ being dual to \overline{E}_{ii} . This can be seen from the calculations

$$\begin{aligned} [\overline{J}_{11}, \varphi_1] &= \varphi_1, & [\overline{J}_{22}, \varphi_1] &= 0, \\ [\overline{J}_{33}, \varphi_1] &= 0, & [\overline{J}_{44}, \varphi_1] &= -\varphi_1, \end{aligned} \quad (2.87)$$

combined with the commutator identity

$$[f(A), B] = f'(A)[A, B] \quad \text{if} \quad [A, [A, B]] = 0. \quad (2.88)$$

It is a highest weight since it is annihilated by all raising operators,

$$[\overline{J}_{ij}, \varphi_1] = 0 \quad \text{for all } i < j. \quad (2.89)$$

2.3 Point contacts and point contact conductances

In the following, we will explain why we expect

$$\mathbb{E}\{\mathcal{Z}_1(\mathbf{r}, \mathbf{c})\} = \langle B_-^\dagger B_-(\mathbf{r})\pi_0(\mathbf{c}) \rangle_{\mathcal{V}} \quad (2.90)$$

to show pure scaling behavior with the distance $|\mathbf{r} - \mathbf{c}|$ between contact and observation link. To this end, we also need to give another perspective on the vacuum projector (2.45) which was employed to establish the connection between vertex and network model observables and its connection with point-contact conductances. Let O be a charge-conserving operator on \mathcal{V} and X an arbitrary element of the global Lie superalgebra, which we can write by the representation (2.77) as $X = \sum_{\text{links } l} X(\mathbf{r}_l)$. The image of the unitary time evolution operator $\rho(U)$ is $\mathfrak{gl}_{2|2}$ -invariant, $[X, \rho(U)] = 0$, and by cyclicity of the supertrace we have the Ward identity

$$\langle [X, O] \rangle_{\mathcal{V}} = 0. \quad (2.91)$$

A point contact is most faithfully modeled by the vertex model operator

$$P(\mathbf{c}) = b_+^\dagger(\mathbf{c})b_-^\dagger(\mathbf{c})|0_{\mathbf{c}}\rangle\langle 0_{\mathbf{c}}| \in \text{End}(V_{\mathbf{c}}). \quad (2.92)$$

We will now use the Ward identity to show that, apart from a constant prefactor, the vacuum projector can be replaced by the point contact operator in

$$\langle \varphi_q(\mathbf{r})\pi_0(\mathbf{c}) \rangle_{\mathcal{V}} \propto \langle \varphi_q(\mathbf{r})P(\mathbf{c}) \rangle_{\mathcal{V}}. \quad (2.93)$$

In the following, let $O = \varphi_q(\mathbf{r})\pi_0(\mathbf{c})$. We first choose $X = \sum_{\mathbf{r}'} \varphi_1(\mathbf{r}')$. From

$$[X, O] = \varphi_q(\mathbf{r})(e^{i\alpha}\pi_0(\mathbf{c})b_+(\mathbf{c})b_-(\mathbf{c}) - e^{-i\alpha}b_+^\dagger(\mathbf{c})b_-^\dagger(\mathbf{c})\pi_0(\mathbf{c})) \quad (2.94)$$

we obtain the identity

$$\langle \varphi_q(\mathbf{r})e^{i\alpha}\pi_0(\mathbf{c})b_+(\mathbf{c})b_-(\mathbf{c}) \rangle_{\mathcal{V}} = \langle \varphi_q(\mathbf{r})e^{-i\alpha}b_+^\dagger(\mathbf{c})b_-^\dagger(\mathbf{c})\pi_0(\mathbf{c}) \rangle_{\mathcal{V}}. \quad (2.95)$$

Now, let $X = \sum_{\mathbf{r}'} (B_-^\dagger B_+)(\mathbf{r}')$. From $[X, \varphi_1(\mathbf{r})] = 2\varphi_1(\mathbf{r})$ we get $[X, \varphi_q(\mathbf{r})] = 2q\varphi_q(\mathbf{r})$. Using the Ward identity again for this choice and combining the result

with (2.95), we arrive at

$$\begin{aligned} \langle \varphi_q(\mathbf{r})\pi_0(\mathbf{c}) \rangle_{\mathcal{V}} &= -\frac{1}{q} e^{-i\alpha} \langle \varphi_q(\mathbf{r})P(\mathbf{c}) \rangle_{\mathcal{V}} \\ &= -\frac{1}{q} e^{i\alpha} \langle \varphi_q(\mathbf{r})P^\dagger(\mathbf{c}) \rangle_{\mathcal{V}} . \end{aligned} \quad (2.96)$$

We are now in a position to explain more precisely what was meant in section 1.7 when we spoke about the broadness of the point contact operator. Positive integer moments of the two-point contact conductance can be expressed as Fock space averages as

$$\begin{aligned} T_{\mathbf{c}_1\mathbf{c}_2}^{\tilde{q}} &= \frac{1}{\tilde{q}!^2} \left\langle |0_{\mathbf{c}_2}\rangle \langle 0_{\mathbf{c}_2}| (b_+(\mathbf{c}_2)b_-(\mathbf{c}_2))^{\tilde{q}} (b_+^\dagger(\mathbf{c}_1)b_-^\dagger(\mathbf{c}_1))^{\tilde{q}} |0_{\mathbf{c}_1}\rangle \langle 0_{\mathbf{c}_1}| \right\rangle_{\mathcal{F}} \\ &=: \left\langle P_{\tilde{q}}^\dagger(\mathbf{c}_2)P_{\tilde{q}}(\mathbf{c}_1) \right\rangle_{\mathcal{F}} , \end{aligned} \quad (2.97)$$

where we used Wick's theorem and the fact that positive- and negative-charge operators commute. The \tilde{q} appearing here has to be distinguished from the index in φ_q .

We now change perspective and regard the point contact operators, being endomorphisms on a vertex model module V , as elements in $V \otimes V^*$. The reduction of this tensor product (or rather of its completion with respect to a hermitean scalar product) was carried out in the context of an antiferromagnetic chain of two super-spins in [Z94], which involves a so-called single continuous series of representation of $\mathrm{GL}_{2|2}$.

The latter object is a Lie supergroup which is, morally speaking, in an analogous relationship with the Lie superalgebra $\mathfrak{gl}_{2|2}$ as it is the case for \mathfrak{su}_N and $\mathrm{SU}(N)$. However, due to the presence of odd parts, naïve exponentiation of the Lie superalgebra is ill-defined. To make sense of such an object, one has to consider a vector bundle E over the base manifold $G \simeq \mathrm{GL}(\mathbb{C}^2) \times \mathrm{GL}(\mathbb{C}^2)$ (which is the Lie group corresponding to the even part $(\mathfrak{gl}_{2|2})_0$) whose fiber over a point is the vector space of G -orbits $\wedge(\mathfrak{gl}_{2|2})_1^*$. $\mathrm{GL}_{2|2}$ is then an algebra of sections of this bundle which carries an action of $\mathfrak{gl}_{2|2}$. Since we do not need the full glory of this global picture and work mainly on the algebraic level, we refrain from giving an extensive overview and remark that a representation of $\mathrm{GL}_{2|2}$ on a graded vector space $V = V_0 \oplus V_1$ is a homomorphism $\rho_* : (\mathfrak{gl}_{2|2})_\tau \rightarrow \mathfrak{gl}(V)_\tau$ together with a compatible homomorphism $\rho : G \rightarrow (\mathrm{GL}(V_0) \times \mathrm{GL}(V_1) \hookrightarrow \mathrm{GL}(V))$ such that $(d\rho)_e = \rho_*|_{(\mathfrak{gl}_{2|2})_0}$.

The representations in the continuous series are of this type and two parameters $\lambda \in \mathbb{R}^+$, $l \in 2\mathbb{N} - 1$ are needed to label them. In the decomposition of $V \otimes V^*$ only $l = 1$ appears, hence one speaks of a *single* continuous series. This comes from the fact that the tensor product of two spin-1/2-representations of SU_2 contains only angular momentum up to 1.

This should be compared to the simplest classical non-compact situation: weight vectors in irreducible unitary representations of $\mathrm{SU}_{1,1}$ are labeled by their weights determined by the action of the subgroup $\mathrm{U}_1 \subset \mathrm{SU}_{1,1}$, which are integer or half-integer depending on the representation, and their Casimir eigenvalues. Since this group arises as the symmetry group of an indefinite bilinear form, the Casimir operator is also indefinite. A simple calculation [BNS65] shows that the negative

eigenvalues can be labeled by an integer. These representations are said to belong to one of the discrete series of $SU_{1,1}$. Positive eigenvalues can belong either to the principal continuous series, labeled by \mathbb{R}^+ , or the complementary series, labeled by the open interval $(-1, 0)$. Together with the trivial representation (being the only unitary finite-dimensional irreducible representation) this list exhausts all unitary irreducible representations of $SU_{1,1}$.

The tensor factor $(b_+^\dagger(\mathbf{c}_1)b_-^\dagger(\mathbf{c}_1))^{\tilde{q}}|0_{\mathbf{c}_1}\rangle$ of the point contact operator $P_{\tilde{q}}$ can be found in the lowest row in figure 2.1 for every $\tilde{q} \in \mathbb{N}_0$. As explained in the last section, these purely bosonic states belong to a discrete series representation of $SU_{1,1}$ sitting in V . Analogous statements are true for the dual module V^* , where figure 2.1 is reflected in the origin. For the combined action of $SU_{1,1}$ on the purely bosonic subspace in $V \otimes V^*$ the point contact operator thus has weight \tilde{q} .

Using the general decomposition of $V \otimes V^*$ from [Z94], the point-contact operator can be decomposed into irreducible representations of $SU_{1,1}$ which belong to the principal continuous series. This calculation was done in [JMZ99], yielding

$$P_{\tilde{q}}^\dagger(\mathbf{c}_1) = \int_{\mathbb{R}^+} \langle V\tilde{q}, V^*0 | \lambda\tilde{q} \rangle \phi_{\lambda\tilde{q}}(\mathbf{c}_1) \mu(\lambda) d\lambda \quad (2.98)$$

$$P_{\tilde{q}}(\mathbf{c}_2) = \int_{\mathbb{R}^+} \langle V0, V^* - \tilde{q} | \lambda - \tilde{q} \rangle \phi_{\lambda-\tilde{q}}(\mathbf{c}_2) \mu(\lambda) d\lambda. \quad (2.99)$$

The first object in the integrand is a Clebsch-Gordan coefficient and $\mu(\lambda)d\lambda$ is the Plancherel measure for the continuous series. $\phi_{\lambda\tilde{q}}$ lies in the irreducible representation of $SU_{1,1}$ with continuous quantum number λ and has discrete weight \tilde{q} . These representations are regarded as subrepresentations of the single continuous series of $GL_{2|2}$ mentioned before. In this sense we can think of the point contact operator as being broad in representation space.

As explained in chapter 1, there is strong evidence that there exists an underlying conformal field theory of the integer quantum Hall transition to which the critical vertex model flows under renormalization. We thus come to the

Central Conjecture: The operators $\phi_{\lambda q}$
are lattice discretizations of conformal primary fields.

Strictly speaking, at this point it would be sufficient to assume that their correlator is of the form

$$\langle \phi_{\lambda q}(\mathbf{c}_1) \phi_{\lambda'-q}(\mathbf{c}_2) \rangle = \frac{\delta(\lambda - \lambda')}{\mu(\lambda)} |\mathbf{c}_1 - \mathbf{c}_2|^{-2\tilde{\Delta}_\lambda} + \dots, \quad (2.100)$$

but we will see that in order to make contact with numerical simulations in the Chalker-Coddington model conformal invariance is needed as well. The dots indicate that in a discretization subleading contributions may be present which vanish in the continuum theory. The presence of the prefactor is necessary to maintain orthonormality of inequivalent irreducible representations of the continuous infinite series appearing in the decomposition of $V \otimes V^*$. The conformal dimensions $\tilde{\Delta}_\lambda$ are related to the multifractal spectrum Δ_q by analytic continuation, $q = \frac{1}{2} + i\lambda$. The

two-point contact conductance is thus given by

$$\mathbb{E}\{T_{\mathbf{c}_1\mathbf{c}_2}^{\tilde{q}}\} = 2 \int_0^\infty |\langle V\tilde{q}, V^*0|\lambda\tilde{q}\rangle|^2 |\mathbf{c}_1 - \mathbf{c}_2|^{-2\tilde{\Delta}_\lambda} \mu(\lambda) d\lambda. \quad (2.101)$$

The Clebsch-Gordan coefficients as well as the measure $\mu(\lambda)$ have been calculated explicitly in [JMZ99]:

$$\mu(\lambda) d\lambda = \lambda \tanh(\pi\lambda) d\lambda \quad (2.102)$$

$$|\langle V\tilde{q}, V^*0|\lambda\tilde{q}\rangle|^2 = \frac{\Gamma(\tilde{q} - \frac{1}{2} - i\lambda)\Gamma(\tilde{q} - \frac{1}{2} + i\lambda)}{\Gamma(\tilde{q})^2}. \quad (2.103)$$

Although the formula has been derived for $\tilde{q} \in \mathbb{N}$, it is possible to continue the result analytically to $\tilde{q} \in \mathbb{R}$. (2.101) remains valid for $\tilde{q} \geq \frac{1}{2}$. A particularly important observation to make is that in the asymptotic limit $r := |\mathbf{c}_1 - \mathbf{c}_2| \rightarrow \infty$ all these moments decay with the same power $\tilde{\Delta}_0$, which we called termination of the spectrum in section 1.5. For $\tilde{q} < \frac{1}{2}$ we must take into account that the integration contour crosses the poles of the numerator at $\lambda = \pm i(\tilde{q} - 1/2)$ and receives a contribution from the residues of the integrand at these points. This leads to

$$\mathbb{E}\{T^{\tilde{q}}\} = \frac{1}{\Gamma^2(\tilde{q})} \left(\int_0^\infty |\Gamma(\tilde{q} - \frac{1}{2} - i\lambda)|^2 r^{-2\tilde{\Delta}_\lambda} \mu(\lambda) d\lambda + 2\pi \cot(\tilde{q}\pi) \Gamma(2\tilde{q}) r^{-2\tilde{\Delta}_{i(\tilde{q}-1/2)}} \right). \quad (2.104)$$

Here, the symmetry property $\tilde{\Delta}_\lambda = \tilde{\Delta}_{-\lambda}$, which follows from $\text{GL}_{2|2}$ -invariance, has been employed. From (2.104) it immediately follows that $\langle T^0 \rangle = r^{-2\tilde{\Delta}_{-i/2}}$, but on the other hand normalization implies $\langle T^0 \rangle = 1$, so that we can infer $\tilde{\Delta}_\lambda = (\lambda^2 + 1/4)F(\lambda^2)$. A priori, no further information about the scaling dimension $\tilde{\Delta}_\lambda$ can be extracted. However, the symmetry puts another strong constraint on it, namely that it has to be the eigenvalue of some linear combination of $\text{GL}_{2|2}$ Casimir invariants, the lowest one being quadratic with eigenvalue $\lambda^2 + 1/4$ on the representations we consider here, which corresponds to a parabolic spectrum of the multifractal dimensions.

The typical two-point contact conductance can be obtained from (2.104) by the identity

$$\left. \frac{d}{dq} \right|_{\tilde{q}=0} \mathbb{E}\{T^{\tilde{q}}\} = \mathbb{E}\{\ln T\}. \quad (2.105)$$

The first term in (2.104) gives no contribution and one has to notice $2\pi \cot(\tilde{q}\pi)\Gamma(2\tilde{q}) = 1 + \mathcal{O}(q^2)$, so the two-point contact conductance shows pure scaling behavior [JMZ99]:

$$\exp \mathbb{E}\{\ln T\} = |\mathbf{c}_1 - \mathbf{c}_2|^{-X_{\text{typ}}}, \quad X_{\text{typ}} = 2F\left(-\frac{1}{4}\right). \quad (2.106)$$

The operators $\varphi_q = (B^\dagger B)^q$ all lie in a representation space V_λ with $q = \frac{1}{2} + i\lambda$, but they do not have definite weight with respect to the subgroup K with Lie superalgebra $\mathfrak{gl}_{1|1} \oplus \mathfrak{gl}_{1|1}$ as $\phi_{\lambda\tilde{q}}$ does. To make contact between these two objects,

one has to average φ_q with respect to K :

$$\phi_{\lambda 0} = \int_K \varphi_{\frac{1}{2}(1+i\lambda)} dk . \quad (2.107)$$

We point out here that the analytic continuation in the parameter λ is, from the viewpoint of mathematics, at this point only a formal calculation, since the corresponding representations are not well understood. The left-hand side rests on firm grounds—a slightly less superficial discussion can be found in section 2.8—while the right-hand side represents uncharted territory so far. But, as we will see as we proceed, the results we produce are perfectly sensible.

Now, by combining φ_q and a vacuum projector in a vertex model average, the properties of the supertrace enforce that only a single contribution in (2.98) survives. This gives the basis for our prediction that the network model observables $\mathbb{E}\{|\psi(\mathbf{r})|^2\}$ in the plane decay as pure powers with the distance from the point contact.

For the rest of this chapter, we will introduce observables of increasing complexity which share with φ_q the property of being highest weight operators and translate them into network model observables. By the same reasoning as before, we also expect these to show pure scaling behavior.

2.4 Multi-point observables for $\mathfrak{gl}_{2|2}$, several contacts

Until now, we discussed observables which could be defined using only a single link of the network model. Let us now broaden the context and consider a set of n links $\mathbf{r}_1, \dots, \mathbf{r}_n$. To simplify the notation, we use summation convention together with upper/lower indices (instead of arguments) on the uppercase operators defined in (2.82):

$$B_{+,j}^\dagger B_+^j := \sum_{j=1}^n (b_+^\dagger(\mathbf{r}_j) - e^{-i\alpha} b_-(\mathbf{r}_j))(b_+(\mathbf{r}_j) - e^{i\alpha} b_-^\dagger(\mathbf{r}_j)) . \quad (2.108)$$

Furthermore, we continue to write \bar{J}_{ab} for the operator coming from the global Lie superalgebra which acts as $\bar{C}_a(\mathbf{r}_j)C_b(\mathbf{r}_j)$ on every link space \mathcal{F}_j ,

$$\bar{J}_{ab} = \sum_{j=1}^n \bar{C}_a(\mathbf{r}_j)C_b(\mathbf{r}_j) . \quad (2.109)$$

It is understood that \bar{J}_{ab} acts as the identity everywhere else. The operator

$$\begin{aligned} \varphi_{q,p} &:= \left(B_{-j}^\dagger B_-^j \right)^{q-p} \left(\left(F_{+j}^\dagger F_-^j \right) \left(B_{-j}^\dagger B_-^j \right) - \left(F_{+j}^\dagger B_-^j \right) \left(B_{-j}^\dagger F_-^j \right) \right)^p \\ &= 2^{q+p} (\bar{J}_{14})^{q-p} (\bar{J}_{23}\bar{J}_{14} - \bar{J}_{24}\bar{J}_{13})^p \\ &= \varphi_{q,0}(\varphi_{0,1})^p \end{aligned} \quad (2.110)$$

is a more general highest weight operator for the action of the Cartan subalgebra and corresponds to the superdeterminant of the upper-right block. The last equality

follows from the fact that both quadrilinears commute. From

$$[\bar{J}_{11}, \varphi_{0,1}] = \varphi_{0,1}, \quad [\bar{J}_{22}, \varphi_{0,1}] = \varphi_{0,1}, \quad (2.111)$$

$$[\bar{J}_{33}, \varphi_{0,1}] = -\varphi_{0,1}, \quad [\bar{J}_{44}, \varphi_{0,1}] = -\varphi_{0,1} \quad (2.112)$$

we infer that $\varphi_{q,p}$ has weight $(q, p, -p, -q)$ and again, this operator is annihilated by the action of all \bar{J}_{ij} for $i < j$. In order to establish a relation between $\varphi_{q,p}$ and network model observables we first notice that (2.52) generalizes to the new situation,

$$\langle B_{-,l}^\dagger B_{-,l}' \pi_0(\mathbf{c}) \rangle_{\mathcal{F}} = \langle F_{+,l}^\dagger F_{-,l}' \pi_0(\mathbf{c}) \rangle_{\mathcal{F}} = \overline{\psi(\mathbf{r}_l)} \psi(\mathbf{r}_l'), \quad (2.113)$$

if the distance between the contact and the observation links is greater than one. If n distinct contacts are present, the last lines in the calculation (2.52) are modified according to

$$\begin{aligned} & \langle \mathbf{r} | (1 - U^{-1}Q)^{-1} U^{-1} (1 - Q) U (1 - U)^{-1} | \mathbf{r}' \rangle \\ &= \langle \mathbf{r} | (1 - U^{-1}Q)^{-1} U^{-1} \left(\sum_{i=1}^n |\mathbf{c}_i\rangle \langle \mathbf{c}_i| \right) U (1 - U)^{-1} | \mathbf{r}' \rangle \\ &= \sum_{i=1}^n \psi_i(\mathbf{r}) \overline{\psi_i(\mathbf{r}')}. \end{aligned} \quad (2.114)$$

For n distinct contacts and observation links we will now show that

$$\langle \varphi_{1,n-1} \pi_0(C) \rangle_{\mathcal{V}} \propto \mathbb{E} \{ A_n \}, \quad (2.115)$$

where A_n is the open-system analogue of one of the antisymmetrized observables introduced in [GMZ13]:

$$A_n = |\text{Det}(\psi_i(\mathbf{r}_j))|^2 \quad 1 \leq i, j \leq n. \quad (2.116)$$

Since operators on different links (anti-)commute, the last (anti-)commutation relation (2.83) is modified according to

$$[B_{\pm i}, B_{\mp}^{j\dagger}] = \{F_{\pm j}, F_{\mp}^{j\dagger}\} = 2\delta_i^j. \quad (2.117)$$

In (2.110), the bilinears in $\varphi_{q,p}$ commute and we have $(F_{+j}^\dagger B_{-}^j)^2 = 0$, so that we can rewrite and expand

$$\begin{aligned} \varphi_{1,n-1} &= \left(F_{+j}^\dagger F_{-}^j \right)^{n-2} \left(\left(F_{+j}^\dagger F_{-}^j \right) \left(B_{-j}^\dagger B_{-}^j \right) - (n-1) \left(F_{+j}^\dagger B_{-}^j \right) \left(B_{-j}^\dagger F_{-}^j \right) \right) \\ &= F_{+i_1}^\dagger F_{-}^{j_1} \delta_{j_1}^{i_1} \dots F_{+i_{n-2}}^\dagger F_{-}^{j_{n-2}} \delta_{j_{n-2}}^{i_{n-2}} \\ &\quad \times F_{+i_{n-1}}^\dagger F_{-}^{j_{n-1}} B_{-i_n}^\dagger B_{-}^{j_n} \left(\delta_{j_{n-1}}^{i_{n-1}} \delta_{j_n}^{i_n} - (n-1) \delta_{j_n}^{i_{n-1}} \delta_{j_{n-1}}^{i_n} \right) \\ &= (-1)^{|(n \ k)|} F_{+i_1}^\dagger F_{-}^{j_1} \dots F_{+i_{n-1}}^\dagger F_{-}^{j_{n-1}} B_{-i_n}^\dagger B_{-}^{j_n} \\ &\quad \times \delta_{j_1}^{i_1} \dots \delta_{j_{k-1}}^{i_{k-1}} \delta_{j_k}^{i_n} \delta_{j_{k+1}}^{i_{k+1}} \dots \delta_{j_{n-1}}^{i_{n-1}} \delta_{j_n}^{i_k}. \end{aligned} \quad (2.118)$$

$|(n\ k)|$ denotes the sign of the transposition of the letters k and n . Due to the anti-commutativity of the fermionic operators we can replace the above sums over the indices i_1, \dots, i_{n-1} and j_1, \dots, j_{n-1} by the anti-symmetrization over these indices. The additional sum over k could be incorporated into the sum over the permutations of S_{n-1} by noting that every $\tau \in S_n$ can be written as a concatenation of an element $\sigma \in S_{n-1}$ and a transposition $(n\ k)$, $\tau = \sigma \circ (n\ k)$. We can thus rewrite

$$\varphi_{1,n-1} = \frac{1}{(n-1)!} \epsilon_{i_1 \dots i_n} \epsilon_{j_1 \dots j_n} F_{+i_1}^\dagger F_-^{j_1} \dots F_{+i_{n-1}}^\dagger F_-^{j_{n-1}} B_{-i_n}^\dagger B_-^{j_n}. \quad (2.119)$$

When performing the Fock space average, there are $(n-1)!$ possible Wick contractions for the $2(n-1)$ fermionic operators, so the factor in front gets canceled. Apart from that, the presence of n contacts generates a sum of n contributions in (2.113), one for each contact, giving

$$\begin{aligned} \langle \varphi_{1,n-1} \pi_0(C) \rangle_{\mathcal{F}} &= \epsilon_{i_1 \dots i_n} \epsilon_{j_1 \dots j_n} \overline{\psi_{k_1}(\mathbf{r}_{i_1})} \psi_{k_1}(\mathbf{r}_{j_1}) \dots \overline{\psi_{k_n}(\mathbf{r}_{i_n})} \psi_{k_n}(\mathbf{r}_{j_n}) \\ &= n! A_n. \end{aligned} \quad (2.120)$$

The framework we used so far is too narrow to allow for arbitrary moments of A_n to be expressed as highest weights operators for $\mathfrak{gl}_{2|2}$ in the vertex model. This issue will be addressed in section 2.6 by enhancing the symmetry to $\mathfrak{gl}_{2n|2n}$.

2.5 $n + 1$ -point functions of φ_q

Another case in which an easy relation between operators and observables is available are $n + 1$ -point functions of φ_q , by which we mean that n operators φ_q at different positions are inserted together with a single vacuum projector in a Fock space average,

$$\langle \varphi_{q_1}(\mathbf{r}_1) \dots \varphi_{q_n}(\mathbf{r}_n) \pi_0(\mathbf{c}) \rangle_{\mathcal{F}} = \Gamma(q_1 + \dots + q_n + 1) |\psi(\mathbf{r}_1)|^{2q_1} \dots |\psi(\mathbf{r}_n)|^{2q_n}. \quad (2.121)$$

At first we restrict ourselves to positive integers q_i . Apart from the correlators (2.113) we also have

$$\langle B_-^\dagger(\mathbf{r}_i) B_-^\dagger(\mathbf{r}_j) \pi_0(\mathbf{c}) \rangle_{\mathcal{F}} = \langle B_-(\mathbf{r}_i) B_-(\mathbf{r}_j) \pi_0(\mathbf{c}) \rangle_{\mathcal{F}} = 0, \quad (2.122)$$

which immediately follows from expanding the bilinears in terms of the lower case operators b, b^\dagger and using that correlators involving different charge indices or two annihilation resp. creation operators vanish. From (2.113) we also see that in the elementary case $B^\dagger B$ taking the Fock space average in the presence of a contact \mathbf{c} amounts to the replacements

$$B_-^\dagger(\mathbf{r}_i) \rightarrow \psi(\mathbf{r}_i) \quad B_-(\mathbf{r}_j) \rightarrow \overline{\psi(\mathbf{r}_j)}. \quad (2.123)$$

In (2.121) we have q_i operators $B_-^\dagger(\mathbf{r}_i)$ and $B_-(\mathbf{r}_i)$ respectively, which are $\sum_i q_i$ operators of each type in total. There are $(q_1 + \dots + q_n)!$ possibilities to build pairs $B^\dagger B$, and each individual product which arises due to Wick's theorem gives the result $|\psi(\mathbf{r}_1)|^{2q_1} \dots |\psi(\mathbf{r}_n)|^{2q_n}$. Since $\Gamma(n+1) = n!$ for $n \in \mathbb{N}$, analytic continuation gives the result (2.121).

2.6 Multi-point observables for $\mathfrak{gl}_{2n|2n}$

To proceed further, we now introduce n replicas of charged bosons and fermions for every link. So far we considered \mathbb{C} as a link space and passed to the link Fock spaces

$$\mathcal{F}_l = \wedge \mathbb{C} \otimes \wedge \mathbb{C}^* \otimes S\mathbb{C} \otimes S\mathbb{C}^* . \quad (2.124)$$

From a conceptual perspective it is useful to regard every copy of the link space as a tensor product $\mathbb{C} \simeq \mathbb{C} \otimes \mathbb{C}$ and to consider the space

$$\tilde{V} = U \otimes \mathbb{C} = \mathbb{C}^{2|2} \otimes \mathbb{C} \quad (2.125)$$

with $U = (U_1^+ \oplus U_1^-) \oplus (U_0^+ \oplus U_0^-)$, where $U_1^\pm = \mathbb{C}^{1|0}$, $U_0^\pm = \mathbb{C}^{0|1}$. The intention for introducing the tensor product is the fact that we have two commuting actions of subalgebras $\mathfrak{gl}_{2|2}, \mathfrak{u}_1 \subset \mathfrak{gl}(\tilde{V})$, which is then accounted for by letting the first algebra act on the first tensor factor and vice versa. Especially when passing to network models where the physical links are duplicated, for example in the unitary symplectic symmetry class C where \mathfrak{u}_1 is replaced by \mathfrak{sp}_2 , it is important to separate these actions.

With this concept at hand we can briefly digress and give a larger mathematical perspective on the nature of the vertex model modules and explain the notion of Howe duality. On the space $W = \tilde{V} \oplus \tilde{V}^*$ one can define a canonical alternating form

$$\begin{aligned} A : W_0 \times W_0 &\rightarrow \mathbb{C} \\ P(v + \phi, v' + \phi') &= \phi(v') - \phi'(v) , \end{aligned} \quad (2.126)$$

a canonical symmetric form

$$\begin{aligned} S : W_1 \times W_1 &\rightarrow \mathbb{C} \\ S(v + \phi, v' + \phi') &= \phi(v') + \phi'(v) , \end{aligned} \quad (2.127)$$

and introduce a so-called orthosymplectic form $Q = S + A$ which restricts to S on W_1 and to A on W_0 and for which the spaces W_0 and W_1 are orthogonal. One can then consider the subspace $\mathfrak{osp}(W) \subset \text{End}(W)$ of those endomorphisms X which are skew-symmetric with respect to Q , i.e.

$$Q(Xv, v') + (-1)^{|X||v|} Q(v, Xv') = 0 \quad (2.128)$$

for all homogeneous $v, v' \in W$. This set together with the bracket is called the orthosymplectic Lie superalgebra of W .

In our situation, the pair $(\mathfrak{gl}_{2|2}, \mathfrak{gl}_1)$ is a so-called classical reductive supersymmetric Howe dual pair in $\mathfrak{osp}(W)$. By this one means that both $\mathfrak{gl}_{2|2}$ and \mathfrak{gl}_1 are Lie sub-superalgebras in $\mathfrak{osp}(W)$, \mathfrak{gl}_1 is a classical Lie algebra which acts reductively on W and that $\mathfrak{gl}_{2|2}$ is the centralizer of \mathfrak{gl}_1 in $\mathfrak{osp}(W)$. In our case \mathfrak{gl}_1 acts by complex-linear extension of its compact real form \mathfrak{u}_1 , which is often denoted as a Howe dual pair with compact group, $(\mathfrak{gl}_{2|2}, U_1)$. In this situation one has a decomposition of Fock space which is, morally speaking, much like the correspondence between irreducible representations of U_N and S_n on an n -fold tensor product of \mathbb{C}^N known as

Schur-Weyl-duality. In Howe duality the supersymmetric Fock space decomposes multiplicity-free, i.e. every irreducible representation of the compact group appearing is in correspondence with an irreducible representation of the Howe dual partner superalgebra. This is the mathematical background of the appearance of the vertex model modules, since calculating the disorder average amounts to projection onto the U_1 -invariant subspaces, i.e. on the trivial representation.

We now have a parameter at our disposal which allows us to enlarge the supersymmetry, namely the even and odd dimension of the first tensor factor in (2.125). In what follows, we consider the general setup $\tilde{V} = \mathbb{C}^{2n|2n} \otimes \mathbb{C}$, where Howe duality tells us that the U_1 -invariants in the enlarged Fock space are in one-to-one correspondence with an irreducible representation of $\mathfrak{gl}_{2n|2n}$. In terms of operators on Fock space, we enhance bosonic and fermionic operators by internal or replica indices, i.e. to every link we assign n species of positive and negative bosons and fermions, for which we introduce an additional subscript as in $b_{+,i}^\dagger$. Notice that the notation has changed in contrast to section 2.6, where a subscript resp. superscript without comma denoted a link index for brevity in notation. From now on, the position of the link to which specific Fock space operators are assigned will be denoted as an argument. The representation is again generated by the action of $4n^2$ charge-conserving bilinears $b_{+,i}^\dagger b_{-,j}^\dagger$, $b_{+,i}^\dagger f_{-,j}^\dagger$, $f_{+,i}^\dagger b_{-,j}^\dagger$, $f_{+,i}^\dagger f_{-,j}^\dagger$ on the Fock space vacuum. In the following we concentrate on the boson-boson sector, i.e. those elements of $\mathfrak{gl}_{2n|2n}$ which translate into purely bosonic bilinears as Fock space operators. To this end, we introduce another pair of formal vectors

$$\bar{b} = \left(b_{+,1}^\dagger \quad \cdots \quad b_{+,n}^\dagger \quad -b_{-,1} \quad \cdots \quad -b_{-,n} \right), \quad (2.129)$$

$$b = \left(b_{+,1} \quad \cdots \quad b_{+,n} \quad b_{-,1}^\dagger \quad \cdots \quad b_{-,n}^\dagger \right)^T \quad (2.130)$$

and change the basis using the operators [B14]

$$U = \frac{1}{\sqrt{2}} (E_{++} \otimes \mathbb{I}_n + E_{-+} \otimes D_n + E_{+-} \otimes T_n - E_{--} \otimes D_n T_n) \quad (2.131)$$

$$U^{-1} = \frac{1}{\sqrt{2}} (E_{++} \otimes \mathbb{I}_n + E_{+-} \otimes D_n^{-1} + E_{-+} \otimes T_n - E_{--} \otimes T_n D_n^{-1}) \quad (2.132)$$

where we defined $T = \sum_{k=1}^n E_{n-k+1,k}$ and $D_n = \text{diag}(e^{i\alpha_1}, \dots, e^{i\alpha_n})$. Notice that for $n = 1$ the boson-boson sector of (2.80) is recovered. For the moment we left the link Fock space(s) on which the operators act open—this issue will be discussed shortly. We now define the boson-boson part of a Lie superalgebra representation by

$$E_{kl} \mapsto \bar{B}_k B_l, \quad 1 \leq a, b, \leq 2n. \quad (2.133)$$

The formal vectors \bar{B}, B are given by

$$\bar{B} = \bar{b} \cdot U = \frac{1}{\sqrt{2}} \left(B_{-,1}^\dagger \quad \cdots \quad B_{-,n}^\dagger \quad B_{+,n}^\dagger \quad \cdots \quad B_{+,1}^\dagger \right), \quad (2.134)$$

$$B = U^{-1} \cdot b = \frac{1}{\sqrt{2}} \left(B_{+,1} \quad \cdots \quad B_{+,n} \quad B_{-,n} \quad \cdots \quad B_{-,1} \right)^T, \quad (2.135)$$

where, as before, we defined

$$B_{\pm,k} = b_{+,k} \pm e^{-i\alpha_k} b_{-,k}^\dagger, \quad B_{\pm,k}^\dagger = b_{+,k}^\dagger \pm e^{i\alpha_k} b_{-,k}. \quad (2.136)$$

Notice that the replica indices in the second halves of \bar{B}, B are decreasing from n to 1 , so that we have

$$E_{kl} \mapsto \begin{cases} B_{-,k}^\dagger B_{+,l} & \text{if } 1 \leq k, l \leq n, \\ B_{-,k}^\dagger B_{-,2n-l+1} & \text{if } 1 \leq k \leq n, n+1 \leq l \leq 2n, \\ B_{+,2n-k+1}^\dagger B_{+,l} & \text{if } n+1 \leq k \leq 2n, 1 \leq l \leq n, \\ B_{+,2n-k+1}^\dagger B_{-,2n-l+1} & \text{if } n+1 \leq k, l \leq 2n. \end{cases} \quad (2.137)$$

For convenience in notation we arrange these operators into a formal matrix,

$$S = \left(\begin{array}{c|c} B_{-,k}^\dagger B_{+,l} & B_{-,k}^\dagger B_{-,2n-l+1} \\ \hline B_{+,2n-k+1}^\dagger B_{+,l} & B_{+,2n-k+1}^\dagger B_{-,2n-l+1} \end{array} \right). \quad (2.138)$$

We will now show that the determinant D_m of an upper-right $m \times m$ block of S with $m \leq n$,

$$D_m = \text{Det} \begin{pmatrix} S_{1,2n-m+1} & \cdots & S_{1,2n} \\ \vdots & & \vdots \\ S_{m,2n-m+1} & \cdots & S_{m,2n} \end{pmatrix}, \quad (2.139)$$

is a highest weight vector for the diagonal Cartan subalgebra $\mathfrak{h} = \{\bar{B}_k B_k\}$ and the choice of positive root vectors $\{\bar{B}_k B_l | k < l\}$. The charge subscripts on the operators are dropped henceforth, since all operators in the upper right block carry the negative ones. We first notice that D_m is well-defined, since the all operators appearing in S commute. The weights of D_m with respect to \mathfrak{h} are easily calculated. We first record two ways of writing D_m ,

$$\begin{aligned} D_m &= S_{a_1,2n-m+1} \cdots S_{a_m,2n} \epsilon_{a_1 \dots a_m} \\ &= S_{1,2n-m+a_1} \cdots S_{m,2n-m+a_m} \epsilon_{a_1 \dots a_m}. \end{aligned} \quad (2.140)$$

Using the first one we get

$$[S_{kk}, D_m] = \sum_{i=1}^m S_{a_1,2n-m+1} \cdots [S_{kk}, S_{a_i,2n-m+i}] \widehat{S_{a_i,2n-m+i}} \cdots S_{a_m,2n} \epsilon_{a_1 \dots a_m} \quad (2.141)$$

$$= \sum_{i=1}^m (\delta_{ka_i} - \delta_{k,2n-m+i}) S_{a_1,2n-m+1} \cdots S_{a_m,2n} \epsilon_{a_1 \dots a_m} \quad (2.142)$$

$$= \sum_{i=1}^m (\delta_{ki} - \delta_{k,2n-m+i}) D_m. \quad (2.143)$$

The hat symbol means that the corresponding factor is omitted. The weight is thus

given by

$$\mu_m = \sum_{i=1}^m (\Phi_i - \Phi_{2n-m+i}), \quad (2.144)$$

where $\Phi_i \in \mathfrak{h}^*$ is dual to S_{ii} . It remains to show that D_m is annihilated by the operators which lie above the diagonal in (2.138). Since $1 \leq m \leq n$ in D_m this is obviously true for the upper-right block of S . In the upper left block of S we have $1 \leq k < l \leq n$ above the diagonal. From $[S_{kl}, S_{i,2n-m+a_i}] = \delta_{li} S_{k,2n-m+a_i}$ we see that applying the commutator only gives a nonzero result on the l th factors in the second line of (2.140). We thus have

$$\begin{aligned} [S_{kl}, D_m] &= S_{1,2n-m+a_1} \cdots S_{l-1,2n-m+a_{l-1}} S_{k,2n-m+a_l} S_{l+1,2n-m+a_{l+1}} \cdots \\ &\quad \times \cdots S_{m,2n-m+a_m} \epsilon_{a_1 \dots a_m}. \end{aligned} \quad (2.145)$$

Since $k < l$ a term $S_{k,2m-n+a_k}$ appears to the left of $S_{k,2n-m+a_l}$ in this product. a_k and a_l are anti-symmetrized, so the commutator vanishes. Finally, the same argument applies to the lower-right block, so that we have shown that D_m is indeed a highest weight vector.

We now address the question of the links involved. It is immediately obvious that we need at least m different positions for nonvanishing D_m , but in the following we will focus on exactly m links and record identities for D_m which follow directly from the properties of the determinant:

$$\begin{aligned} (-1)^{\lfloor \frac{m}{2} \rfloor} D_m &= (-1)^{\lfloor \frac{m}{2} \rfloor} \text{Det} \left(\sum_i B_k^\dagger(\mathbf{r}_i) B_{m-l+1}(\mathbf{r}_i) \right)_{k,l=1}^m \\ &= \text{Det} \left(\sum_{i=1}^m B_k^\dagger(\mathbf{r}_i) B_l(\mathbf{r}_i) \right)_{k,l=1}^m \\ &= \text{Det} \left(\sum_{k=1}^m B_k^\dagger(\mathbf{r}_i) B_k(\mathbf{r}_j) \right)_{i,j=1}^m \\ &= \text{Det} \left(B_k^\dagger(\mathbf{r}_i) \right)_{i,k=1}^m \text{Det} \left(B_k(\mathbf{r}_i) \right)_{i,k=1}^m. \end{aligned} \quad (2.146)$$

The last equation allows us to prove that D_m is a positive operator for arbitrary $m \leq n$. Recall that for the case $m = 1$ we showed in (2.48) that B does not annihilate any state. Every summand in

$$\text{Det} (B_k(\mathbf{r}_i)) = \epsilon_{i_1 \dots i_m} B_1(\mathbf{r}_{i_1}) \cdots B_m(\mathbf{r}_{i_m}) \quad (2.147)$$

acts on different link Fock spaces and thus does not annihilate any state *individually*. However, since the determinant is totally antisymmetric, any given combination of link and replica indices does appear in exactly one summand, so that there is no possibility of terms adding up to zero. Now, by the same argument as around (2.48), D_m is positive and we can consider arbitrary complex powers of it.

By the Leibniz rule for the commutator, the operator

$$\varphi_\lambda(R) = D_1^{q_1 - q_2} D_2^{q_2 - q_3} \cdots D_n^{q_n} \quad (2.148)$$

is a highest weight operator for arbitrary $q_i \in \mathbb{C}$ with weight

$$\lambda = \sum_{i=1}^{m-1} (q_i - q_{i+1}) \mu_i + q_n \mu_n \equiv (q_1, \dots, q_n) \quad (2.149)$$

and observation links $R \equiv \{\mathbf{r}_1, \dots, \mathbf{r}_m\}$. To make contact with the scaling observables from [GMZ13] we restrict to integers q_i subject to $q_1 \geq q_2 \geq \dots \geq q_n \geq 0$, but in the end we will get a result which could be analytically continued to arbitrary q_i . Such a descending sequence defines a partition of λ , to which we can assign a Young diagram with $|\lambda| = \sum_i q_i$ boxes, see figure 2.2. These diagrams are well-known from the representation theory of U_n , since every diagram with at most n rows is in one-to-one correspondence with an isomorphism class of irreducible U_n -representations. We follow [GMZ13] by using Young tableaux to relate vertex model averages of φ_λ to network model observables.

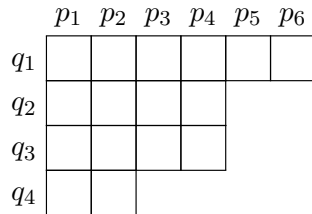


Figure 2.2: Young diagram $\lambda = (6^1, 4^2, 2) = [4^2, 3^2, 2^2]$.

Young tableaux are Young diagrams where the boxes are filled with positive integers less or equal than $N = |\lambda|$. The symmetric group S_N acts on a Young tableaux by permuting the contents of its boxes. There are two distinct subgroups of S_N , namely the group of row stabilizers $R(\lambda)$ and the group of column stabilizers $C(\lambda)$ which leave the contents of each individual row resp. column of a given Young tableau invariant. Given a group G , one can pass to the group algebra $\mathbb{K}[G]$ over the field \mathbb{K} , which consists of finite formal linear combinations of elements of G . We can thus define the row symmetrizer and column antisymmetrizer in $\mathbb{C}[S_N]$,

$$a_\lambda = \sum_{\sigma \in R(\lambda)} \sigma, \quad b_\lambda = \sum_{\tau \in C(\lambda)} (-1)^{|\tau|} \tau, \quad (2.150)$$

where $|\tau|$ denotes the sign of $\tau \in S_N$. These can now be employed to define the Young symmetrizers

$$c_\lambda = b_\lambda a_\lambda, \quad \tilde{c}_\lambda = a_\lambda b_\lambda. \quad (2.151)$$

All these operators are idempotent up to a factor,

$$a_\lambda^2 = n_R a_\lambda, \quad b_\lambda^2 = n_C b_\lambda, \quad c_\lambda^2 = n_\lambda c_\lambda, \quad \tilde{c}_\lambda^2 = n_\lambda \tilde{c}_\lambda. \quad (2.152)$$

n_R and n_C are the orders of $R(\lambda)$ and $C(\lambda)$ and $n_\lambda = \frac{|\lambda|!}{\dim V_\lambda}$, where $\dim V_\lambda$ is the dimension of $\mathbb{C}[S_N c_\lambda]$ in $\mathbb{C}[S_N]$ [FH04]. A special type of tableau which we need in the following is called minimal semistandard tableau T_λ^{\min} , where all boxes in the

i th row are filled with the integer i . For example, the minimal semistandard tableau for $\lambda = (5, 3, 1)$ is

$$T_{(5,3,1)}^{\min} = \begin{array}{|c|c|c|c|c|} \hline 1 & 1 & 1 & 1 & 1 \\ \hline 2 & 2 & 2 & & \\ \hline 3 & & & & \\ \hline \end{array} . \quad (2.153)$$

In this case it is clear that the row symmetrizers a_λ act as multiples of the identity. The notion of Young tableaux was extended in [GMZ13] to pairings in the following sense: Given λ , we take two diagrams of this shape and fill them with objects that can be paired, for example wavefunctions ψ_i and positions \mathbf{r}_j . This gives two tableaux T_ψ and T_r , for which the elements in the corresponding boxes are paired according to

$$\Psi_\lambda(T_\psi, T_r) = \prod_{i \in \lambda} \psi_i(\mathbf{r}_i) . \quad (2.154)$$

For example, the pairing of the two tableaux of shape $(3, 2, 1)$,

$$T_\psi = \begin{array}{|c|c|c|} \hline \psi_2 & \psi_4 & \psi_5 \\ \hline \psi_1 & \psi_5 & \\ \hline \psi_3 & & \\ \hline \end{array} , \quad T_r = \begin{array}{|c|c|c|} \hline \mathbf{r}_1 & \mathbf{r}_2 & \mathbf{r}_3 \\ \hline \mathbf{r}_1 & \mathbf{r}_3 & \\ \hline \mathbf{r}_4 & & \\ \hline \end{array} , \quad (2.155)$$

yields

$$\Psi_{(3,2,1)}(T_\psi, T_r) = \psi_1(\mathbf{r}_1)\psi_2(\mathbf{r}_1)\psi_3(\mathbf{r}_4)\psi_4(\mathbf{r}_2)\psi_5^2(\mathbf{r}_3) . \quad (2.156)$$

This construction can be extended by the action of group algebra elements $s = \sum_j s_j \sigma_j \in \mathbb{C}[S_N]$ in the natural way,

$$\Psi_\lambda(sT_\psi, T_r) = \sum_j s_j \prod_{i \in \lambda} \psi_{\sigma(i)}(\mathbf{r}_i) , \quad (2.157)$$

$$\Psi_\lambda(T_\psi, sT_r) = \sum_j s_j \prod_{i \in \lambda} \psi_i(\mathbf{r}_{\sigma_j(i)}) . \quad (2.158)$$

It immediately follows that $\Psi_\lambda(sT_\psi, sT_r) = \Psi_\lambda(T_\psi, T_r)$ for all $s \in \mathbb{C}[S_{|\lambda|}]$ and $\Psi_\lambda(T_\psi, \sigma T_r) = \Psi_\lambda(\sigma^{-1}T_\psi, T_r)$ for all $\sigma \in S_{|\lambda|}$. Thus we have for the (anti-)symmetrizers

$$\begin{aligned} \Psi_\lambda(T_\psi, a_\lambda T_r) &= \Psi_\lambda(a_\lambda T_\psi, T_r) , & \Psi_\lambda(T_\psi, b_\lambda T_r) &= \Psi_\lambda(b_\lambda T_\psi, T_r) , \\ \Psi_\lambda(T_\psi, c_\lambda T_r) &= \Psi_\lambda(\tilde{c}_\lambda T_\psi, T_r) , & \Psi_\lambda(T_\psi, \tilde{c}_\lambda T_r) &= \Psi_\lambda(c_\lambda T_\psi, T_r) . \end{aligned} \quad (2.159)$$

For two Young tableaux S, T of shape λ we also define the self-adjoint operator

$$\mathcal{N}_\lambda(T, S) = \left(\prod_{i \in \lambda} B_{T_\lambda^{\min(i)}}^\dagger(\mathbf{r}_{T(i)}) \right) \left(\prod_{i \in \lambda} B_{T_\lambda^{\min(i)}}(\mathbf{r}_{S(i)}) \right) \quad (2.160)$$

$$= \prod_{i \in \lambda} B_{T_\lambda^{\min(i)}}^\dagger(\mathbf{r}_{T(i)}) B_{T_\lambda^{\min(i)}}(\mathbf{r}_{S(i)}) . \quad (2.161)$$

The boxes in the tableaux S, T are counted from left to right and top to bottom. The general highest weight operator in (2.148) can then be rewritten as

$$\varphi_\lambda(R) = \mathcal{N}_\lambda(b_\lambda T_\lambda^{\min}, b_\lambda T_\lambda^{\min}), \quad (2.162)$$

where $R = \{\mathbf{r}_1, \dots, \mathbf{r}_n\}$ is a set of n distinct points for observation. Recall the definition of the operator g in (2.50),

$$g = QU(1 - QU)^{-1} + (1 - U^{-1}Q)^{-1}, \quad (2.163)$$

in the presence of n distinct point contacts, $Q = 1 - \sum_{i=1}^n |0_{\mathbf{c}_i}\rangle \langle 0_{\mathbf{c}_i}|$. Recall further that

$$g_{ij} = \sum_{k=1}^n \psi_k(\mathbf{r}_i) \overline{\psi_k(\mathbf{r}_j)}. \quad (2.164)$$

Now, if we define

$$\mathcal{G}_\lambda(T, S) = \prod_{i \in \lambda} g_{T(i), S(i)}, \quad (2.165)$$

we can express a product of powers of the determinant observables A_n from (2.116) using the minimal tableau:

$$\mathcal{G}(b_\lambda T_\lambda^{\min}, T_\lambda^{\min}) = A_1^{q_1 - q_2} A_2^{q_2 - q_3} \dots A_n^{q_n}. \quad (2.166)$$

Finally, we will now relate the Fock space average with observables,

$$\langle \mathcal{N}_\lambda(T, S) \pi_0(C) \rangle_{\mathcal{F}} = \mathcal{G}_\lambda(S, a_\lambda T), \quad (2.167)$$

for two tableaux S, T of shape λ . This result is proven as follows:

$$\begin{aligned} \langle \mathcal{N}_\lambda(T, S) \pi_0(C) \rangle_{\mathcal{F}} &= \left\langle B_1^\dagger(T(1)) \cdots B_1^\dagger(T(q_1)) B_1(S(1)) \cdots B_1(S(q_1)) \pi_0(C) \right\rangle_{\mathcal{F}} \cdots \\ &\quad \left\langle B_n^\dagger(T(|\lambda| - q_n + 1)) \cdots B_n^\dagger(T(|\lambda|)) \right. \\ &\quad \left. \cdot B_n(S(|\lambda| - q_n + 1)) \cdots B_n(S(|\lambda|)) \pi_0(C) \right\rangle_{\mathcal{F}} \\ &= \sum_{\pi_1 \in S_{q_1}} g_{S(1), T(\pi_1(1))} \cdots g_{S(q_1), T(\pi_1(q_1))} \cdots \\ &\quad \sum_{\pi_n \in S_{q_n}} g_{S(|\lambda| - q_n + 1), T(\pi_n(|\lambda| - q_n + 1))} \cdots g_{S(|\lambda|), T(\pi_n(|\lambda|))} \\ &= \sum_{\pi \in R(\lambda)} g_{S(1), T(\pi(1))} \cdots g_{S(q_1), T(\pi(q_1))} \cdots \\ &\quad \cdots g_{S(|\lambda| - q_n + 1), T(\pi(|\lambda| - q_n + 1))} \cdots g_{S(|\lambda|), T(\pi(|\lambda|))} \\ &= \sum_{\pi \in R(\lambda)} \mathcal{G}_\lambda(S, \pi T) \quad (2.168) \\ &= \mathcal{G}_\lambda(S, a_\lambda T). \quad (2.169) \end{aligned}$$

The first equality uses the fact that different replica indices do not mix in Fock space

averages. The second is Wick's theorem, where S_{q_1} acts on $\{1, 2, \dots, q_1\}$, which are the box numbers in the first row, S_{q_2} acts on $\{q_1 + 1, \dots, q_1 + q_2\}$, which are the box numbers in the second row and so on. This is then rewritten using $R(\lambda)$, which is the row stabilizer of the *normal* tableau of shape λ , i.e. the one where each box is filled with its number. To arrive at the desired result, we apply this formula to the case $S = T = b_\lambda T_\lambda^{\min}$ and use that row stabilizers reproduce the minimal semistandard tableau by a factor, $a_\lambda T_\lambda^{\min} = n_R T_\lambda^{\min}$:

$$\begin{aligned}
\langle \mathcal{N}_\lambda(b_\lambda T_\lambda^{\min}, b_\lambda T_\lambda^{\min}) \pi_0(C) \rangle_{\mathcal{F}} &= \mathcal{G}_\lambda(b_\lambda T_\lambda^{\min}, a_\lambda b_\lambda T_\lambda^{\min}) \\
&= \frac{1}{n_R} \mathcal{G}_\lambda(b_\lambda a_\lambda T_\lambda^{\min}, a_\lambda b_\lambda T_\lambda^{\min}) \\
&= \frac{n_\lambda}{n_R} \mathcal{G}_\lambda(b_\lambda a_\lambda T_\lambda^{\min}, T_\lambda^{\min}) \\
&= n_\lambda \mathcal{G}_\lambda(b_\lambda T_\lambda^{\min}, T_\lambda^{\min}) \\
&= n_\lambda A_1^{q_1 - q_2} A_2^{q_2 - q_3} \dots A_n^{q_n}. \tag{2.170}
\end{aligned}$$

Since the operators appearing in the definition of φ_λ descend to vertex model operators, we finally arrive at

$$\mathbb{E}\{(A_1^{q_1 - q_2} A_2^{q_2 - q_3} \dots A_n^{q_n})(R, C)\} \propto \langle (D_1^{q_1 - q_2} D_2^{q_2 - q_3} \dots D_n^{q_n})(R) \pi_0(C) \rangle_{\mathcal{V}}. \tag{2.171}$$

2.7 Casimir eigenvalues

The universal enveloping superalgebra $U(\mathfrak{g})$ is the unital associative algebra generated by elements of \mathfrak{g} with the Lie superbracket relations imposed. A version of the Poincaré-Birkhoff-Witt theorem is also available in the super case [CW12]. The elements in the center $Z_{U(\mathfrak{g})}$ of $U(\mathfrak{g})$ are called Casimir invariants and have, by definition, the property that they commute with all elements of \mathfrak{g} . Of special importance to us is the fact that highest weight vectors of representations are eigenvectors for Casimir invariants. To see this one has to use that every element in the center can be decomposed into a part lying in $U(\mathfrak{h})$ and a part lying in $U(\mathfrak{g})\mathfrak{n}^+ \cap \mathfrak{n}^- U(\mathfrak{g})$.

The scaling dimensions of the observables (and thus of the conformal dimensions of the underlying conformal field theory) must be linear combinations of an algebraically independent set of eigenvalues of such invariants. Explicit expressions for these eigenvalues on highest weight representations of $\mathfrak{gl}_{m|n}$ were obtained by Scheunert [S83], which we now adapt to our situation. We first notice that the supertrace induces an isomorphism $\mathfrak{h}^* \ni \mu \mapsto H_\mu \in \mathfrak{h}$ by

$$\mu(H) = \text{STr}(H_\mu H) \quad \text{for all } H \in \mathfrak{h}. \tag{2.172}$$

Furthermore, the Weyl vector ρ is defined by half the sum of the positive roots, each one counted with its parity:

$$2\rho := \sum_{\alpha \in \Delta^+} (-1)^{|\alpha|} \alpha. \tag{2.173}$$

Scheunert then introduces

$$r_i = s_i \rho(E_{ii}) = \frac{1}{2} \left(\sum_{j>i} s_j - \sum_{j<i} s_j \right), \quad (2.174)$$

$$l_i = s_i(\lambda + \rho)(E_{ii}) = s_i \text{STr}(H_{\lambda+\rho} E_{ii}) = (H_{\lambda+\rho})_{ii}, \quad (2.175)$$

where s_i are the components of the formal grading vector (2.66) and λ is a highest weight. The eigenvalue c_n of the n th order Casimir operator on the highest weight representation labeled by λ is then a polynomial in

$$Q_m = \sum_i s_i (l_i^m - r_i^m) \quad (2.176)$$

with the property that $c_n - Q_n$ has degree less than n . With other words, the Q_m can be taken as generators of invariant polynomials. Notice in particular that, by the definition of l_i and r_i , Q_m is invariant under the so-called Weyl group $W = S_m \times S_n$ which permutes even and odd root separately.

For $\mathfrak{gl}_{2n|2n}$ the second sum vanishes for all m , $\sum_i s_i r_i^m = 0$. We can then rewrite the expression for Q_m as

$$Q_m = \text{STr}(H_{\lambda+\rho}^m). \quad (2.177)$$

Recall that for the ordering (2.64) of the basis elements of \mathfrak{h}^* we have the even roots

$$\begin{aligned} \Phi_i - \Phi_j & \quad 1 \leq i < j \leq n, \\ \Phi_{n+i} - \Phi_{n-j} & \quad 1 \leq i < j \leq n, \\ \Phi_i - \Phi_{n+j} & \quad 1 \leq i, j \leq n, \\ \Psi_i - \Psi_j & \quad 1 \leq i < j \leq 2n \end{aligned} \quad (2.178)$$

and the odd roots

$$\Phi_i - \Psi_j, \quad \Psi_j - \Phi_{n+i}, \quad 1 \leq i \leq n, 1 \leq j \leq 2n. \quad (2.179)$$

The Weyl vector is then

$$\begin{aligned} 2\rho &= \sum_{i=1}^n \{(-2i+1)\Phi_i + (2n-2i+1)\Phi_{n+i}\} + \sum_{i=1}^{2n} (2n-2i+1)\Psi_i \\ &= (-1, -3, \dots, -2n+1; 2n-1, 2n-3, \dots, 1, \\ &\quad -1, -3, \dots, -2n+1; 2n-1, 2n-3, \dots, 1). \end{aligned} \quad (2.180)$$

The most general operators φ_λ we want to consider have weight

$$\lambda = \sum_{i=1}^n q_i (\Phi_i - \Phi_{2n-i+1}) \quad (2.181)$$

with respect to this choice of basis. In this particular situation Q_m vanishes for odd m and, by an easy calculation, we arrive at

$$\frac{1}{2}Q_{2k} = \sum_{i=1}^n \left(q_i - i + \frac{1}{2} \right)^{2k} - \sum_{i=1}^n \left(i - \frac{1}{2} \right)^{2k}. \quad (2.182)$$

From the requirement that the scaling dimensions Δ_λ are polynomials in Q_{2k} Weyl group invariance has some remarkable implications: (2.182) is easily seen to be invariant under the transformations

$$\begin{aligned} q_i &\mapsto 2i - 1 - q_i \quad \text{for all } q_i \text{ or} \\ q_i &\mapsto q_j + i - j \wedge q_j \mapsto q_i + j - i. \end{aligned} \quad (2.183)$$

For $n = 2$ and $q_1 = q_2 = 0$ we have

$$\mathbb{E}\{A_1^{0-0} A_2^0(R, C)\} = \mathbb{E}\{1\} = 1 \quad (2.184)$$

and thus $\Delta_{0,0} = 0$. By applying (2.183) we get a sequence of nontrivial vanishing scaling dimensions, for example $\Delta_{2,2} = \Delta_{-1,1} = \Delta_{0,3} = 0$ which directly implies that the leading contribution of a priori nontrivial ensemble averages of network model observables are constant, e.g.

$$\mathbb{E}\{A_1^{-2} A_2(R, C)\} = \text{const.} + \text{subleading}. \quad (2.185)$$

In particular, for $n = 1$ we recover the symmetry relation (1.45).

2.8 The conceptual background of φ_q

Throughout this chapter we presented several highest weight vertex model operators and related them to observables in the network model. Although, or maybe more appropriately *because* the treatment was quite elementary, meaning that we only employed superalgebra rather than superanalysis, the question arises why these observables were only found in 2013. There are at least two reasons, one being superficial and the other being mathematical: Although the case $n = 1$ corresponds to the ensemble average of moments of wavefunction amplitudes in the presence of a point contact, which seems quite a simple object to consider, there is no obvious correspondence between this theoretical vehicle and an experiment.

This has to be seen in contrast with, say, a two-point conductance, which could easily be imagined to be an idealization of an actual transport measurement. The constructions presented here also apply for general transport variables, as was shown in [GMZ13]: Take n contacts in the region C_1 and n contacts in the region C_2 . Now, consider the set of stationary scattering states ψ_1, \dots, ψ_n which correspond to the region C_1 . To each state we can assign a transmission probability from $\mathbf{c}_i \in C_1$ to $\mathbf{c}_j \in C_2$ by $t_{ij} = \psi_i(\mathbf{c}_j)$. A construction analogous to that of A_m , i.e. taking B_m as the absolute value squared of the determinant of the upper-left $m \times m$ -corner of the matrix $T = (t_{ij})$ gives the transport observable

$$M_{q_1 \dots q_n} = \langle B_1^{q_1 - q_2} B_2^{q_2 - q_3} \dots B_n^{q_n} \rangle. \quad (2.186)$$

The leading scaling behavior of this observable with the distance $|C_1 - C_2|$ is given by $2\Delta_{q_1 \dots q_n}$. As in the case of the two-point contact conductance, it does not decay as a pure power but rather has an admixture of a continuum of subleading exponents, which jeopardize numerical investigations.

On the other hand, from a heuristic viewpoint it was crystal clear how to proceed since the decomposition (2.98) of the point-contact operator became available in 1999: One *just* has to write down an appropriate highest weight operator in $\text{End}(V)$. Unfortunately, the decomposition of $V \otimes V^*$ into a principal continuous series is quite complicated and no systematic method existed to find these operators. The original construction of the modules V and V^* was as representations of a supergroup in terms of a super generalization of the Borel-Weil correspondence, i.e. as holomorphic resp. antiholomorphic sections of a line bundle over the super coset space $G_{\mathbb{C}}/K_{\mathbb{C}} = \text{GL}_{2n|2n}/\text{GL}_{n|n} \times \text{GL}_{n|n}$ which is the complexification of $G/K = \text{U}_{n,n|2n}/\text{U}_{n|n} \times \text{U}_{n|n}$. The product of both types of sections then gives an ordinary function $f \in C^\infty(G/K)$. In summary, we have the correspondences

$$\text{End}(V) \simeq V \otimes V^* \simeq \text{Hol}(G/K, L) \otimes \text{Hol}(G/K, L^*) \rightarrow C^\infty(G/K) . \quad (2.187)$$

The last correspondence is also well-known from the classical case: All irreducible representations of SO_3 have a realization as ordinary functions on the sphere called spherical harmonics $Y_m^l \in C^\infty(S^2)$. Here, one should notice

$$S^2 \simeq SO_3 / SO_2 \simeq SU_2 / U_1 . \quad (2.188)$$

Each of these representations is also an irreducible representation of the group SU_2 . However, the odd-integer¹ representations of SU_2 do not appear as ordinary functions, but rather as holomorphic sections of a line bundle over S^2 . Let us explain what we mean by this notion: By $V_m \simeq \mathbb{C}$ we denote the one-dimensional U_1 -representation given by the highest weight m for SU_2 . $g = e^{i\phi\sigma_3} \in U_1$ acts on V by multiplication of $\rho(g) = e^{im\phi}$. The representation ρ allows us to pass from the trivial vector bundle $G \times V$ to the associated bundle $G \times_\rho V$, where we identify $(gk, v) = (g, \rho(k)v)$. The sections of this bundle are isomorphic to the SU_2 -representation induced by U_1 ,

$$\Gamma(SU_2 / U_1, V_m) \simeq C^\infty(SU_2, V_m)^{U_1} , \quad (2.189)$$

where the latter object is the set of all U_1 -equivariant complex-valued smooth functions on SU_2 ,

$$C^\infty(SU_2, V_m)^{U_1} = \{f \in C^\infty(SU_2, V) | f(gk) = \rho(k)^{-1}f(g), k \in U_1\} . \quad (2.190)$$

To explain the notion of holomorphicity, it is customary to pass to the complexified setting, where we have

$$S^2 \simeq SU_2 / U_1 \simeq SL_{2,\mathbb{C}} / B . \quad (2.191)$$

The so-called Borel subgroup B is the unique connected subgroup in $SL_{2,\mathbb{C}}$ which

¹This is the way mathematicians label the highest weights; in physics, one would call them half-integer.

has Lie algebra $\mathfrak{b} = \mathfrak{gl}_1 \oplus \mathfrak{n}^+$. In the standard matrix representation of $\mathrm{SL}_{2,\mathbb{C}}$ these are the matrices of the form $\begin{pmatrix} a & b \\ 0 & a^{-1} \end{pmatrix}$. We can extend the representation ρ of U_1 on V_m to a representation ρ_B of B by

$$\rho_B \begin{pmatrix} a & b \\ 0 & a^{-1} \end{pmatrix} = a^m. \quad (2.192)$$

The holomorphic sections in $\Gamma(\mathrm{SU}_2 / U_1, V_m)$ then correspond to the holomorphic functions in $C^\infty(\mathrm{SL}_{2,\mathbb{C}}, V_m)^B$. With this very explicit realization it is easy to work out the details on 2×2 matrices, which shows that the holomorphic sections are the homogeneous polynomials of degree m on the first column of $\mathrm{SL}_{2,\mathbb{C}}$ matrices [S07]. An analogous story can now be told in the antiholomorphic case, where the only difference is that instead of V_m one has to use the dual representation $V_m^* = V_{-m}$. Thus, multiplying a holomorphic and an antiholomorphic B -equivariant function f_1 resp. f_2 on $\mathrm{SL}_{2,\mathbb{C}}$ we end up with a B -invariant function, since the contributions of the one-dimensional B -representations on V_m and V_m^* cancel each other:

$$(f_1 \otimes f_2)(g) = \rho_B(b)f_1(gb) \otimes \rho_B(b^{-1})f_2(gb) = (f_1 \otimes f_2)(gb). \quad (2.193)$$

Since $\mathrm{SL}_{2,\mathbb{C}}/B \simeq S^2$ this product can then be regarded as an ordinary function on the sphere S^2 .

The good objects to consider as gradientless pure scaling operators for the nonlinear sigma models at the Anderson transition are functions on the target space G/K which are eigenfunctions of all Laplace-Casimir operators on G/K . The reason is that infinitesimal RG transformations acting on sigma model operators A are equivalent to differential operators acting on A considered as a function on the target space. Under the assumption that the action is G -invariant, infinitesimal RG transformations correspond to G -invariant differential operators, a complete set of which is furnished by Laplace-Casimir operators. The main advancement in [GMZ13] was then to relate these functions back to properly symmetrized expressions involving critical wavefunctions.

At this point we would also like to stress that the open-network situation we consider is conceptually superior: The second term in the sigma model action

$$S[Q] = \frac{1}{16\pi t} \int d^d r \mathrm{Tr}(\nabla Q)^2 + h \int d^d r \mathrm{Tr}(Q\Lambda) \quad (2.194)$$

serves the purpose of infrared regularization in infinite volume, but breaks invariance under the full group G down to invariance under the subgroup K . In the closed network model this is related to the fact that an infinitesimal imaginary energy shift is needed to make Green's functions well-defined. From the viewpoint of symmetry opening the network is a better way of regularization, because it preserves invariance under G away from the contact. Furthermore, the correspondence between network and vertex models furnished by Howe duality (and thus the correspondence between our operators and observables) is exact, while in [GMZ13] this is only the case approximately.

With the connection between pure scaling operators and eigenfunctions uncovered we can now use a systematic way to relate a polynomial eigenfunction $f \in C^\infty(G/K)$

of all Laplace-Casimir operators, which is a highest weight for the action

$$(\hat{X}f)(gK) = \left. \frac{d}{dt} \right|_{t=0} f(e^{-tX}gK) \quad (2.195)$$

of $X \in \mathfrak{g}$ as a first-order differential operator \hat{X} on $C^\infty(G/K)$, to vertex model operators. The function

$$Q : G/K \rightarrow \mathfrak{gl}_{2n|2n}, \quad Q(g) = g(i\Sigma_3)g^{-1}, \quad (2.196)$$

where $\Sigma_3 = \sigma_3 \otimes \mathbb{I}_{2n}$, intertwines the action of G on $C^\infty(G/K)$ by left multiplication with the one on $\mathfrak{gl}_{2n|2n}$ by conjugation,

$$Q(hgK) = hg(i\Sigma_3)g^{-1}h^{-1} = \text{Ad}(h)Q(gK). \quad (2.197)$$

A correspondence between $\mathfrak{gl}_{2n|2n}$ and highest weights in $C^\infty(G/K)$ can be established by employing the moment map

$$\mu : G/K \rightarrow \mathfrak{gl}_{2n|2n}^*, \quad gK \mapsto (X \mapsto \text{STr}(XQ(gK))) \quad (2.198)$$

which has a pullback

$$\mu^* : S(\mathfrak{gl}_{2n|2n}) \rightarrow C^\infty(G/K). \quad (2.199)$$

Notice that the symmetric algebra $S(\mathfrak{gl}_{2n|2n})$ is isomorphic to the polynomial functions on the dual $\mathfrak{gl}_{2n|2n}^*$. Evaluation of these polynomials, by finite-dimensionality of the Lie superalgebra, is understood in the canonical sense

$$v(\vartheta) = \vartheta(v) \quad \text{for } v \in V \simeq (V^*)^*, \vartheta \in V^*. \quad (2.200)$$

Applying (2.195) to the moment map and using the G -equivariance of Q and the cyclicity of the supertrace we see that elements in $S(\mathfrak{gl}_{2n|2n})$ which are annihilated by the adjoint action of \mathfrak{n}^+ can be related to polynomial highest weight functions on G/K . The second-quantized operators associated with the former objects then have the desired properties.

We close this section with a remark on the nature of the operators φ_q . The attentive reader has noticed that the representations of the continuous series do not contain any highest weight vectors. The functions on G/K which are eigenfunctions of all invariant differential operators form a so-called eigenspace representation of G —see [H09] for details in the classical case. Our highest weight vertex model operators live, morally speaking, on the boundary of G/K . Focusing on the purely bosonic sector, $\text{SU}_{1,1}$ can be interpreted as the group of Bogoliubov transformations which relates the operators b_\pm, b_\pm^\dagger to a new set $\tilde{b}_\pm, \tilde{b}_\pm^\dagger$ which still obey CCR:

$$\begin{pmatrix} e^{i\beta} \cosh t & -e^{i(\alpha+\beta)} \sinh t \\ -e^{-i(\alpha+\beta)} \sinh t & e^{i\beta} \cosh t \end{pmatrix} \begin{pmatrix} b_+ \\ b_-^\dagger \end{pmatrix} = \begin{pmatrix} \tilde{b}_+ \\ \tilde{b}_-^\dagger \end{pmatrix}. \quad (2.201)$$

The space of vacua resp. U_1 -equivalence classes of operators is $\text{SU}_{1,1}/U_1$, which can be modeled as the Poincaré disc. In this picture the operators (2.82) sit at the

boundary and cannot be reached by any proper Bogoliubov transformation, which explains their peculiar commutation relations (2.83) and the fact the transformation (2.79) does not correspond to a unitary transformation on Fock space.

Chapter 3

Numerical Tests

Nachdem er einmal Doktorarbeiten aus dem Institut von Ludwig Prandtl, immerhin eines weltberühmten Strömungsmechanikers und Aerodynamikers, in die Hand bekommen hatte, bezeichnete er fortan derartige Arbeiten, die sich mit Fragen der Anwendung befassten, nur noch ironisch-despektierlich als „Schmieröl“ und die zugehörige Wissenschaft als „Schmieröl-Mathematik“.

Aus dem deutschen wikipedia-Artikel über Edmund Landau

In this chapter we report our numerical results, starting with an explanation of the program used in our simulations. The source code can be found in appendix B. We continue by investigating falsifiability, or, in other words, whether or not we can distinguish between a network observable showing pure algebraic decay—the typical two-point contact conductance—and one that does not. After receiving an affirmative answer, we critically recapitulate the results from our letter [BWZ14] for the observables A_n , $1 \leq n \leq 3$, on long cylinders, as well as on $2 + 1$ -point functions. We then present a recent attempt to refine these results which takes into account finite size scaling. Finally, we investigate A_1 in the corner of a rectangle, again using finite size scaling.

Throughout this chapter the dimensions of the network are counted in plaquette units, as explained in section 3.1. Error bars in the numerical data are always standard errors of the mean. All fits are produced by the Mathematica 9 routine `NonlinearModelFit`. The weights are given by the inverse variance of the numerical data as suggested by the Mathematica documentation, `MaxIterations` is set to 10^4 and the numerically robust method `Levenberg-Marquardt` is used in multi-parameter fits. Unless stated otherwise, further options for this routine are the standard ones. If the fit object is called `nlm`, the error bars of the parameters are the ones given by `nlm[\"ParameterErrors\"]`. The choice of weights is such that the goodness of fit measure χ_{red}^2 can be found by `nlm[\"EstimatedVariance\"]`. Recall that this quantity is defined as [BR03]

$$\chi_{\text{red}}^2 = \frac{1}{\nu} \sum_{i=1}^n \frac{(y_i - Y_i)^2}{\sigma_i^2}. \quad (3.1)$$

Here, ν is the number of degrees of freedom¹, y_i the measured value, σ_i its variance and Y_i the prediction. Values of χ_{red}^2 around 1 are considered as very good fits. More precisely, the value χ_{red}^2 should be compared with quantiles of the χ^2 -distribution for the corresponding number of degrees of freedom. The distribution function is

$$f(\chi^2) = \frac{1}{2^{\nu/2}\Gamma(\nu/2)} e^{-\chi^2/2} (\chi^2)^{\nu/2-1}, \quad (3.2)$$

which is derived from the assumption that the measured values are normally distributed. $\chi^2 = 1$ is the mean of the distribution, the median being slightly smaller and depending on ν . To perform a statistical test, one has to specify a level α such that

$$\int_{\chi_{\nu,\alpha}^2}^{\infty} f(\chi^2) d\chi^2 = \alpha, \quad (3.3)$$

meaning that the probability of having the correct model at hand, but finding $\chi_{\text{red}}^2 > \chi_{\nu,\alpha}^2/\nu$ from a measurement or simulation is less than α . As an orientation we will state values for $\alpha = 0.05$ in the appropriate places. However, also a word of caution is in order, since such a statistical test must not be (ab)used as the single criterion for assessing the validity of a fit. Thus, we will comment on the results in every single case.

In this chapter we put strong emphasis on an accurate and transparent description of the numerical procedures involved to produce our results in order to allow for full reproducibility and (justified) criticism.

3.1 Description of the program code

We now explain how to calculate the scattering states introduced in section 1.7 numerically by constructing a matrix representation of the closed-network unitary (discrete) time evolution operator U with respect to the basis given by the link states. To this end, we view the Chalker-Coddington network as a rectangular network consisting of LW plaquettes, where we henceforth call L the length and W the width of the network as measured in plaquette units, see figure 3.1. Notice that for cylindrical or toric geometries one or both of these dimensions will play the role of a circumference.

For reasons of convenient implementation the counting of links starts at 0. On a given plaquette, links are counted clockwise starting from upper right—this one we call a link of type 0, the other ones accordingly type 1, 2 and 3—and probability flux is scattered counterclockwise. The minus signs which ensure unitarity are placed in the lower and the right corner. With other words, the lower scattering node is of the type shown in figure 1.5 and we keep the convention $\begin{pmatrix} \psi_1 \\ \psi_3 \end{pmatrix} = \frac{1}{\sqrt{2}} \begin{pmatrix} 1 & -1 \\ 1 & 1 \end{pmatrix} \begin{pmatrix} \psi_0 \\ \psi_2 \end{pmatrix}$. The counting of plaquettes starts at the top left corner and then proceeds row-wise, so that the links in the i th row are numbered from $4(i-1)L$ to $4iL-1$. After each

¹The reader may tolerate that this standard symbol collides with the localization length exponent, which is not used in this chapter. Furthermore, we use $\nu = n - p$, where p is the number of parameters.

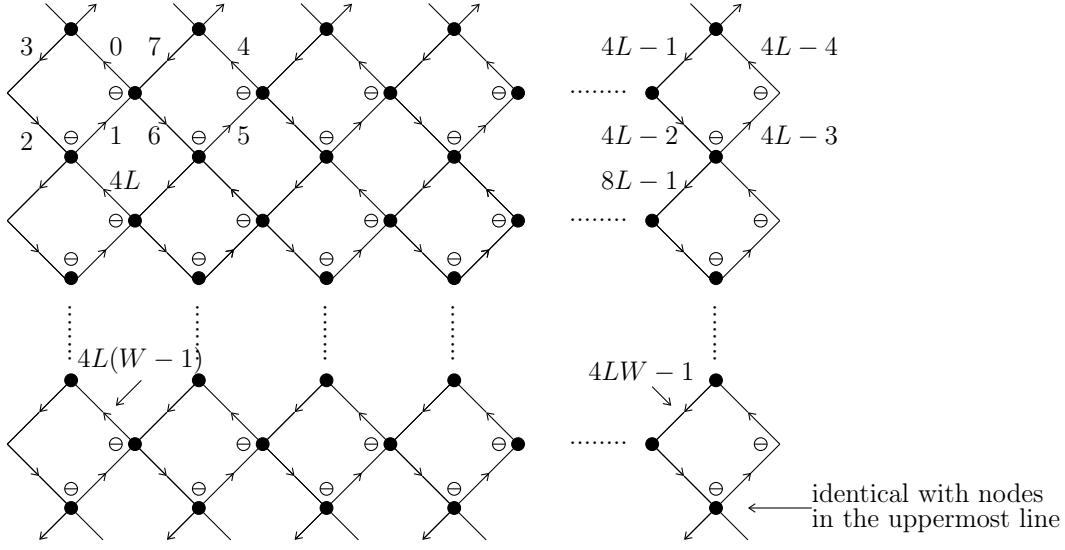


Figure 3.1: The Chalker-Coddington network on a cylinder as a network of plaquettes.

discrete time step, the four links on the plaquette in the i th row and j th column of the network receive contributions from neighboring links as shown in figure 3.2 and summarized in table 3.1.

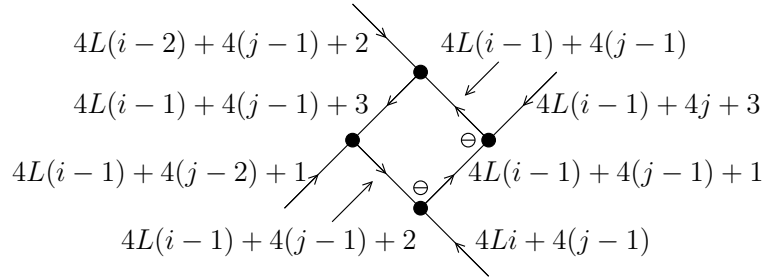


Figure 3.2: Scattering in a generic plaquette in the bulk of the network.

link	receives contribution from	sign
$4L(i-1) + 4(j-1)$	$4L(i-1) + 4(j-1) + 1$ $4L(i-1) + 4j + 3$	\ominus \oplus
$4L(i-1) + 4(j-1) + 1$	$4L(i-1) + 4(j-1) + 2$ $4Li + 4(j-1)$	\ominus \oplus
$4L(i-1) + 4(j-1) + 2$	$4L(i-1) + 4(j-1) + 3$ $4L(i-1) + 4(j-2) + 1$	\oplus \oplus
$4L(i-1) + 4(j-1) + 3$	$4L(i-1) + 4(j-1)$ $4L(i-2) + 4(j-1) + 2$	\oplus \oplus

Table 3.1: Link contributions in the bulk of the network.

In this thesis we consider two types of boundary conditions: reflecting (RBC) and periodic (PBC). Let us have a look at two examples to see what changes in contrast

edge of network	BC	link	receives contribution from
right	RBC	$4iL - 4$	$4iL - 3$
	PBC		$4iL - 3$ $4L(i - 1) + 3$
lower	RBC	$4L(W - 1) + 4(j - 1) + 1$	$4L(W - 1) + 4(j - 1) + 2$
	PBC		$4L(W - 1) + 4(j - 1) + 2$ $4(j - 1)$
left	RBC	$4L(i - 1) + 2$	$4L(i - 1) + 3$
	PBC		$4L(i - 1) + 3$ $4iL - 3$
upper	RBC	$4(j - 1) + 3$	$4(j - 1)$
	PBC		$4(j - 1)$ $4L(W - 1) + 4(j - 1) + 2$

Table 3.2: Link contributions at the boundary of the network.

to bulk plaquettes: For RBC at the right side of the network, the wave function amplitude on link type 1 is scattered into link type 0 at any given plaquette, whereas no change is needed for scattering into link type 1. If we consider PBC instead, a link of type 0 on the rightmost column is fed by link type 1 on the same plaquette as well as by link type 3 on the leftmost part of the network. Conversely, link type 2 on the left-hand side receives a contribution from link type 3 on the same plaquette and from link type 1 on the right-hand side. The general situation is summarized in table 3.1. With this preliminary work done it is now easy to set up a sparse matrix representation of U for a given network size L , W and boundary conditions. We then want to calculate the open-network scattering wavefunction

$$|\psi_k\rangle = U(1 - QU)^{-1} |\mathbf{c}_k\rangle \quad (3.4)$$

with projector $Q = 1 - \sum_{l=1}^n |\mathbf{c}_l\rangle \langle \mathbf{c}_l|$. Since we are ultimately interested in studying observables of the type introduced in chapter 2, we only need to consider the amplitudes of $|\psi_k\rangle$ on links which do not lie in the direct vicinity of the contact, i.e. which are more than one scattering event away. Thus we can multiply both sides of (3.4) by U^{-1} without changing the amplitude on these links:

$$(1 - QU) |\psi'_k\rangle = |\mathbf{c}_k\rangle . \quad (3.5)$$

This representation has the advantage that no numerical inversion is needed anymore since $|\psi'_k\rangle$ is now the solution of a system of linear equations and coincides with $|\psi_k\rangle$ on all links which are not directly connected to the contact(s).

3.2 Results on long cylinders

Recall from the introductory chapter that a preferred geometry for numerical studies is the quasi one-dimensional long cylinder, where an explicit and easy formula is available for the decay of two-point functions of conformal primary fields. In section 1.6 we derived

$$\langle \phi(w_1, w_1^*) \phi(w_2, w_2^*) \rangle = \left| \frac{W}{\pi} \sinh \left(\frac{\pi}{W} w_{12} \right) \right|^{-2\Delta}, \quad (3.6)$$

where w is a complex coordinate on the cylinder. In the following we will use the coordinates τ and σ for the horizontal resp. vertical distance from the point contact(s), see figure 3.3. The presence of the network introduces a non-universal length scale parameter a , which could be interpreted as a lattice constant, so that we will use

$$\left| \frac{W}{\pi a} \sinh \left(\frac{\pi}{W} (\tau - \tau' + i\sigma - i\sigma') \right) \right|^{-2\Delta} \quad (3.7)$$

as a fitting function. In the case of the typical two-point conductance, it is however common to denote the exponents as X_{typ} .

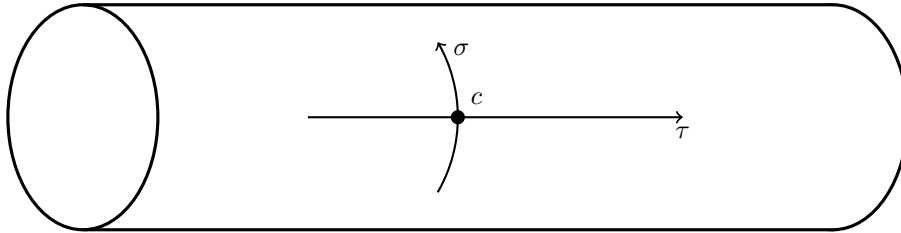


Figure 3.3: Coordinate system on the cylinder

3.2.1 Two-point contact conductances

We begin by addressing the question of falsifiability, meaning whether or not we can even distinguish between observables that show pure scaling behavior and those that do not. To this end, we consider the two-point contact conductance T given in (1.66) and the typical two-point contact conductance. From the results of [JMZ99] presented in section 2.3 we expect the ensemble average of the latter to show pure scaling behavior, while the former should display deviations due to a continuum of subleading scaling dimensions. We investigate this question on cylinders of length $L = 400$ and different circumferences $W = 19, 22, \dots, 40$ at an ensemble size $N = 10^6$. The first contact sits in the center ($0|0$) of the cylinder, the second contact lies at $(\tau|0)$, $10 \leq \tau \leq 80$. We use reflecting boundary conditions at the left and right end of the cylinder, so that we want to take the observation region in the bulk of the cylinder. The method comes with the drawback that the second contact moves, so that 10^6 runs of the program are needed for *each* data point. While this problem can be circumvented by employing the Klesse-Zirnbauer formula (1.67) which relates this particular observable to eigenstates of the closed network, no generalization is available for more general transport observables like the ones mentioned in (2.186).

The results for the typical two-point contact conductance are shown in figure 3.4. The main part shows the numerical data and the fitted curves, where the smallest circumference $W = 19$ corresponds to the bottom curve. The visual impression of a perfect fit between numerical data and the predicted behavior is substantiated by the goodness of fit measure χ_{red}^2 displayed in table 3.3. In this case we have $\chi_{\nu,0.05}^2 = 1.3$. The fitted exponents show a slow decay with the circumference of the system, as is expected from our discussion of finite size scaling in section 1.3. A value of about 0.53 is in accordance with the value 0.57 ± 0.05 found in [KZ01]. This discrepancy as well as the much larger error bars come from the fact that the latter was not obtained by a fitting procedure, but rather from visual inspection of a collapse plot (as shown in set inset of figure 3.4) for different values of Δ [K13]. For producing this type of plot one plots $\mathbb{E}\{\ln T\} + X_{\text{typ}} \ln W$ versus $\ln \frac{\tau}{W}$. For the correct choice of X_{typ} this makes the curves collapse onto a single one, as long as the non-universal parameter a does not change drastically (which would shift individual curves vertically). However, even if we include a numerically cheap data point for $W = 3$, which gives the fitting value $X_{\text{typ}} = 0.53868(3)$, our collapse plot does not show the broadening visible in figure 2 of [KZ01], so that from visual inspection we would infer $X_{\text{typ}} = 0.53 \pm 0.02$. The situation differs drastically for the two-point contact conductance, which is shown in figure 3.5. The visual impression of a "bad fit"—every curve is missing almost all data points in a systematic way—is underpinned by values of χ_{red}^2 ranging from 28 for $W = 40$ to 103 for $W = 19$. One should note that the argument of the fitting function contains the ratio $\frac{\tau}{W}$, so that for larger circumferences a smaller interval of the continuum curve is probed by the data points, which results in a slightly better fit.

The optimal values for χ_{red}^2 in the case of a pure scaling observable in combination with the large values of this measure for an observable which is expected to suffer from continuous subleading contributions justifies to use the goodness of fit as a criterion for the pure scaling nature of the observables A_n .

W	19	22	25	28
X_{typ}	0.5356(1)	0.5345(1)	0.5338(1)	0.5330(1)
χ_{red}^2	1.03	0.98	0.75	1.23
W	31	34	37	40
X_{typ}	0.5322(1)	0.5320(2)	0.5312(2)	0.5306(1)
χ_{red}^2	0.95	1.25	1.19	0.80

Table 3.3: Numerical results on the typical two-point conductance.

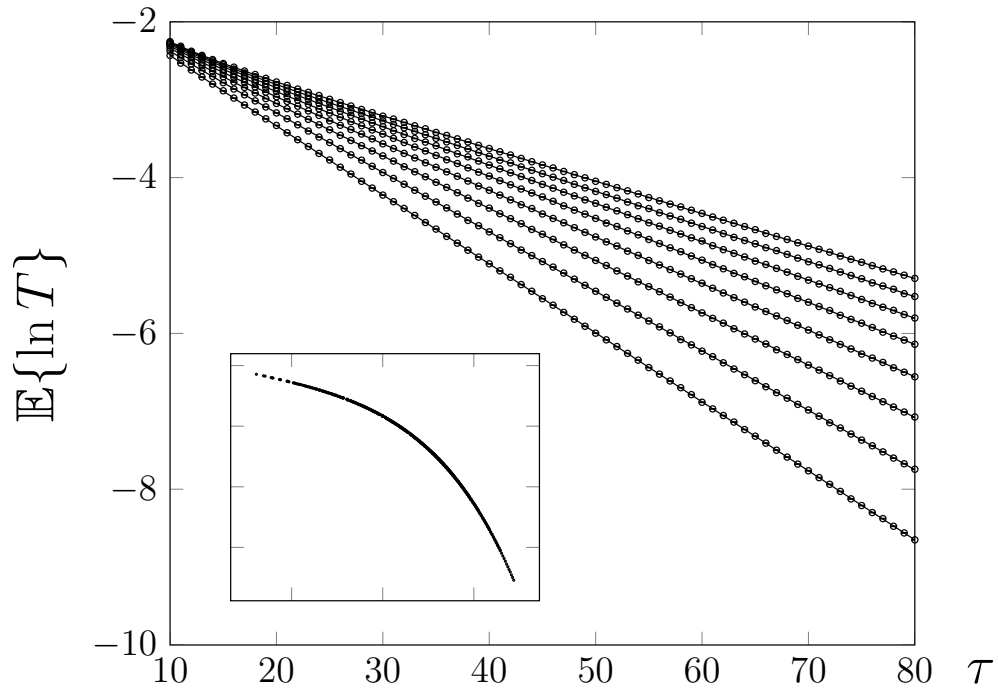


Figure 3.4: Numerical results for the typical two-point contact conductance. Inset: Collapse of the data under rescaling. For a discussion, see the main text.

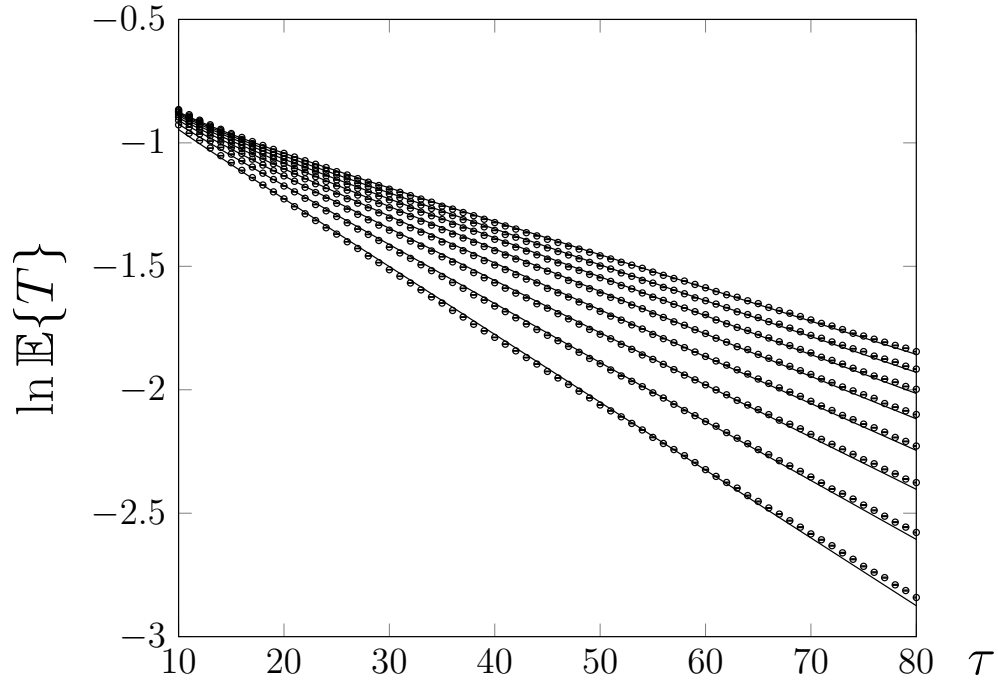


Figure 3.5: Numerical results for the two-point contact conductance. For a discussion, see main text.

3.2.2 First results on the observables A_1 , A_2 , A_3

In this section we recall and critically reinvestigate the numerical results we already presented in [BWZ14]. These were produced in a few weeks on the rather small cluster IBM THP which only allows for 250 parallel jobs, imposing restrictions on both ensemble and system size. We thus had to restrict ourselves to the setup we also used for the two-point contact conductance, i.e. $L = 400$, $19 \leq W \leq 40$ and $N = 10^6$ with distances $10 \leq \tau \leq 80$ between observation region R and contact region C . For the observables A_n with $n > 1$ we placed the links in C resp. R as close as possible, namely on equivalent links on plaquettes on top of each other. This setup is shown in figure 3.6 for $n = 2$.

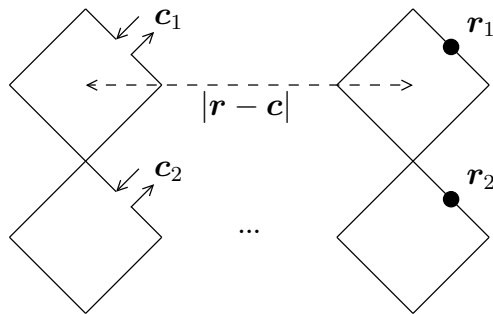


Figure 3.6: Setup for the contact and observation links (dots).

Figure 3.7 displays the goodness of fit for $n = 1, 2, 3$ and $|q| \leq 0.7$ using the prediction (3.7), which was not contained in our letter. For A_1 and A_2 the data are accurately described. The results for A_3 are still acceptable for most values of q and the goodness of fit is, depending on the circumference of the system, between one and two orders of magnitude smaller than the one we found for the two-point contact conductance. Figure 3.8 shows a comparison of numerical data and a fit for $A_3^{0.5}$. These results thus strongly imply that the observables A_n indeed show pure scaling behavior.

Notice that since A_n is defined as an $n \times n$ -determinant of a matrix containing only small elements, one has to proceed with caution especially in the range of negative q . The values of A_3 can underflow available data types, but at the same time the smallest values give the most important contributions for negative q . The extracted exponents should thus be used with more caution than the ones for $n = 1, 2$. We will come back to this point shortly.

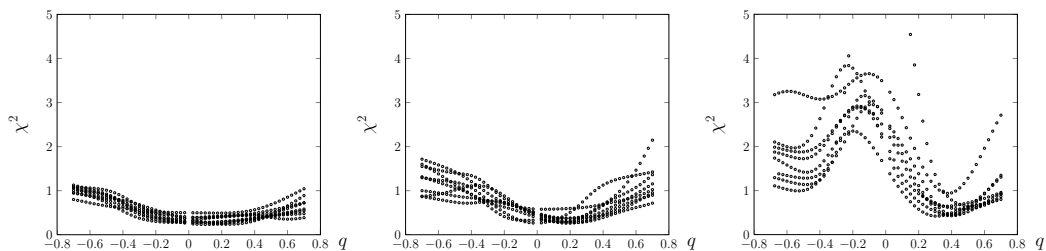


Figure 3.7: Goodness of fit for A_1 (left), A_2 (center), A_3 (right)

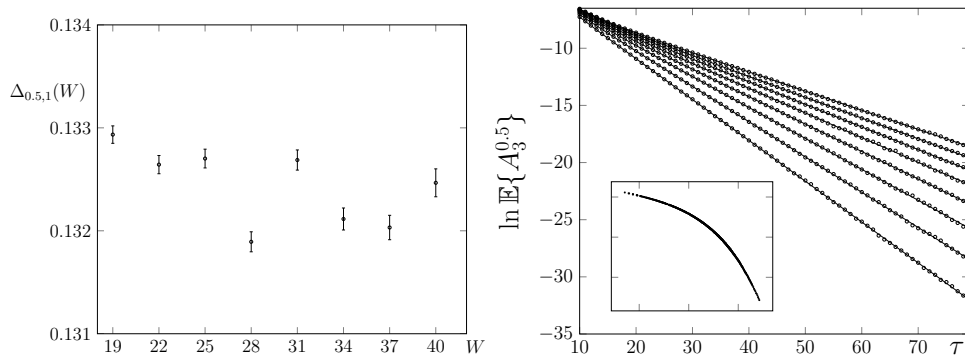


Figure 3.8: Fluctuations of the exponents $\Delta_{q,0.5}$ with the circumference (left), comparison of numerical data and fit for $A_3^{0.5}$ and a collapse plot of the curves (right, figure taken from [BWZ14]).

Already due to the narrow interval of circumferences a finite size scaling analysis for the data set at hand is doomed to fail, but also individually fitted scaling dimensions $\Delta_{q,n}(W)$ suffer from fluctuations as functions of the circumference, as is shown in the left part of figure 3.8. To specify a scaling dimension $\Delta_{q,n}$ we thus limited ourselves to giving the mean and standard deviation for each set of eight exponents $\{\Delta_{q,n}(19), \dots, \Delta_{q,n}(40)\}$. The collapse plot of $A_3^{0.5}$ in the inset of figure 3.8 was generated using such a mean exponent $\Delta_{0.5,3}$.

We now address the important question of (non-)parabolicity of the multifractal spectrum obtained from the numerical exponents $\Delta_{q,n}$. Recall from section 2.3 that the only terms allowed to appear here are eigenvalues of $\mathfrak{gl}_{2n|2n}$ Casimir invariants evaluated on the irreducible representation to which φ_q belongs. The expression (2.182) can be specified to this case to give

$$C_2(q, n) = nq(n - q) \quad C_4(q, n) = -n(q(n - q))^2 + n(n^2 - 1/2)q(n - q). \quad (3.8)$$

Up to quartic terms, the scaling dimensions then have the form

$$\Delta_{q,n} = a_0 C_2(q, n) + a_1 C_2(q, n)^2 + a_2 C_4(q, n). \quad (3.9)$$

On a microscopic level the theory should be described by a $\mathfrak{gl}_{2|2}$ -invariant Hamiltonian, so the parameters are independent of q and n and a fit of this ansatz to the numerical data has to explain all numerical exponents at once. To compare the results for $n = 1$ directly with the literature, we can convert this expression to the form

$$2\Delta_{q,1} = q(1 - q)(b_0 + b_1(q - 1/2))^2, \quad (3.10)$$

which has been used by Evers et al. [EMM08] and Obuse et al. [OSF⁺08]. Only two parameters b_0, b_1 appear here, because for $n = 1$ the eigenvalues $C_4(q, n)$ are not algebraically independent of $C_2(q, n)$ and $C_2(q, n)^2$. Recall from section 1.5 that the first set of authors found $b_0 = 0.1291(2)$, $b_1 = 0.0029(3)$ by a finite size scaling analysis of moments of the local density of states on squares of dimension up to 1000×1000 , while Obuse et al. found $b_0 = 0.1300$, $b_1 = 0.0032$ for the same

observable in cylindrical geometry without giving error bars. From our data we arrive at $b_0 = 0.1327(1)$, $b_1 = 0.0036(1)$ at $\chi_{\text{red}}^2 = 0.7$. Keeping in mind that we could not employ finite size scaling for our data and we are thus missing at least one type of systematic errors, these results are in reasonable accordance. Fitting our data sets for $n = 1$ and $n = 2$ simultaneously, we find $a_0 = 0.2637(2)$, $a_1 = 0.0028(1)$ and $a_2 = 0.0075(1)$ at $\chi_{\text{red}}^2 = 1.17 < 1.25 = \chi_{\nu,0.05}^2/\nu$. A comparison between data and fit is shown in figure 3.9. This fit is stable under restriction of the data set: If we discard, e.g., half of the data points by restricting to $|q| < 0.35$, this leaves the parameters unchanged while only increasing the statistical error in the last significant digit of a_1 by one, meaning that we can perfectly extrapolate to the rest of our data set. At the same time, we find it impossible to explain our data by a strictly parabolic spectrum, as the simultaneous fit shown in figure 3.10 reveals ($\chi_{\text{red}}^2 = 228$). Notice in particular that the finite size scaling results in [EMM08] imply that the exponents (for positive q) should decrease with system size, while improving the parabolic fit would require increasing exponents.

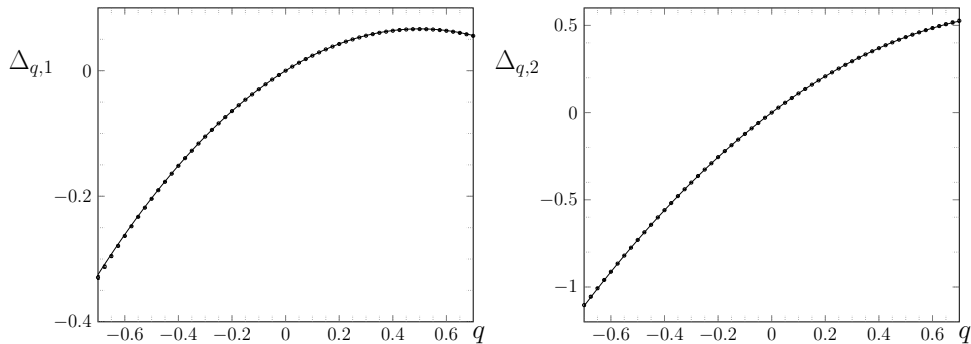


Figure 3.9: Simultaneous fit of $\Delta_{q,n}$ for $n = 1$ (left) and $n = 2$ (right) using the full ansatz (3.9)

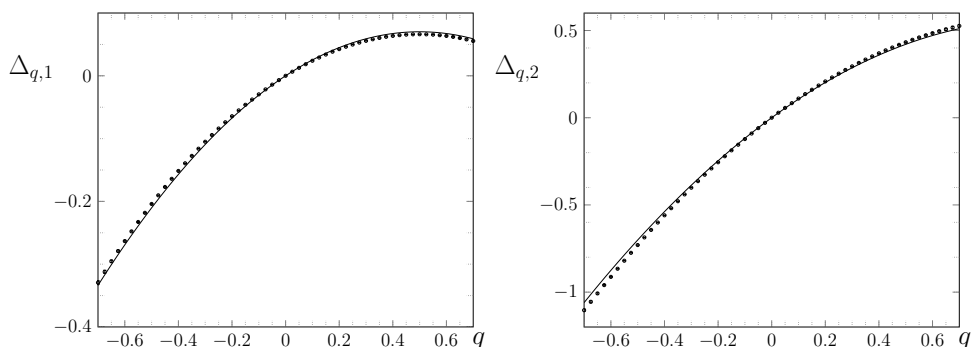


Figure 3.10: Simultaneous fit of $\Delta_{q,n}$ for $n = 1$ (left) and $n = 2$ (right), including only the quadratic term $C_2(q, n)$ in (3.9)

Although our discussion of the observable A_3^q indicates that our numerical exponents $\Delta_{q,3}$ should be taken with caution, the author was tempted to present a simultaneous fit of (3.9) for $n = 1, 2, 3$ in [BWZ14] which he wants to revise at this point. The plot presented there might give the visual impression that the fit is accurate, but

a reinvestigation shows that this is not the case at all ($\chi_{\text{red}}^2 = 110$). In fact, we cannot find an acceptable fit for this situation if we include only quartic terms. We thus take the stability of the fitting parameters for $n = 1$ under inclusion of $n = 2$ as a further indication for the fact that the results for A_3 should be regarded only as qualitative evidence for the pure scaling nature of the observables. Notice that this does not change the conclusion drawn in our letter: We still find it necessary to include quartic terms into the scaling dimension in order to explain the numerical data, but our closer look now reveals that the ansatz (3.9) gives a stable simultaneous fit for A_1 and A_2 in the range $|q| \leq 0.7$.

3.2.3 2+1-point functions

As a further test for conformal invariance, we checked in [BWZ14] whether the nontrivial prediction for the decay of the 2+1-point function (1.61), which we recall here for convenience,

$$\langle \phi_1(z_1, z_1^*) \phi_2(z_2, z_2^*) \phi_3(z_3, z_3^*) \rangle = \frac{C_{123}}{z_{12}^{\Delta_1 + \Delta_2 - \Delta_3} z_{13}^{\Delta_1 + \Delta_3 - \Delta_2} z_{23}^{\Delta_2 + \Delta_3 - \Delta_1}} \quad (3.11)$$

matches with numerical results. On the cylinder, the infinite-plane distances z_{ij} have to be replaced by the fitting function (3.7) evaluated at the appropriate points. Recall further that the term "2+1-point function" originates from the vertex model observables (2.121), where two highest weight operators are paired with one point contact.

We chose the setup displayed in figure 3.11. On a cylinder of length $L = 400$ and circumference $W = 50$ we fixed the contact at the center $(0|0)$. One observation point lies at $\mathbf{r}_1 = (\tau_1|0)$, the second one moves around the cylinder at the same horizontal distance $\mathbf{r}_2 = (\tau_1|\sigma_2)$, where we chose $\tau_1 = 10, 20, \dots, 60$. The observable we considered is $\mathbb{E}\{|\psi(\mathbf{r}_1)|^{0.5} |\psi(\mathbf{r}_2)|^{0.5}\}$, i.e. we chose $q_1 = q_2 = \frac{1}{4}$. The average was taken over $N = 10^6$ realizations of disorder. Since we multiplied two strongly fluctuating numbers at distant positions before carrying out the ensemble average, it is no surprise that the observable also suffers from large fluctuations if we choose larger values of q_i , but it turned out that our intermediate choice gives good results. Figure 3.12 shows a comparison between the numerical data and the prediction (1.61). We emphasize that the only fit parameter involved here is the non-universal lattice constant a (in which the constant C_{123} is absorbed), while we used the scaling dimensions determined in the previous section. Nevertheless, we get an impressive match ($\chi_{\text{red}}^2 = 0.8$), which provides further strong evidence for the pure scaling nature of the observables.

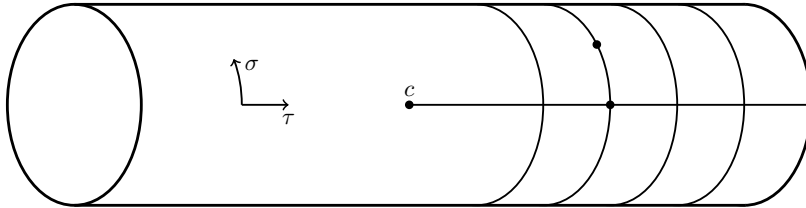


Figure 3.11: Numerical setup for the three-point function.

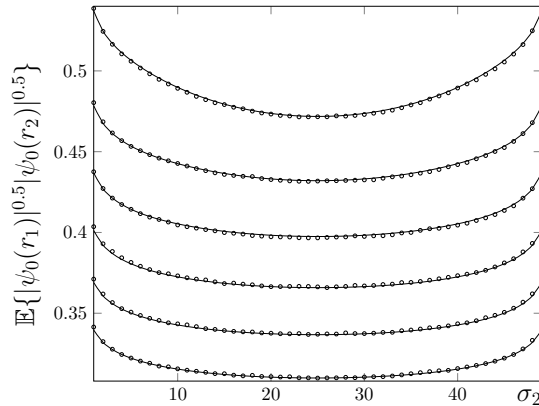


Figure 3.12: Match between numerical results and theoretical prediction for the $2 + 1$ -point function. Figure taken from [BWZ14].

3.2.4 An attempt at finite size scaling for A_1

In an attempt to improve the results presented in section 3.2.2, we change some aspects of the numerical simulation: The ensemble size is increased by one order of magnitude to $N = 10^7$ and we consider cylinders of size $15W \times W$ for $W = 5, 10, 20, 30, 40, 50, 60, 80, 100$. The contact is placed at distance $2W$ from the boundary, and we restrict the observation region to $aW \leq \tau \leq bW$. The reason for this choice are twofold. On one hand, the whole setup is just scaled up with the circumference, so that we always probe the same region of the fitting function's argument. On the other hand, placing the contact near the boundary is not expected to change the results, since amplitude reflected at the boundary might exit through the contact; only the observation region we still keep far from the boundary. We checked that for positive q different choices for $a < b$ give compatible results for the exponents within error bars, but the growth of the observable renders fluctuations in the data far away from the contact large for negative q , so that in these cases no fit is possible. This especially happens for the larger circumferences. We thus restrict the fits to the region $2W \leq \tau \leq 5W$, which captures sufficiently many points for the small circumferences but avoids large fluctuations at remote distances from the contact. The scaling dimensions $\Delta_{q,1}(W)$ are extracted as described in section 3.2.2. We then tried to fit them using the usual finite size scaling size with one irrelevant exponent

$$\Delta_{q,1}(W) = \Delta_{q,\infty} + \frac{a_q}{W^y}. \quad (3.12)$$

The results turn out to be discouraging: Only for $0 < q \leq 0.4$ is it possible to do such a fit at all. For smaller or larger q the fitting routine produces nonsensical irrelevant exponents less than 10^{-6} combined with asymptotic scaling dimensions $\Delta_{q,1,\infty} < -10^3$. The results for the former range are displayed in figure 3.13. The irrelevant exponents are clearly not constant within error bars, although there should be only one universal y independent of q . Dividing the asymptotic dimensions by the functional dependence $q(1-q)$ of the quadratic Casimir eigenvalue, parabolicity of the spectrum corresponds to a constant result which we do not find here; in fact

not even the symmetry of this reduced asymptotic dimension around $q = 1/2$ is recovered. We take these findings as an indication that the finite size scaling study of A_1 (and thus also for $n > 1$), at least using this approach, should be postponed until more computing power is available.

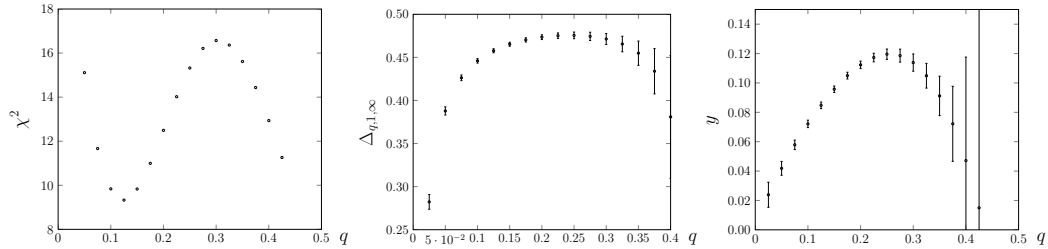


Figure 3.13: Finite size scaling analysis: Goodness of fit (left), Asymptotic exponents $\Delta_{q,1,\infty}$ (center), irrelevant exponents (right).

3.3 Results on the rectangle

As we mentioned in section 1.5, more pronounced fluctuations as well as a new set of multifractal dimensions arise near the surface of a critical system. If deviations from parabolicity are present in the spectrum, they are expected to be stronger near the surface. We take this as motivation to study the observable A_1 in rectangular geometry. More specifically, we consider a rectangle \mathcal{R} with corners in $\pm \frac{L}{2}, \pm \frac{L}{2} + iW$ shown in figure 3.14 as well as the rectangle \mathcal{R}' with L and W interchanged.

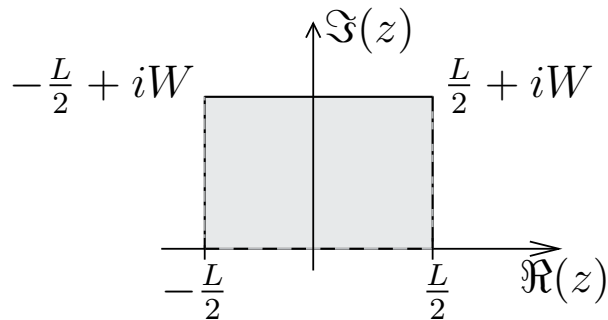


Figure 3.14: A rectangle in the upper half plane used for our simulations.

In terms of corner primary fields Ψ^c , we consider the ratio

$$Z(\tau) = \frac{\langle \Psi^c(-\frac{L}{2}) \Psi^c(\frac{L}{2}) \rangle_{\mathcal{R}}}{\langle \Psi^c(-\frac{W}{2}) \Psi^c(\frac{W}{2}) \rangle_{\mathcal{R}'}} \quad (3.13)$$

with $\tau = i\frac{W}{L}$. By the calculation presented in appendix A we expect it to scale with the aspect ratio as

$$Z(\tau) = 2^{-8\Delta^c} \left(\frac{\eta(\frac{\tau}{2})}{\eta(2\tau)} \right)^{16\Delta^c}, \quad (3.14)$$

where c indicates that we study a corner exponent. In our simulations we replace one field by a point contact sitting at the lower left corner of the network and the other by an observation link at the lower right corner. For \mathcal{R} we have $\mathbf{c} = -\frac{L}{2}$ and $\mathbf{r} = \frac{L}{2}$, i.e. the numerator of $Z(\tau)$ corresponds to $\mathbb{E}\{\psi(\mathbf{r})\}$, evaluated in a network of size $L \times W$.

To the best of our knowledge, a ratio of two-point functions in the corners of a rectangle has not been put on numerical trial in the literature so far. Obuse et al. [OSF⁺07b] considered the scaling of the local density of states near corners with different angles θ to provide numerical evidence for the relation

$$\Delta_q^\theta = \frac{\pi}{\theta} \Delta_q^s \quad (3.15)$$

predicted by conformal field theory. The exponent on the right-hand side refers to a straight edge and was studied in [OSF⁺08].

We first establish that the scaling behavior in (3.14) holds and then consider the finite size scaling of this observable on rectangles of fixed aspect ratio $L = 2W$. Since we work in a situation where $\theta = \frac{\pi}{2}$, we expect the exponent $h_q := 2\Delta_q^c$ to coincide with previous results on Δ_q^s .

3.3.1 Establishing the scaling behavior of $Z(\tau)$

Expecting large fluctuations, we are particularly careful in our try to establish the so-far unknown scaling behavior (3.14). Firstly, we choose a large nontrivial system, i.e. aspect ratio different from one, so that the observable is non-constant. As we discussed in section 1.7, scattering states obey the symmetry relation

$$\langle |\psi(\mathbf{r})|^{2q} \rangle = \langle |\psi(\mathbf{r})|^{2(1-q)} \rangle. \quad (3.16)$$

We use the restoration of this symmetry for $0 \leq q \leq 1$ in the numerical data as a criterion for an appropriate ensemble size. After checking on a very small system that this is possible at all, we went to a rather large network of size 200×100 . The results for ensemble sizes between 10^4 and 10^8 are shown in figure 3.15, from which we conclude that only the largest one is sufficient for our purposes. As a comparison, the symmetry in the bulk observable A_1^q on long cylinders is already restored at two orders of magnitude less.

Now, we consider networks of width $W = 100$ and varying length $L = 150, 175, \dots, 300$. The intention behind these large rectangles is that it lies in the very nature of the observable (3.14) to be studied on systems of different aspect ratios, so we want to keep possible changes in the exponent h due to finite size scaling with L as small as possible. Occupying 1500 CPU cores in parallel, the simulation of the largest system took ten days on CHEOPS. The comparison between the numerical data for $q = 0.5$ and the fitting function $Z^{0.5}(\tau)$ is shown in figure 3.17. The inset of this figure displays the goodness of fit in the range $0 \leq q \leq 0.5$. To get a comparable χ_{red}^2 by a generic fitting function one has to use a polynomial of degree 5—i.e. six parameters for seven data points—an ansatz which does not only overfit the data, but is also not capable of reproducing the trivial value $Z(i) = 1$ for $L = W$ as an extrapolation. The results thus clearly imply that our one-parameter fitting function (3.14) does indeed describe the observable correctly.

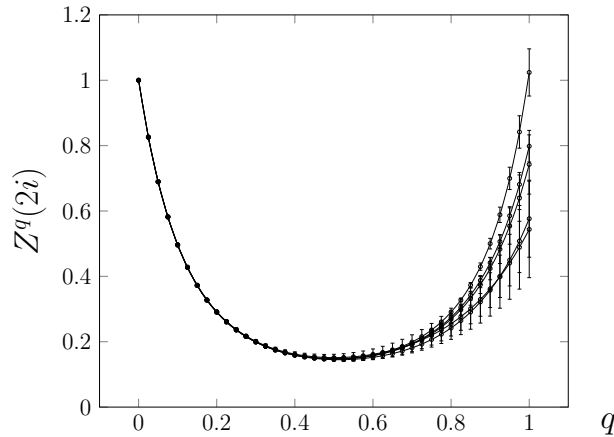


Figure 3.15: Comparison of different ensemble sizes, from 10^4 (bottom) to 10^8 (top). Solid lines are meant as a guide to the eye.

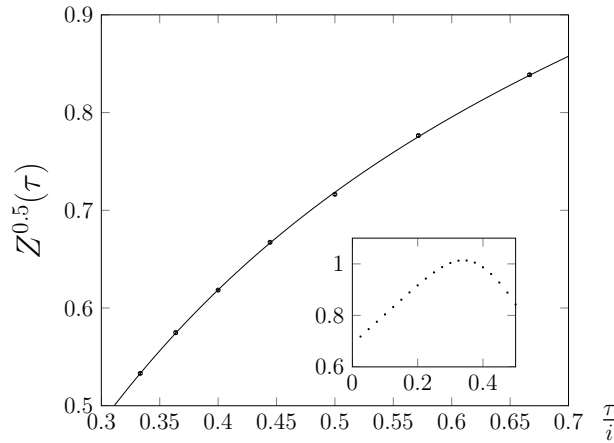


Figure 3.16: Numerical data and fit for $Z^{0.5}(\tau)$. Inset: χ_{red}^2 in the range $0 \leq q \leq 0.5$.

3.3.2 Finite size scaling on the rectangle

Now that we have numerically established (3.14) as the correct decay behavior of the observable $Z(\tau)$, we address the question of finite size scaling on the rectangle. In view of the large ensemble sizes needed and the desire to study at least one order of magnitude both in length and width of the rectangles under consideration, we decided to investigate the aspect ratio $\frac{1}{2}$ at an ensemble size of $N = 10^8$. The system widths we consider are $W = 5, 7, 10, 15, 20, 25, 30, 40, 50, 60, 80, 100$. Since $\tau = \frac{i}{2}$ is fixed, we can invert (3.14) for given q and W to extract the exponent $h_{q,W}$. For fixed q these data points are then fitted against the usual finite size scaling ansatz

$$h_q(W) = h_{q,\infty} + \frac{a_q}{W^{2y}}. \quad (3.17)$$

Notice that a_q is a non-universal parameter which may depend on q and we are only interested in the asymptotic exponents $h_{q,\infty}$ as well as the most important irrelevant exponent y . Both length and width are scaled up at constant ratio, thus a factor

of 2 appears in front of y . The goodness of fit of $h_q(W)$ for $|q| \leq 0.5$ lies between $0.8 \leq \chi_{\text{red}}^2 \leq 4.0$. Figure 3.17 shows a comparison between the numerical data $h_{q,W}$ and the fitted function, which indicates that the larger values of χ_{red}^2 are most likely due to underestimated statistical errors. However, from its definition (3.1) one immediately sees that switching from a 68% confidence interval $[y_i - \sigma_i, y_i + \sigma_i]$ to a 95% interval $[y_i - 2\sigma_i, y_i + 2\sigma_i]$ reduces χ_{red}^2 by a factor of 4. Another way for improving the goodness of fit would be to discard the data points for $W = 15$ and $W = 100$ as outliers, but this method is less controlled and also decreases the error bars on the parameters of interest. From a statistical viewpoint a goodness of fit measure up to 2 is still acceptable at $\alpha = 0.05$, the large value coming from the fact that less degrees of freedom are involved. But as we will see, even if we would declare this criterion as our impeccable source of truth and discard all asymptotic exponents outside $-0.05 \leq q \leq 0.3$, the statement on the form of the spectrum would remain unchanged.

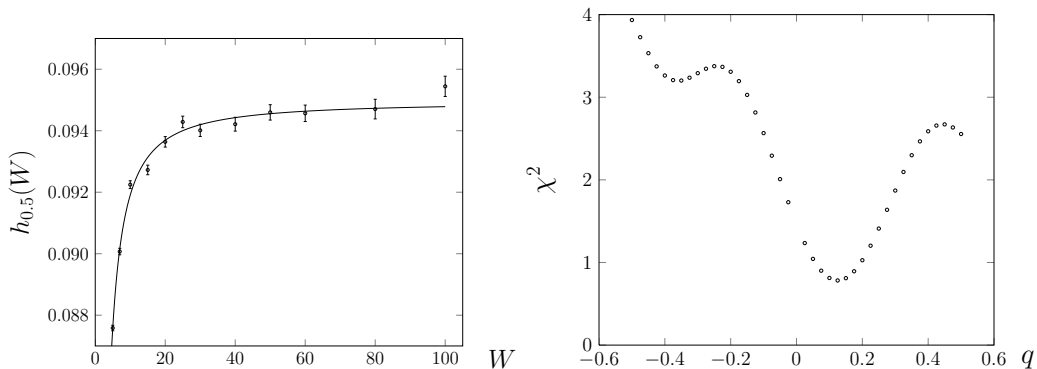


Figure 3.17: Comparison between numerical data and fit for $Z^{0.5}(\tau)$ (left), goodness of fit for the finite scaling ansatz (3.17) (right).

Although we cannot improve on the size of the error bars, our result $y \approx 0.6$ for the irrelevant exponent shown in figure 3.18 is compatible with the ones recently found [OBL⁺13]. This is quite remarkable, because there is no a priori reason why the leading irrelevant exponent in a corner should coincide with its bulk counterpart. Furthermore, in view of the problems discussed in section 3.2.4 it is also remarkable that we are able to get meaningful results in a finite size scaling analysis in the rectangular geometry. Here, the exponent in a system of dimension 100×50 differs by less than 1% from the fitted asymptotic one. We can only speculate that this may be related to the fact that the rectangular geometry could be studied exactly in a numerical simulation. This has to be seen in contrast to the infinite cylinder, for which we had to choose artificial reflecting boundaries.

Finally, we turn to the corner multifractal spectrum. Since we are interested in particular in the (non-)parabolicity of $h_{q,\infty}$ as a function of q , we divide by the functional dependence $q(1-q)$ of the quadratic term and consider

$$\tilde{h}(q) = \frac{h_{q,\infty}}{q(1-q)} = c_0 + c_1 \left(q - \frac{1}{2}\right)^2 + c_2 \left(q - \frac{1}{2}\right)^4 + \dots, \quad (3.18)$$

where the expansion matches the symmetry of the spectrum.

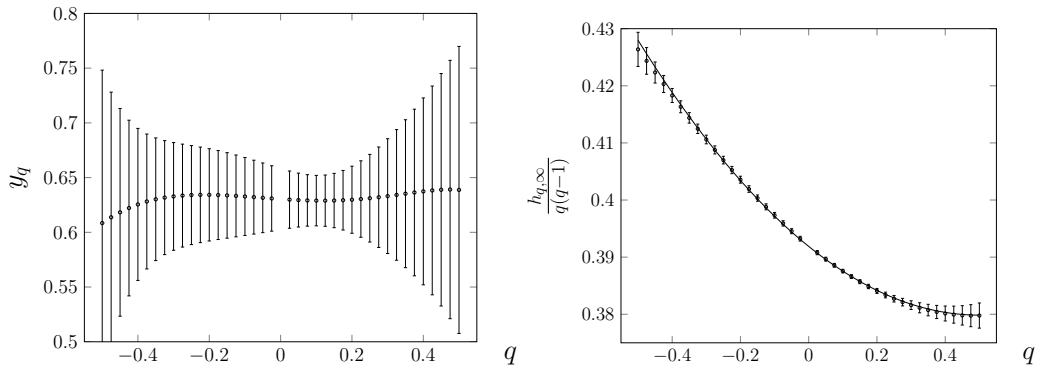


Figure 3.18: Irrelevant exponents obtained from fitting $h_q(W)$ (left), numerical data for $\tilde{h}(q)$ together with fit $0.37986 + 0.0481(q - \frac{1}{2})^2$ (right).

Firstly, parabolicity of the corner spectrum is clearly not in accordance with the numerical data shown in figure 3.18.

A two-parameter fit with $c_0 = 0.37986(4)$, $c_1 = 0.0481(1)$ gives a perfect explanation of the numerical data ($\chi_{\text{red}}^2 = 0.08$). Inclusion of the next order gives $c_0 = 0.37955(2)$, $c_1 = 0.0507(1)$ and $c_2 = -0.0035(1)$, but comes at the price of overfitting the data ($\chi_{\text{red}}^2 = 0.004$). Therefore, we accept the two-parameter fit. These results are in reasonable accordance with the ones found in [OSF⁺08], where the scaling of the local density of states, coarse-grained over strips of unit width along the boundaries, was investigated. In this case $c_0 = 0.370$ and $c_1 = 0.042$ was found without giving error bars. We interpret the plot shown in figure 3.19 as an indication that the ensemble size used by these authors was not sufficient to restore the symmetry of the spectrum. Our own results in figure 3.15 strongly imply that exponents for $q < \frac{1}{2}$ are far more trustworthy than the ones for $q > \frac{1}{2}$ when one employs a comparably small ensemble. Taking this into account the exponents show stronger deviations from parabolicity than the plotted solid curve implies. Recall that we consider reduced scaling dimensions, so a parabolic spectrum would correspond to a constant plot. The difference in the constant c_0 could come from the fact that a coarse-graining procedure of the local density of states along narrow strips along the boundary of the system was used, while in our case the contact and the observation links sit right at the corner of the system.

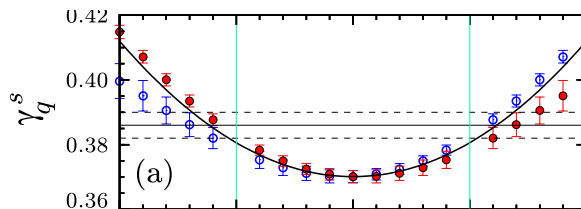


Figure 3.19: Surface exponents $\gamma_q^s = \Delta_q^s/(q(1-q))$, taken from [OSF⁺08]. Filled symbols represents numerical data, open symbols are reflected at the axis $q = 1/2$.

In conclusion, if we accept the extrapolation of the data to the continuum limit using the finite size scaling ansatz (3.17) we must infer that the corner multifractal

spectrum is not parabolic. Although no strong statement could be made about the connection between bulk and surface exponents for an arbitrary conformal field theory, deviations from parabolicity at the boundary at least rule out Wess-Zumino-Witten models for the bulk *and* the boundary at the same time [OSF⁺08].

Chapter 4

Summary and outlook

*Erstens kommt es anders,
und zweitens als man denkt.*
Wilhelm Busch

In this thesis we introduced a broad class of highest weight operators φ_q in the supersymmetric $\mathfrak{gl}_{2n|2n}$ vertex model and related their vertex model averages in the presence of vacuum projectors to open-network observables in the Chalker-Coddington model. Each individual constituent of the vertex model, called vertex model module, corresponds to a link in the network. The observables are built of local intensities of a basis of stationary scattering states, where the observation points correspond to the modules where the operators act and the point contacts correspond to the vacuum projectors.

Based on symmetry arguments, it was then natural to conjecture that our operators constitute lattice discretizations of a conformal field theory which emerges as the continuum limit of the network model. We thus expected the observables to feature pure scaling behavior with the distance between the region C of point contacts and the region R of observation links. If the model indeed describes the universal features of the integer quantum Hall plateau transition—at least it has been introduced with this intention and, apart from a comment in [NKS14], we are not aware of any serious doubts at this point—then our statements also hold true in this physical situation.

We presented strong numerical evidence in favor of the expected behavior by investigating the decay of the observables A_n in the presence of up to $n = 3$ point contacts in cylindrical geometry. Moreover, we found that the data for a 2+1-point function (two observation links and one contact) is in perfect agreement with predictions from conformal field theory. Due to limited computational resources we did not succeed in determining the asymptotic values of the multifractal exponents extracted from these simulations by finite size scaling. Nevertheless, we tried to use a fitting ansatz for the spectrum which included the three lowest order terms compatible with the symmetry. Fitting the results for $n = 1$ and $n = 2$ simultaneously, it is impossible to explain these numerical exponents using only a parabolic spectrum which is in accordance with previous results [EMM08][OSF⁺08].

Furthermore, we considered a rectangle of length L and width W with a point con-

tact in the lower left corner and observed A_1 in the lower right corner. The ratio of this observable and its counterpart for a rectangle with L and W interchanged is predicted by conformal field theory to be a ratio of Dedekind eta functions which depends only on the aspect ratio of the system. We established this scaling behavior numerically, which provides further strong evidence for the pure scaling nature of the observable A_1 . Finally, we used this result in order to study the finite size scaling of moments of A_1 on rectangles of constant aspect ratio $L = 2W$ up to $W = 100$ at an ensemble size of 10^8 . If the extrapolation of the numerical exponents to the continuum limit is accepted, it is necessary to include a non-parabolic term in the spectrum. This agrees with the results in [OSF⁺08].

We close this section by offering some directions for future work: The story we told in chapter 2 can be repeated for the network model in class C [KHA⁺99] which describes the spin quantum Hall transition. This model has link space \mathbb{C}^2 , i.e. two separate channels for each spin orientation. The deterministic part of the unitary time evolution is the same as in class A, independently for each channel, and additionally there is USp_2 -disorder mixing the channels. After disorder averaging one arrives at a $\mathfrak{sl}_{2|1}$ -vertex model.

From the perspective of mathematics it is desirable to gain a better understanding of the eigenspace representations to which the operators φ_q belong. Up to now nothing is known about reducibility or if these representations are related to a super generalization of conical distributions [H09].

The pure scaling nature of our observables in combination with our results on the spectrum raises the question of the corresponding continuum limit of the Chalker-Coddington network model. A first (numerical) step towards this goal could be made by calculating the operator product expansion coefficients from three- and four-point functions numerically. As these observables generally suffer from the large fluctuations of the scattering states, we were not able to carry out this program.

In a recent preprint [S14], Suslov showed that a set of consistency equations for the multifractal dimensions which follow from the heuristic reasoning presented in section 1.5 imply a strictly parabolic spectrum. The assumption that the moments of critical wavefunctions become essentially uncorrelated once the distance between the points is of order of the system size is wrong for our scattering states. Nevertheless, we will show how to arrive at the same set of consistency equations in [BWZ15].

Arguing along Suslov's lines then implies a strictly parabolic spectrum. However, the systems considered in simulations or in actual experiments are obviously different from the infinite plane: Our cylindrical geometries correspond to an annulus with reflecting boundaries, whereas the rectangle corresponds to the upper half plane. Although much work has been done to arrive at a conclusive answer, it remains unclear if "the observed deviations [from parabolicity] can be related with slow convergence to the thermodynamic limit" [S14] as Suslov claims to show in a preprint not published to date or if they are due to the very presence of boundaries. In view of the results on the boundary exponents, the author currently favors the latter interpretation.

Appendix A

Two-point function on the rectangle

In this appendix we relate the two-point function of two boundary conformal fields sitting on the real line, which is in this case regarded as the boundary of the upper half plane, to the two-point function of two primary fields in the corners of a rectangle. That the notions of conformal field theory generalize to this situation is not entirely obvious, but a detailed discussion of this fact does not contribute to the understanding of the following calculation. The interested reader is thus referred to the introductory article [C04].

The upper half plane \mathbb{H} (coordinate w) can be mapped conformally to a rectangle \mathcal{R} (coordinate z) by the Schwarz-Cristoffel-transformation

$$z = f(w) = \alpha \int_0^w \frac{1}{\sqrt{(1-t^2)(1-k^2t^2)}} dt, \quad \alpha \in \mathbb{R}. \quad (\text{A.1})$$

Specifically, the points $\pm\frac{1}{k}$, ± 1 on the real axis are mapped to the corners according to

$$f\left(\pm\frac{1}{k}\right) = \alpha(\pm K + iK') \quad f(\pm 1) = \pm\alpha K, \quad (\text{A.2})$$

where $K := K(k^2) = \frac{1}{\alpha} f(1)$ is the complete elliptic integral of first kind and $K' := K(1-k^2)$. By an appropriate choice of α and k we can arrange the length $L = 2\alpha K$ and width $W = \alpha K'$ to match prescribed values, see also figure A.1.

This goes as follows: Using $q := e^{2\pi i\tau}$, the Jacobi theta functions θ_i are defined as

$$\theta_2(\tau) = \sum_{n \in \mathbb{Z}} q^{\frac{1}{2}(n+\frac{1}{2})^2} \quad (\text{A.3})$$

$$\theta_3(\tau) = \sum_{n \in \mathbb{Z}} q^{\frac{1}{2}n^2} \quad (\text{A.4})$$

$$\theta_4(\tau) = \sum_{n \in \mathbb{Z}} (-1)^n q^{\frac{1}{2}n^2}. \quad (\text{A.5})$$

From the theory of special functions [AS72] it is known that for the special choice $k = \frac{\theta_2^2(2\tau)}{\theta_3^2(2\tau)}$ one has $K(k) = \frac{1}{2}\pi\theta_3^2(2\tau)$ and $K'(k) = -2i\tau K(k)$, i.e. $\tau = \frac{iK'}{2K}$. Thus,

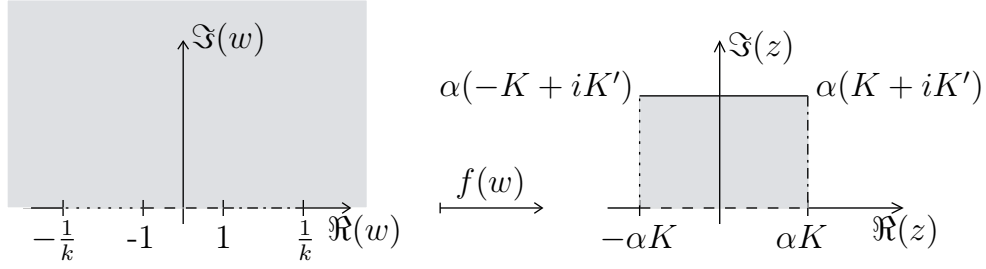


Figure A.1: The Schwarz-Cristoffel transformation from the upper half plane to a rectangle. Different line styles indicate which part of the real axis is mapped to which edge of the rectangle.

for $\tau = i\frac{W}{L}$ and $\alpha = \frac{L}{2K}$ we arrive at

$$f\left(\pm\frac{1}{k}\right) = \pm\frac{L}{2} + iW \quad f(\pm 1) = \pm\frac{L}{2}. \quad (\text{A.6})$$

The inverse transformation of (A.1) is given by the Jacobi elliptic function

$$w = \text{sn}\left(\frac{z}{\alpha}, k^2\right). \quad (\text{A.7})$$

For $x \in \left(-\frac{L}{2}, \frac{L}{2}\right)$, the derivative needed to transform correlators of boundary primary field from \mathbb{H} to \mathcal{R} is

$$(f'(w(x)))^{-h} = \alpha^{-h} \left((1 - \text{sn}\left(\frac{x}{\alpha}, k^2\right))^2 (1 - k^2 \text{sn}\left(\frac{x}{\alpha}, k^2\right))^2 \right)^{\frac{h}{2}} \quad (\text{A.8})$$

This expression vanishes as we approach the corners. More specifically, if we expand around $x = \pm\frac{L}{2}$ we find

$$(f'(w(x)))^{-h} = \alpha^{-2h} (1 - k^2)^h \left(z \pm \frac{L}{2} \right) + \mathcal{O}\left(\left(z \pm \frac{L}{2} \right)^2 \right). \quad (\text{A.9})$$

Since the primaries in the upper half plane are not supposed to vanish $w \rightarrow \pm 1$, one defines the corner primary fields to behave as $(z - z_c)\Psi^c(z_c)$, where the subscript stands for 'corner'. Using this definition the singularity of the Jacobian is canceled. In order to give a streamlined answer for the two-point function between two corners of \mathcal{R} we remind ourselves of the Dedekind eta function and its relation to Jacobi theta functions,

$$\eta(\tau) = q^{\frac{1}{24}} \prod_{n=1}^{\infty} (1 - q^n) = \left(\frac{\theta_2(\tau)\theta_3(\tau)\theta_4(\tau)}{2} \right)^{\frac{1}{3}}. \quad (\text{A.10})$$

Combining this with the transformation law for primaries (1.55), (A.8) and the

relation $K = \frac{\pi}{4}(\theta_3^2(\tau) + \theta_4^2(\tau))$ we arrive at

$$\begin{aligned}
\left\langle \Psi^c \left(-\frac{L}{2} \right) \Psi^c \left(\frac{L}{2} \right) \right\rangle_{\mathcal{R}} &= \alpha^{-4h} (1 - k^2)^{2h} \left| \frac{L}{2} - \left(-\frac{L}{2} \right) \right|^{-2h} \\
&= 2^{-2h} L^{-4h} (2K)^{4h} (1 - k^2)^{2h} \\
&= 2^{-2h} L^{-4h} 2^{4h} \left(\left(\frac{\pi}{4} (\theta_3^2(\tau) + \theta_4^2(\tau)^2) \right)^2 \frac{\theta_4^4(2\tau)}{\theta_3^4(2\tau)} \right)^{2h} \\
&= \left(\frac{\pi^2}{2} \right)^{4h} L^{-4h} \eta^{16h}(\tau) \eta^{-8h}(2\tau). \tag{A.11}
\end{aligned}$$

Notice that the appearance of the factor L^{-4h} is related to log-contributions to the free energy at the corners [CP88]. Again, as in the case of the cylinder, the presence of L introduced a non-universal lattice constant in the discretized setup we study using the network model. It is preferable to introduce a rectangle \mathcal{R}' which results from a rotation of \mathcal{R} by $\frac{\pi}{2}$ and to consider the ratio

$$Z(\tau) = \frac{\langle \Psi^c \left(-\frac{L}{2} \right) \Psi^c \left(\frac{L}{2} \right) \rangle_{\mathcal{R}}}{\langle \Psi^c \left(-\frac{W}{2} \right) \Psi^c \left(\frac{W}{2} \right) \rangle_{\mathcal{R}'}}. \tag{A.12}$$

The denominator is obtained from (A.11) by interchanging L and W :

$$\begin{aligned}
\left\langle \Psi^c \left(-\frac{W}{2} \right) \Psi^c \left(\frac{W}{2} \right) \right\rangle_{\mathcal{R}'} &= \left(\frac{\pi^2}{2} \right)^{4h} W^{-4h} \eta^{16h} \left(-\frac{1}{\tau} \right) \eta^{-8h} \left(-\frac{2}{\tau} \right) \\
&= \left(\frac{\pi^2}{2} \right)^{4h} W^{-4h} (-i\tau)^{4h} 2^{4h} \eta^{16h}(\tau) \eta^{-8h} \left(\frac{\tau}{2} \right) \\
&= \left(\frac{\pi^2}{2} \right)^{4h} \left(\frac{L}{2} \right)^{4h} \eta^{16h}(\tau) \eta^{-8h} \left(\frac{\tau}{2} \right) \tag{A.13}
\end{aligned}$$

where the modular property $\eta \left(-\frac{1}{\tau} \right) = \sqrt{-i\tau} \eta(\tau)$ was used. We thus arrive at the result

$$Z(\tau) = 2^{-4h} \left(\frac{\eta \left(\frac{\tau}{2} \right)}{\eta(2\tau)} \right)^{8h}. \tag{A.14}$$

Notice that we concentrated on the holomorphic sector, so in order to relate h to known results of boundary or corner spectra a factor of 2 has to be taken into account.

Appendix B

Program code

```
/* wfamp.cpp
compile using 'icpc wfamp.cpp solver.cpp generate_coefficient_matrix.cpp
bubblesort.cpp mtrand.cpp complex_functions.cpp getMilliCount.cpp
-lmkl_intel_lp64 -lmkl_core -lmkl_sequential -lpthread -O3 -o wfamp.out'

./wfamp.out L W N nc bc does the following for N disorder realizations:

- set up the (random phase) unitary time evolution operator U for a
Chalker-Coddington network with boundary conditions bc
(0:cylinder, 1:rectangle, 2:torus)
consisting of L*W plaquettes as a sparse matrix and calculate QU-1,
where Q is the projector
 $1 - \sum_i^{nc} |m_i\rangle\langle m_i|$  and  $m_i$  are the positions
of nc point contacts
(this is done by generate_coefficient_matrix)

- solve the linear system  $(QU-1)|\Psi_i\rangle = |m_i\rangle$  for the scattering wavefunction  $|\Psi_i\rangle$ 
(Notice that the results do not change by considering QU-1 instead of 1-QU,
since they are related by a global phase factor  $\exp(i\pi)$ . This way,
many minus signs are avoided in the code.)
(this is done by solve_unsym_complex)

- generate and print the absolute value squared of the desired wave function
amplitudes,
here for plaquettes with horizontal separation between 1 and 100 from m

A C++-port by Bedaux (http://www.bedaux.net/mtrand/mtrand.zip,
retrieved 13/10/02) of the original Mersenne Twister code by Matsumoto
and Nishimura (ACM Transactions on Modeling and Computer Simulation,
Vol. 8, No. 1, January 1998, pp. 3-30) is used for random number generation.

The MKL solver PARDISO is used to solve the linear system, initialization
and calls are adapted from the PARDISO project manual
(http://www.pardiso-project.org/manual/pardiso\_unsym\_complex.cpp, retrieved
13/09/20)
*/

#include <iostream>
#include <mkl_types.h>
#include <mkl.h>
#include <mkl_spblas.h>
#include "mtrand.h"
#include "generate_coefficient_matrix.h"
#include "generate_observable.h"
#include "solver.h"
#include "getMilliCount.h"
```

```

using namespace std;

int main(int argc, const char* argv[])
{
    int i,bc(1),nc(1),ensemblesize(1),L(200),W(1),run(0),n(800);

    switch (argc)
    {
        case 6:
            // boundary conditions
            bc=int(atof(argv[5]));
            // number of contacts, has to be smaller than 4.
            nc=int(atof(argv[4]));
            ensemblesize=int(atof(argv[3]));
            W = int(atof(argv[2]));
            L = int(atof(argv[1]));
            break;
        default:
            cout << "usage: ./wfamp.out_L_W_N_nc_bc" << endl;
            cout << "L: system length (plaquette units)" << endl;
            cout << "W: system width (plaquette units)" << endl;
            cout << "N: ensemble size" << endl;
            cout << "nc: number of contact (1,2,3)" << endl;
            cout << "bc: boundary conditions (0:cylinder, 1:rectangle, 2:torus)" << endl;
            return 0;
    }

    if(bc>2)
    {
        cout << "invalid boundary conditions" << endl;
        return 0;
    }
    if(nc>3||nc==0)
    {
        cout << "use at least one and less than four contacts" << endl;
        return 0;
    }

    int *m = new int[nc];

    // Position of first point contact is m[0]. m[0]=2*L is the center of first row.
    for(i=0;i<nc;i++)
    {
        m[i]=2*L+4*L*i;
    }

    n = 4*L*W; // number of links

    // Number of nonzero entries in 1-QU.
    // For n' contacts this is 3*n-2*n'.
    // (Every link scatters into (at most) two links,
    // the diagonal has n entries, and 2*n' are deleted
    // to account for the presence of point contacts.
    int nonzeroes=3*n-2*nc;

    // initialization of MT19937 by system time in milliseconds
    MTRand drand(getMilliCount());

    while(run<ensemblesize)
    {
        // Solution vector psi and rhs of the system
        // (QU-1)|Psi>=|m>
        // To calculate a basis of scattering states |Psi_k>
        // in presence of n' contacts, n' systems
        // (QU-1)|Psi_k>=|m_k>
        // have to be solved; notice that the coefficient matrix

```

```

// does not change. psi and rhs are
// vectors with nn' entries and when PARDISO is finished
// |\Psi_k> is stored in psi[(k-1)n] ... psi[kn-1].
MKL_Complex16 *psi = new MKL_Complex16[n*nc]; // solution vector
MKL_Complex16 *rhs = new MKL_Complex16[n*nc]; // rhs of linear system

for(i=0;i<n*nc;i++)
{
    psi[i].real=0;psi[i].imag=0;
    rhs[i].real=0; rhs[i].imag=0;
}

for(i=0;i<nc;i++)
{
    rhs[m[i]+n*i].real=1;
}

// Ucsr, iU, jU stores QU-1 in compressed row storage form
MKL_Complex16 *Ucsr = new MKL_Complex16[nonzeroes];
int *jU = new int[nonzeroes];
int *iU = new int[n+1];

generate_coefficient_matrix(bc, n, nonzeroes, nc, m, L, W, iU, jU, Ucsr,
    drand);

solve_unsym_complex(n,nc,Ucsr,iU,jU,rhs,psi);

int max_hdist = 100; // maximal horizontal distance between point contact
    and observation
double *psi_abs2 = new double[max_hdist]; // stores |\Psi|^2

generate_observable(n, nc, max_hdist, m, psi, psi_abs2);

// Output.

for(i=1;i<=max_hdist;i++)
{
    cout << i << "_" << psi_abs2[i] << endl;
}

run++;

delete [] rhs;
delete [] iU;
delete [] jU;
delete [] Ucsr;
delete [] psi;
delete [] psi_abs2;
} // end while

return 0;
}

// getMilliCount.cpp
#include <sys/timeb.h>

int getMilliCount(){
    timeb tb;
    ftime(&tb);
    int nCount = tb.millitm + (tb.time & 0xffff) * 1000;
    return nCount;
}

```

```

/* solver.cpp
The MKL solver PARDISO is used to solve the linear system, initialization
and calls are adapted from the PARDISO project manual
(http://www.pardiso-project.org/manual/pardiso\_unsym\_complex.cpp, retrieved
13/09/20) */

#include <iostream>
#include "mkl_types.h"
#include <mkl.h>

using namespace std;

void solve_unsym_complex(int n, int nrhs, MKL_Complex16 *A, int *iA, int *jA,
    MKL_Complex16 *rhs, MKL_Complex16 *solution){

    // PARDISO variables
    MKL_INT      mtype = 13;          /* Complex unsymmetric matrix */

    /* Internal solver memory pointer pt,
    /* 32-bit: int pt[64]; 64-bit: long int pt[64]
    /* or void *pt[64] should be OK on both architectures
    void      *pt[64];
    /* Pardiso control parameters.
    MKL_INT      iparm[64];
    MKL_INT      maxfct, mnum, phase, error, msglvl;

    MKL_Complex16 ddum;          /* Double dummy */
    MKL_INT      idum;          /* Integer dummy.

    /* ----- */
    /* .. Setup Pardiso control parameters.
    /* ----- */
    for (int i = 0; i < 64; i++) {
        iparm[i] = 0;
    }
    iparm[0] = 1; /* No solver default */
    iparm[1] = 2; /* Fill-in reordering from METIS */
    /* Numbers of processors, value of OMP_NUM_THREADS */
    iparm[2] = 1;
    iparm[3] = 0; /* No iterative-direct algorithm */
    iparm[4] = 0; /* No user fill-in reducing permutation */
    iparm[5] = 0; /* Write solution into x */
    iparm[6] = 0; /* Not in use */
    iparm[7] = 2; /* Max numbers of iterative refinement steps */
    iparm[8] = 0; /* Not in use */
    iparm[9] = 13; /* Perturb the pivot elements with 1E-13 */
    iparm[10] = 1; /* Use nonsymmetric permutation and scaling MPS */
    iparm[11] = 0; /* Not in use */
    iparm[12] = 1; /* Maximum weighted matching algorithm is switched-on (
        default for non-symmetric) */
    iparm[13] = 0; /* Output: Number of perturbed pivots */
    iparm[14] = 0; /* Not in use */
    iparm[15] = 0; /* Not in use */
    iparm[16] = 0; /* Not in use */
    iparm[17] = -1; /* Output: Number of nonzeros in the factor LU */
    iparm[18] = -1; /* Output: Mflops for LU factorization */
    iparm[19] = 0; /* Output: Numbers of CG Iterations

    maxfct = 1;          /* Maximum number of numerical factorizations.
    mnum = 1;          /* Which factorization to use.

    msglvl = 0;          /* Print statistical information
    error = 0;          /* Initialize error flag

    /* ----- */
    /* .. Initialize the internal solver memory pointer. This is only

```

```

/* necessary for the FIRST call of the PARDISO solver. */
/* ----- */
for (int i = 0; i < 64; i++) {
    pt[i] = 0;
}

/* ----- */
/* .. Reordering and Symbolic Factorization. This step also allocates */
/* all memory that is necessary for the factorization. */
/* ----- */
phase = 11;

PARDISO (pt, &maxfct, &mnum, &mtype, &phase,
         &n, A, iA, jA, &idum, &nrhs,
         iparm, &msglvl, &ddum, &error);

if (error != 0) {
    cout << "ERROR_during_symbolic_factorization:_ " << error << endl;
    exit(1);
}

/* ----- */
/* .. Numerical factorization. */
/* ----- */
phase = 22;

PARDISO (pt, &maxfct, &mnum, &mtype, &phase,
         &n, A, iA, jA, &idum, &nrhs,
         iparm, &msglvl, &ddum, &error);

if (error != 0) {
    cout << "ERROR_during_numerical_factorization:_ " << error << endl;
    exit(2);
}

/* ----- */
/* .. Back substitution and iterative refinement. */
/* ----- */
phase = 33;

iparm[7] = 1;      /* Max numbers of iterative refinement steps. */

PARDISO (pt, &maxfct, &mnum, &mtype, &phase,
         &n, A, iA, jA, &idum, &nrhs,
         iparm, &msglvl, rhs, solution, &error);

if (error != 0) {
    cout << "ERROR_during_solution:_ " << error << endl;
    exit(3);
}

/* ----- */
/* .. Termination and release of memory. */
/* ----- */
phase = -1;      /* Release internal memory. */

PARDISO (pt, &maxfct, &mnum, &mtype, &phase,
         &n, A, iA, jA, &idum, &nrhs,
         iparm, &msglvl, &ddum, &error);
}

```

```

/* generate_observable.cpp
Generate  $|\Psi(x)|^2$  for horizontal distances
between  $x=1$  and  $x=\text{max\_hdist}$  from point contact region.
For more than one contact, LU decomposition is used
to calculate the determinants.*/

#include <mkl_types.h>
#include <mkl.h>
#include <mkl_spblas.h>
#include "complex_functions.h"

void generate_observable(int n, int nc, int max_hdist, int m[], MKL_Complex16 *psi
, double *psi_abs2)
{
    int i;
    switch(nc)
    {
        case 1:
            for(i=1;i<=max_hdist;i++)
            {
                psi_abs2[i]=psi[m[0]+4*i].real*psi[m[0]+4*i].real+psi[m[0]+4*i].
                    imag*psi[m[0]+4*i].imag;
            }
            break;

        case 2:
            for(i=1;i<=max_hdist;i++)
            {
                MKL_Complex16 A[]={ psi[m[0]+4*i], psi[m[1]+4*i],
                    psi[m[0]+4*i+n], psi[m[1]+4*i+n]
                };
                int k=2;
                int INFO;
                int LWORK=10*k;
                int *permutations = new int[2*k];
                zgetrf_( &k, &k, A , &k, permutations , &INFO );
                psi_abs2[i]=cabs2(cmult(A[0],A[3]));
                delete [] permutations;
            }
            break;

        case 3:
            for(i=1;i<=max_hdist;i++)
            {
                MKL_Complex16 A[]={ psi[m[0]+4*i], psi[m[1]+4*i], psi[m[2]+4*i],
                    psi[m[0]+4*i+n], psi[m[1]+4*i+n], psi[m[2]+4*i+n],
                    psi[m[0]+4*i+2*n], psi[m[1]+4*i+2*n], psi[m[2]+4*i+2*n]
                };
                int k=3;
                int INFO;
                int LWORK=10*k;
                int *permutations = new int[2*k];
                zgetrf_( &k, &k, A , &k, permutations , &INFO );
                psi_abs2[i]=cabs2(cmult(cmult(A[0],A[4]),A[8]));
                delete [] permutations;
            }
            break;
    }
}

```

```

\* generate_coefficient_matrix.cpp
Generates the coefficient matrix of the linear system
of equations for different boundary conditions. *\
#include <iostream>
#include <mkl_types.h>
#include <mkl.h>
#include <math.h>
#include "mtrand.h"
#include "bubblesort.h"

void generate_coefficient_matrix(int bc, int n, int nonzeroes, int nc, int m[],
    int L, int W, int *iU, int *jU, MKL_Complex16 *Ucsr, MTRand &drand){
    int i, j, k, x, y;
    MKL_Complex16 z1;
    double randomphase(0);

    // Ucoo,rowind,colind stores U in coordinate form
    MKL_Complex16 *Ucoo = new MKL_Complex16[nonzeroes];
    int *rowind = new int[nonzeroes];
    int *colind = new int[nonzeroes];

    // U2coo,rowind2,colind2 stores QU-1 in coordinate form
    MKL_Complex16 *U2coo = new MKL_Complex16[nonzeroes];
    int *rowind2 = new int[nonzeroes];
    int *colind2 = new int[nonzeroes];

    int count=0;

    bool not_at_contact = true;

    switch(bc)
    {
    case 0: //cylinder
        for(y=0;y<W;y++)
        {
            for(x=0;x<L;x++)
            {
                for(k=0;k<4;k++)
                {

                    i=4*L*y+4*x+k;
                    randomphase=2*M_PI*drand(); // random phase, distributed
                        uniformly on [0,2*pi)
                    z1.real = cos(randomphase)/sqrt(2);
                    z1.imag = sin(randomphase)/sqrt(2);
                    switch(k)
                    {
                    case 0: // scattering into upper right link on plaquette
                        at (x|y)

                    if(x!=L-1)
                    {
                        rowind[count]=i; colind[count]=i+1; Ucoo[count].real = -z1
                            .real; Ucoo[count].imag= -z1.imag; count++;
                        rowind[count]=i; colind[count]=i+7; Ucoo[count] = z1;
                            count++;
                    }
                    else // rightmost column
                    {
                        // Only link type 1 on plaquette (L-1|y) contributes (
                            reflecting bc)
                        rowind[count]=i; colind[count]=i+1; Ucoo[count].real = -
                            sqrt(2)*z1.real; Ucoo[count].imag= -sqrt(2)*z1.imag;
                            count++;
                        // No scattering from leftmost column
                        rowind[count]=i; colind[count]=i+7-4*L; Ucoo[count].real =
                            0; Ucoo[count].imag = 0;count++;
                    }
                }
            }
        }
    }
}

```

```

    }
    break;

    case 1: // lower right
    rowind[count]=i; colind[count]=i+1; Ucoo[count] = z1;
        count++;
    if (y!=W-1)
    {
    rowind[count]=i; colind[count]=i-1+4*L; Ucoo[count] = z1;
        count++;
    }
    else // last row receives contribution from first row (pbc
        )
    {
    rowind[count]=i; colind[count]=i-1-4*L*(W-1); Ucoo[count]
        = z1; count++;
    }
    break;

    case 2: // lower left
    if (x!=0)
    {
    rowind[count]=i; colind[count]=i+1; Ucoo[count] = z1;
        count++;
    rowind[count]=i; colind[count]=i-5; Ucoo[count] = z1;
        count++;
    }
    else // Only link type 3 on plaquette (0|y+1) contributes
    {
    rowind[count]=i; colind[count]=i+1; Ucoo[count].real =
        sqrt(2)*z1.real; Ucoo[count].imag = sqrt(2)*z1.imag;
        count++;
    rowind[count]=i; colind[count]=i-5+4*L; Ucoo[count].real =
        0; Ucoo[count].imag = 0; count++;
    }
    break;

    case 3: // upper left
    rowind[count]=i; colind[count]=i-3; Ucoo[count] = z1;
        count++;
    if (y!=0)
    {
    rowind[count]=i; colind[count]=i-1-4*L; Ucoo[count].real =
        -z1.real; Ucoo[count].imag= -z1.imag; count++;
    }
    else // first row receives contribution from last row
    {
    rowind[count]=i; colind[count]=i-1+4*L*(W-1); Ucoo[count].
        real = -z1.real; Ucoo[count].imag=-z1.imag; count++;
    }
    break;

        } // end switch(k)
    } // end for(k)
} // end for(y)
} // end for(x)
break;
case 1: // rectangle
for (y=0; y<W; y++)
{
for (x=0; x<L; x++)
{
for (k=0; k<4; k++)
{
i=4*L*y+4*x+k;
randomphase=2*M_PI*drand(); // random phase, distributed
uniformly on [0,2*pi)

```

```

z1.real = cos(randomphase)/sqrt(2);
z1.imag = sin(randomphase)/sqrt(2);
switch(k)
{
case 0:

    if(x!=L-1)
    {
rowind[count]=i; colind[count]=i+1; Ucoo[count].real = -z1
    .real; Ucoo[count].imag= -z1.imag; count++;
rowind[count]=i; colind[count]=i+7; Ucoo[count] = z1;
    count++;
    }
    else
    {
rowind[count]=i; colind[count]=i+1; Ucoo[count].real = -
    sqrt(2)*z1.real; Ucoo[count].imag= -sqrt(2)*z1.imag;
    count++;

rowind[count]=i; colind[count]=i+7-4*L; Ucoo[count].real =
    0; Ucoo[count].imag = 0; count++;
    }
    break;

case 1:

rowind[count]=i; colind[count]=i+1; Ucoo[count] = z1;
    count++;

    if(y!=W-1)
    {
rowind[count]=i; colind[count]=i+1; Ucoo[count] = z1;
    count++;
rowind[count]=i; colind[count]=i-1+4*L; Ucoo[count] = z1;
    count++;
    }
    else
    {
rowind[count]=i; colind[count]=i+1; Ucoo[count].real =
    sqrt(2)*z1.real; Ucoo[count].imag = sqrt(2)*z1.imag;
    count++;
rowind[count]=i; colind[count]=i-1-4*L*(W-1); Ucoo[count].
    real = 0; Ucoo[count].imag=0; count++;
    }
    break;

case 2:

    if(x!=0)
    {
rowind[count]=i; colind[count]=i+1; Ucoo[count] = z1;
    count++;
rowind[count]=i; colind[count]=i-5; Ucoo[count] = z1;
    count++;
    }
    else
    {
rowind[count]=i; colind[count]=i+1; Ucoo[count].real =
    sqrt(2)*z1.real; Ucoo[count].imag = sqrt(2)*z1.imag;
    count++;
rowind[count]=i; colind[count]=i-5+4*L; Ucoo[count].real =
    0; Ucoo[count].imag = 0; count++;
    }
    break;

case 3:

```

```

        if (y!=0)
        {
            rowind[count]=i; colind[count]=i-3; Ucoo[count] = z1;
            count++;
            rowind[count]=i; colind[count]=i-1-4*L; Ucoo[count].real =
                -z1.real; Ucoo[count].imag= -z1.imag; count++;
        }
        else
        {
            rowind[count]=i; colind[count]=i-3; Ucoo[count].real =
                sqrt(2)*z1.real; Ucoo[count].imag = sqrt(2)*z1.imag;
            count++;
            rowind[count]=i; colind[count]=i-1+4*L*(W-1); Ucoo[count].
                real = 0; Ucoo[count].imag=0; count++;
        }
        break;
    } // end switch(k)
} // end for(k)
} // end for(y)
} // end for(x)
break;
case 2: //torus
for (y=0;y<W;y++)
{
    for (x=0;x<L;x++)
    {
        for (k=0;k<4;k++)
        {
            i=4*L*y+4*x+k;
            randomphase=2*M_PI*drand(); // random phase, distributed
                uniformly on [0,2*pi)
            z1.real = cos(randomphase)/sqrt(2);
            z1.imag = sin(randomphase)/sqrt(2);
            switch(k)
            {
                case 0:

                rowind[count]=i; colind[count]=i+1; Ucoo[count].real = -z1
                    .real; Ucoo[count].imag= -z1.imag; count++;
                if (x!=L-1)
                {
                    rowind[count]=i; colind[count]=i+7; Ucoo[count] = z1;
                    count++;
                }
                else
                {
                    rowind[count]=i; colind[count]=i+7-4*L; Ucoo[count] = z1;
                    count++;
                }
                break;

                case 1:

                rowind[count]=i; colind[count]=i+1; Ucoo[count] = z1;
                count++;

                if (y!=W-1)
                {
                    rowind[count]=i; colind[count]=i-1+4*L; Ucoo[count] = z1;
                    count++;
                }
                else
                {
                    rowind[count]=i; colind[count]=i-1-4*L*(W-1); Ucoo[count]
                        = z1; count++;
                }
            }
        }
    }
}

```

```

    }
    break;

    case 2:

    rowind[count]=i; colind[count]=i+1; Ucoo[count] = z1;
    count++;

    if(x!=0)
    {
    rowind[count]=i; colind[count]=i-5; Ucoo[count] = z1;
    count++;
    }
    else
    {
    rowind[count]=i; colind[count]=i-5+4*L; Ucoo[count] = z1;
    count++;
    }
    break;

    case 3:

    rowind[count]=i; colind[count]=i-3; Ucoo[count] = z1;
    count++;

    if(y!=0)
    {
    rowind[count]=i; colind[count]=i-1-4*L; Ucoo[count].real =
    -z1.real; Ucoo[count].imag= -z1.imag; count++;
    }
    else
    {
    rowind[count]=i; colind[count]=i-1+4*L*(W-1); Ucoo[count].
    real = -z1.real; Ucoo[count].imag=-z1.imag; count++;
    }
    break;

    } // end switch(k)
} // end for(k)
} // end for(y)
} // end for(x)
break;
}

// QU is calculated from U by deleting the rows corresponding to the
contacts
count=0;
for(i=0;i<2*n;i++)
{
    for(j=0;j<nc;j++)
    {
        if(rowind[i]==m[j]){ not_at_contact=false; }
    }
    if(not_at_contact)
    {
        rowind2[count]=rowind[i]; colind2[count]=colind[i]; U2coo[count]=Ucoo[
        i];
        count++;
    }
    not_at_contact=true;
}

// fill in -1 on the diagonal
count=0;
for(i=nonzeroes-n;i<nonzeroes;i++)

```

```

    {
        rowind2[i]=count; colind2[i]=count; U2coo[i].real=-1; U2coo[i].imag=0;
        count++;
    }

    // Convert U2c00, rowind2, colind2 to column-compressed form Ucsr, jU, iU
    // Notice that mkl_zcsrcoo does not care if the column indices
    // are increasing for any given row, but this is required by the solver.
    // For a description of the format see p.8 of the PARDISO manual
    // http://www.pardiso-project.org/manual/manual.pdf
    int *job= new int[6];
    int *info = new int[1];
    job[0]=1; job[1]=0; job[2]=0; job[3]=0; job[4]=nonzeroes; job[5]=3;
    mkl_zcsrcoo(job, &n, Ucsr, jU, iU, &nonzeroes, U2coo, rowind2, colind2,
        info);
    delete [] job;
    delete [] info;

    // PARDISO routines require the column indices in jU to
    // increase for any given row
    for(i=0;i<n;i++)
    {
        bubblesort(jU,Ucsr,iU[i],iU[i+1]);
    }
    // Indices also have to start from 1 instead from 0
    for(i=0;i<n+1;i++)
    {
        iU[i]++;
    }
    for(i=0;i<nonzeroes;i++)
    {
        jU[i]++;
    }

    delete [] Ucoo;
    delete [] rowind;
    delete [] colind;
    delete [] U2coo;
    delete [] rowind2;
    delete [] colind2;
};

/* complex_functions.cpp
Apparently, no overloaded operators for MKL_Complex16 are available.*/

#include <iostream>
#include <mkl_types.h>

MKL_Complex16 cmult(MKL_Complex16 z1, MKL_Complex16 z2)
{
    double a=z1.real;
    double b=z1.imag;
    double c=z2.real;
    double d=z2.imag;
    MKL_Complex16 z3;
    z3.real = a*c-b*d; z3.imag=b*c+a*d;
    return z3;
}

MKL_Complex16 csub(MKL_Complex16 z1, MKL_Complex16 z2)
{
    double a=z1.real;
    double b=z1.imag;
    double c=z2.real;
    double d=z2.imag;
    MKL_Complex16 z3;
    z3.real = a-c; z3.imag=b-d;
}

```

```

        return z3;
    }

MKL_Complex16 cadd(MKL_Complex16 z1, MKL_Complex16 z2)
{
    double a=z1.real;
    double b=z1.imag;
    double c=z2.real;
    double d=z2.imag;
    MKL_Complex16 z3;
    z3.real = a+c; z3.imag=b+d;
    return z3;
}

double cabs2(MKL_Complex16 z)
{
    double abs;
    abs=z.real*z.real+z.imag*z.imag;
    return abs;
}

// bubblesort.cpp
// PARDISO demands the sparse array in column-compressed form
// with increasing column indices for each row of the matrix.
// Since there are only 3 entries per row, we use a trivial
// sorting algorithm.

#include "mkl_types.h"

void bubblesort(int *indexarray, MKL_Complex16 *valuearray, int startpos, int
    endpos)
{
    bool swapped = true;
    int aux;
    MKL_Complex16 aux2;
    int n = endpos-startpos;
    while(swapped==true)
    {
        swapped=false;
        for(int i=startpos; i<startpos+n-1; i++)
        {
            if(indexarray[i] > indexarray[i+1])
            {
                aux=indexarray[i];
                aux2=valuearray[i];
                indexarray[i]=indexarray[i+1];
                valuearray[i]=valuearray[i+1];
                indexarray[i+1]=aux;
                valuearray[i+1]=aux2;
                swapped = true;
            }
        }
        n = n-1;
    }
}

```


Bibliography

- [AS72] M. Abramowitz, I.A. Stegun (eds.), *Handbook of Mathematical Functions with Formulas, Graphs, and Mathematical Tables* (Dover, 1972)
- [AS10] A. Altland, B. Simons, *Condensed Matter Field Theory* (Cambridge University Press, 2010).
- [AZ97] A. Altland, M.R. Zirnbauer, Phys. Rev. B **55**, 1142 (1997).
- [AS03] J.E. Avron, D. Osadchy, R. Seiler, Physics Today, **56**, August, 38, (2003)
- [BES94] J. Bellisard, A. van Elst, H. Schulz-Baldes, J. Math. Phys. **35**, 5373 (1994).
- [BR03] P.R. Bevington, D.K. Robinson, *Data Reduction and Error Analysis for the physical sciences* (McGraw-Hill, 2003).
- [BKS⁺00] M.J. Bhaseen, I.I. Kogan, O.A. Soloviev, N. Taniguchi, A.M. Tselik, Nucl. Phys. B **580**, 688 (2000).
- [BNS65] L.C. Biedenharn, J. Nuyts, N. Straumann, Ann. Inst. Henri Poincaré **3**, 13 (1965).
- [B14] R. Bondesan, private communication.
- [BWZ14] R. Bondesan, D. Wieczorek, M.R. Zirnbauer, Phys. Rev. Lett. **112**, 186803 (2014).
- [BWZ15] R. Bondesan, D. Wieczorek, M.R. Zirnbauer, in preparation.
- [B88] M. Büttiker, Phys. Rev. B **38**, 9375 (1988).
- [C96] J. Cardy, *Scaling and Renormalization in Statistical Physics* (Cambridge University Press, 1996).
- [C04] J. Cardy, *Boundary Conformal Field Theory*, Encyclopedia of Mathematical Physics, (Elsevier, 2006).
- [C08] J. Cardy, arXiv:0807.3472.
- [CP88] J. Cardy and I. Peschel, Nucl. Phys. B, **300** [FS22], 377 (1988).
- [CC88] J. T. Chalker, P. D. Coddington, J. Phys. C **21**, 2665 (1988).
- [CW12] S. Cheng, W. Wang, *Dualities and Representations of Lie Superalgebras* (AMS, 2012).

- [CFZ05] J.B. Conrey, D.W. Farmer, M.R. Zirnbauer, arXiv:math-ph/0511024.
- [EMM01] F. Evers, A. Mildenberger, A.D. Mirlin, Phys. Rev. B **64**, 241303(R) (2001).
- [EMM08] F. Evers, A. Mildenberger, A.D. Mirlin, Phys. Rev. Lett. **101**, 116803 (2008).
- [EM08] F. Evers, A.D. Mirlin, Rev. Mod. Phys. **80**, 1355 (2008).
- [FMS97] P. Di Francesco, P. Mathieu, D. Senechal, *Conformal Field Theory* (Springer, 1997).
- [FH04] W. Fulton, J. Harris, *Representation Theory: A First Course* (Springer, 2004)
- [GMZ13] I. A. Gruzberg, A. D. Mirlin, M. R. Zirnbauer, Phys. Rev. B **87**, 125144 (2013).
- [H09] S. Helgason, *Geometric Analysis on Symmetric Spaces* (AMS, 2009).
- [H89] R. Howe, Remarks on Classical Invariant Theory, Trans. Amer. Math. Soc. **313**, 539 (1989).
- [H95] B. Huckestein, Rev. Mod. Phys. **67**, 357 (1995).
- [HK97] A. Hansen, J. Kertesz, arXiv:cond-mat/9706066.
- [J94] M. Janßen, Int. J. Mod. Phys. B **8**, 943 (1994)
- [JMZ99] M. Janßen, M. Metzler, M. R. Zirnbauer, Phys. Rev. B **59**, 15836 (1999).
- [JVF⁺94] M. Janßen, O. Viehweger, U. Fastenrath, J. Hajdu, *Introduction to the Theory of the Integer Quantum Hall Effect* (Wiley-VCH, 1994).
- [KHA⁺99] V. Kagalovsky, B. Horovitz, Y. Avishai, J. T. Chalker, Phys. Rev. Lett. **82**, 3516 (1999).
- [KM05] C.L. Kane, E.J. Mele, Phys. Rev. Lett. **95**, 146802 (2005).
- [KS83] A. V. Khaetskii, B. I. Shklovskii, Sov. Phys. JETP **85**, 721 (1983).
- [KDP80] K. von Klitzing, G. Dorda, M. Pepper, Phys. Rev. Lett. **45**, 494 (1980).
- [K85] K. von Klitzing, Nobel Lecture: The Quantized Hall Effect. (1985), retrieved from http://www.nobelprize.org/nobel_prizes/physics/laureates/1985/klitzing-lecture.html, 6 Mar 2015
- [K13] R. Klesse, private communication.
- [KM97] R. Klesse, M. Metzler, Phys. Rev. Lett. **79**, 721 (1997).
- [KZ01] R. Klesse, M.R. Zirnbauer, Phys. Rev. Lett. **86**, 2094 (2001).

- [KOK05] B. Kramer, T. Ohtsuki, S. Kettemann, *Physics Reports* **417** (5-6), 211 (2005).
- [L81] R. Laughlin, *Phys. Rev. B* **23**, 5632 (1981).
- [LVX⁺09] W. Li, C. L. Vicente, J. S. Xia, W. Pan, D. C. Tsui, L. N. Pfeiffer, and K. W. West, *Phys. Rev. Lett.* **102**, 216801 (2009).
- [MS88] G. V. Mil'nikov, I. M. Sokolov, *JETP Lett.* **48**, 536 (1988).
- [MFM⁺06] A.D.Mirlin, Y.V.Fyodorov, A.Mildenberger, F.Evers, *Phys. Rev. Lett.* **97**, 046803 (2006).
- [NKS14] W. Nuding, A. Klüner, A. Sedrakyan, arXiv:1405.4269.
- [OBL⁺13] H. Obuse, S. Bera, A.W.W. Ludwig, I.A. Gruzberg, F. Evers, *Europhys. Lett.* **104**, 27014 (2013).
- [OGE12] H. Obuse, I.A. Gruzberg, F. Evers, *Phys. Rev. Lett.* **109**, 206804 (2012).
- [OSF⁺07a] H. Obuse, A. R. Subramaniam, A. Furusaki, I. A. Gruzberg, A. W. W. Ludwig, *Phys. Rev. Lett.* **98**, 156802 (2007).
- [OSF⁺07b] H. Obuse, A. R. Subramaniam, A. Furusaki, I. A. Gruzberg, A. W. W. Ludwig, *Physica E* **40**, 1404 (2008).
- [OSF⁺08] H. Obuse, A. R. Subramaniam, A. Furusaki, I. A. Gruzberg, A. W. W. Ludwig, *Phys. Rev. Lett.* **101**, 116802 (2008).
- [O68] V. I. Oseledec, *Trans. Moscow Math. Soc.* **19**, 197 (1968)
- [SD87] H. Saleur, B. Duplantier, *Phys. Rev. Lett.* **58**, 2325 (1987).
- [S83] M. Scheunert, *J. Math. Phys.* **24**, 2681 (1983).
- [S07] M.R. Sepanski, *Compact Lie Groups* (Springer, 2007).
- [SGL⁺06] A.R. Subramaniam, I.A. Gruzberg, A.W.W. Ludwig, F. Evers, A. Mildenberger, A.D. Mirlin, *Phys. Rev. Lett.* **96**, 126802 (2006).
- [S14] I.M. Suslov, arXiv:1412.5339.
- [T07] A.M. Tsvelik, *Phys. Rev. B* **75**, 184201 (2007).
- [Z94] M.R. Zirnbauer, *Annalen der Physik* **506**, 513 (1994).
- [Z99] M.R. Zirnbauer, arXiv:hep-th/9905054.

Erklärung

Ich versichere, dass ich die von mir vorgelegte Dissertation selbständig angefertigt, die benutzten Quellen und Hilfsmittel vollständig angegeben und die Stellen der Arbeit – einschließlich Tabellen, Karten und Abbildungen –, die anderen Werken im Wortlaut oder dem Sinn nach entnommen sind, in jedem Einzelfall als Entlehnung kenntlich gemacht habe; dass diese Dissertation noch keiner anderen Fakultät oder Universität zur Prüfung vorgelegen hat; dass sie – abgesehen von unten angegebenen Teilpublikationen – noch nicht veröffentlicht worden ist sowie, dass ich eine solche Veröffentlichung vor Abschluss des Promotionsverfahrens nicht vornehmen werde. Die Bestimmungen der Promotionsordnung sind mir bekannt. Die von mir vorgelegte Dissertation ist von Martin R. Zirnbauer betreut worden.

Köln, den 11. Mai 2015

Daniel Johann Wieczorek

Teilpublikationen:

R. Bondesan, D. Wieczorek and M.R. Zirnbauer, Pure Scaling Operators at the Integer Quantum Hall Plateau Transition, *Phys. Rev. Lett.* **112**, 186803 (2014).

R. Bondesan, D. Wieczorek and M.R. Zirnbauer, in preparation.

Abschließende Worte

Dass Betreuer Interesse am Thema zeigen oder ihre Schützlinge gar betreuen, Eltern Kinder großziehen und (Ehe-)Partner dem Autor während der Erstellung einer solchen Arbeit moralisch zur Seite stehen, statt ihm in den Rücken zu fallen, liest man allenthalben.

Meinem Doktorvater Martin R. Zirnbauer danke ich daher vor allem auch für den Aufbau unserer interdisziplinären Arbeitsgruppe, deren Mitglieder sich mit dem häufig Halbgaren der (theoretischen) Physik nicht zufriedengeben, für exzellente Lehre sowie für die Möglichkeit, trotz meiner zahlreichen Nebentätigkeiten und Eskapaden dabei sein und auch bleiben zu dürfen.

Dem stets motivierten Koautor unserer Veröffentlichung, Roberto Bondesan, möchte ich für zahllose Diskussionen, Anregungen, interne Notizen und Korrekturen danken, die ganz entscheidend zum Gelingen des Projekts beigetragen haben.

Rochus Klesse hat unsere Arbeit, die auch eine späte Fortführung seiner eigenen Forschung darstellt, von Beginn an verfolgt. Ihm danke ich insbesondere für die frühen Hilfen bei der Implementierung und den stets kritischen Blick auf die Ergebnisse, der geholfen hat, anfänglich zu naive Herangehensweisen zu korrigieren.

Für die Vermittlung von Grundlagen der Supermathematik sowie die Hilfe bei der Berechnung der Casimir-Eigenwerte und Erläuterungen zu konischen Distributionen gebührt Alexander Alldridge mein Dank, ebenso wie Thomas Quella in Bezug auf sämtliche Aspekte der konformen Feldtheorie.

Da es sich hierbei bekanntermaßen um Fragen der nationalen Sicherheit handelt, musste ich meine „frühere Freundin und derzeitige Ehefrau“ (in Anlehnung an ein Zitat von P.A.M. Dirac) jahrelang über den eigentlichen Inhalt meiner Arbeit im Dunkeln tappen lassen, was sie im Alltag immer wieder aufs Neue in die Bredouille brachte, niemandem auf Nachfrage genau erklären zu können, woran ihr Ehegatte – der im Übrigen von ihr nicht als derzeitig bezeichnet wird – denn arbeite. Es gehe um Lie-Gruppen und den Quanten-Hall-Effekt, wobei man sich zunächst an den klassischen Hall-Effekt, den man noch aus der Schule kenne, erinnern müsse. Zum Gelingen hat sie über das bereits Gesagte hinaus dennoch mehr beigetragen, als ich durch Hilfe bei Regressionsmodellen hätte abgelten können.

Mit meinen Freunden „Captain Neven“, „dem Dänen“, „Hipster-Jochen“ (auch: „Johchen P. Schutter“), Jan, Max L. „Schäfer (mit ae)“, „Dr. Ricky, Fernmeldetechniker a.D.“, „dem Terroristen“, „de verrückte Mongol“ und „Dr. Wolfi“ hatte ich dienstlich wie privat eine formidable Zeit. Moritz Fabian Ernst, der frühere Pvd (Prokrastinator vom Dienst), zählt auch zu dieser Liste, möchte seinen tatsächlichen, politisch unkorrekten Spitznamen hier allerdings nicht lesen. Unser ehemaliger Fernmeldetechniker hat zudem derart viele nicht-triviale Tippfehler gefunden, dass er in der Befürchtung, das Programm arbeite vollkommen falsch, zwei Wochen vor Abgabe entsetzt anrief; zum Glück war nur die Orientierung in Abbildung 3.1 und die Nummerierung in Abbildung 3.2 falsch.

„Grothendieck II“ hat unser aller Horizont in vielerlei Hinsicht erweitert.

Zwei geschätzten langjährigen Kollegen möchte ich, auch im Namen von Moritz Ernst, für die außergewöhnlich gute Zusammenarbeit im Übungsbetrieb danken.

Meine ausdrückliche Enttäuschung möchte ich an dieser Stelle noch zum Verhalten der Bonn-Cologne Graduate School of Physics and Astronomy und auch der Deutschen Forschungsgemeinschaft als Dachorganisation in Bezug auf die (höchstwahrscheinlich nicht nur mich betreffende) Problematik der Stipendien für Empfänger von Ausbildungsförderung gem. BAföG zu Protokoll geben. Wie von mir mehrfach detailliert dargelegt, konnte diese Gruppe bis zum Wintersemester 2011/2012 aufgrund des Spannungsverhältnisses zwischen BAföG-Darlehen, Studienbeitragskredit und Stipendienzahlungen, welche die Ämter für Ausbildungsförderung als Erwerbseinkommen werten mussten, in einer rationalen finanziellen Entscheidung nur zu dem Schluss kommen, die Stipendienzahlungen bis zum Ende der Regelstudienzeit abzulehnen und auf die Inanspruchnahme von Reisekostenerstattung zu verzichten. Aufgrund der geringen relativen Größe dieser Gruppe hätte die aus meiner Sicht angemessene Reaktion von offizieller Seite nur lauten können, die Ausschüttung der Zahlungen auf diesen Zeitpunkt zu verschieben, da der zu erwartende positive Effekt eines Stipendiums in dieser Gruppe deutlich größer ausfällt als für diejenigen Studenten, deren Familien vollständig für das Studium aufkommen können und für die somit im Nachhinein auch keine Rückzahlungsverpflichtungen bestehen. Zusammenfassend sehe ich hierin eine Ausprägung nicht-intentionaler institutioneller Diskriminierung, und zwar in derjenigen Form, die aus der Anwendung gleicher Regeln auf Ungleiche resultiert. Die Stipendienzahlungen sind selbstverständlich auch auf den Unterhaltsanspruch eines Studenten, der keine Ausbildungsförderung bezieht, anzurechnen. Die unterhaltspflichtigen Eltern setzen allerdings im Gegensatz zum Staat – und darin liegt meiner Meinung nach der Ursprung der resultierenden Benachteiligung – in der Regel gegen ihre studierenden Sprößlinge keine Unterhaltskürzungen durch. Als persönliche Konsequenz war daher in meinem Fall bereits vor Beginn der Diplomarbeit klar, dass ich nach der Promotion auf gar keinen Fall im Universitätsbetrieb verbleiben würde.

Dass diese Arbeit abgeschlossen wurde ist nicht zuletzt auch dem glücklichen Zufall zu verdanken, dessen tragende Rolle in der Wissenschaft nur allzu gerne verschwiegen wird. Wären die Observablen nur einige Wochen später entdeckt worden, so hätte ich wohl kürzlich (bezogen auf den Termin der mündlichen Prüfung) meinen Vorbereitungsdienst an der Martin-Luther-Schule in Marburg abgeschlossen.